Collective properties of nucleons in the abnormal-parity states

K. H. Bhatt,[1,3] S. Kahane,[2,3] and S. Raman[4]
[1]*Department of Physics and Astronomy, University of Mississippi, University, Mississippi 38677*
[2]*Nuclear Research Center–Negev, Beer-Sheva, Israel*
[3]*Joint Institute for Heavy-Ion Research, Oak Ridge, Tennessee 37831*
[4]*Physics Division, Oak Ridge National Laboratory, Oak Ridge, Tennessee 37831*
(Received 12 October 1999; published 22 February 2000)

In the first part of this work, we study the quadrupole collective properties of $N_a=2$, 4, 6, and 8 nucleons occupying the abnormal-parity intruder single-particle states with high angular momenta $j_a=\frac{9}{2}$, $\frac{11}{2}$, $\frac{13}{2}$, and $\frac{15}{2}$. This study is essential for a detailed understanding of the contribution made by these nucleons to the quadrupole collectivity of the yrast states of deformed nuclei. The properties studied include (i) the distribution of the angular momenta J contained in the intrinsic state of N_a particles in the $|j_a k_a\rangle$ states, (ii) the relationship between the quadrupole moment $Q_0(j_a,N_a)$ of such an intrinsic state and the maximum angular momentum $J_{\max}$ contained in it, (iii) the complete set of reduced quadrupole matrix elements $(J'||Q||J)$ for transitions between all the states $|J\rangle$ and $|J'\rangle$ projected from the intrinsic state, (iv) the $B(E2{:}J\rightarrow J-2)$ values, (v) the transition moments $Q_t(J)$, and (vi) the spectroscopic quadrupole moment $Q(J)$. We compare these properties with similar properties of an intrinsic state having SU(3) symmetry which contains the same set of angular momenta as contained in the intrinsic state of a particular number of nucleons in a specific j_a configuration. In the second part, we use the input from the first part to study the collective properties of the coupled system of protons and neutrons in abnormal-parity states. We show that the SU(3)-like features observed for the individual groups of abnormal-parity nucleons become stronger for the coupled system. Finally, in the third part, we consider the yrast bands of well-deformed nuclei projected from their Nilsson intrinsic states of valence nucleons in a major shell. We specify the structure of the wave function of each projected yrast state $|J\rangle$ in terms of the nucleons in both normal- and abnormal-parity states. These wave functions can be used to determine the individual contributions of the nucleons in normal- and abnormal-parity states to any specific property of the yrast state. In particular, we calculate the transition moments $Q_t(J)$ of the entire yrast band of even-even $^{160-166}$Yb, ^{156,158}Dy, ^{232}Th, ^{234}U, and ^{236}U projected from their respective Nilsson intrinsic states.

PACS number(s): 21.60.Fw, 21.60.Cs, 27.70.+q, 27.90.+b

I. INTRODUCTION

In a shell-model description of heavy, deformed nuclei, the configuration space for the valence protons and neutrons consists of the single-particle states (with angular momentum j) in major shells appropriate to the proton and neutron numbers. These states in the 28–50, 50–82, 82–126, and 126–184 major shells are listed in Table I. Each shell contains a number of states $|j_n\rangle$ with the same parity—the so-called normal-parity (n) states—and an intruder state $|j_a\rangle$ with a parity opposite to that of the n states. This intruder state is called the abnormal-parity (a) state. The a states in the four major shells listed in Table I have $j_a=\frac{9}{2}$, $\frac{11}{2}$, $\frac{13}{2}$, and $\frac{15}{2}$.

In Refs. [1] and [2], we showed that the trend of the experimental $B(E2{:}0_1^+\rightarrow 2_1^+)$ values for even-even nuclei can be quantitatively understood by assuming that the corresponding intrinsic state (abbreviated as $\mathcal{IS}$) of the valence particles has a mass quadrupole moment close to the maximum value that it can have in a major shell. In Ref. [3], we asked the following question: What is the contribution of the nucleons in the a states (loosely referred to as a nucleons) to the total quadrupole moment of the $\mathcal{IS}$ of a deformed nucleus? We showed that if the asymptotically deformed Nilsson $\mathcal{IS}$ within the configuration space of a major shell is assumed to be a good approximation to the $\mathcal{IS}$ of a well-deformed nucleus (in the rare-earth or actinide regions), the a nucleons contribute about 25% to the total intrinsic quadrupole moment.

In Ref. [4], we posed the next questions: How much do the a nucleons contribute to the total angular momentum J (the unit is $\hbar$, which is usually omitted) of an yrast state of a deformed nucleus, and what are the relative contributions of the a and n nucleons? To answer these questions, we assumed that the structure of the yrast band is well approximated by the states of definite J projected from the asymptotically deformed Nilsson $\mathcal{IS}$. We then showed that although the a nucleons contribute only $\sim$25% to the intrin-

TABLE I. List of single-particle states in four major shells. Pairs of states within brackets are nearly degenerate. They form pseudo-spin-orbit doublets. In each major shell, the state with the highest j value is the abnormal-parity (a) state.

Major shell	Single-particle states n states	a state
28–50	$1p_{1/2},(1p_{3/2},0f_{5/2})$	$0g_{9/2}$
50–82	$(2s_{1/2},1d_{3/2}),(1d_{5/2},0g_{7/2})$	$0h_{11/2}$
82–126	$2p_{1/2},(2p_{3/2},1f_{5/2}),(1f_{7/2},0h_{9/2})$	$0i_{13/2}$
126–184	$(3s_{1/2},2d_{3/2}),(2d_{5/2},1g_{7/2}),(1g_{9/2},0i_{11/2})$	$0j_{15/2}$

sic quadrupole moment, their contribution to the angular momentum of an yrast state is as large as that of the n nucleons.

Starting with Elliott [5,6], several authors have shown that the SU(3) symmetry is, in one form or another, ideally suited for describing quadrupole collectivity. In the $\mathcal{IS}$ of a nucleus, the n nucleons are known to possess good pseudo-SU(3) symmetry [7]. On the other hand, the number N_a of a nucleons in the same $\mathcal{IS}$ are in a $j_a^{N_a}$ configuration, which lacks SU(3) symmetry. In fact, if the pairing interaction is dominant, the symmetry appropriate for the $j_a^{N_a}$ configuration is the symplectic Sp$(2j_a+1)$ symmetry [8,9], which gives rise to bands of states that can be labeled by angular momenta J and seniority v. The properties of the $j_a^{N_a}$ states with definite seniority have been well studied in Refs. [8,9]. The symplectic symmetry is, however, broken to a considerable extent by the strong deformation of the mean field of the nucleus.

Within the framework of the deformed configuration-mixed shell model [10,11], the dynamic structure of the yrast band should be determined largely by the states $|\text{proj};J_n\rangle$ and $|\text{proj};J_a\rangle$ of the n and a nucleons projected from their respective $\mathcal{IS}$'s. The states $|\text{proj};J_n\rangle$ projected from the asymptotic Nilsson $\mathcal{IS}$'s also have pseudo-SU(3) symmetry, and their collective properties have been studied well [12]. By contrast, despite their obvious importance, the collective properties of the states $|\text{proj};J_a\rangle$ have received only scant attention until now primarily because these states do not possess any symmetry. In this work, we have systematically examined (in a numerical fashion) the quadrupole collective properties of the states $|\text{proj};J_a\rangle$ of the $j_a^{N_a}$ configurations projected from the corresponding prolate $\mathcal{IS}$ designated as $\mathcal{F}_K(j_a,N_a)$. We have considered the a states $0g_{9/2}$, $0h_{11/2}$, $0i_{13/2}$, and $0j_{15/2}$ and $N_a=2$, 4, 6, and 8 particles. The collective properties of these states are compared with those of the low-lying states belonging to the appropriate SU(3), SO(6), and Sp$(2j_a+1)$ symmetries to look for some similarities, if any.

In Sec. II, we consider the quadrupole collectivity of the $\mathcal{IS}$ $\mathcal{F}_K(j_a,N_a)$. One aspect of this collectivity is the distribution of angular momenta contained in this $\mathcal{IS}$. In Sec. II A, we summarize how this distribution is calculated for an axially symmetric $\mathcal{IS}$ $\mathcal{F}_K(j_a,N_a)$ and for an $\mathcal{IS}$ $\mathcal{F}_K[\lambda,0]$ belonging to an SU(3) representation $[\lambda,0]$. In Sec. II B, the prolate $\mathcal{IS}$'s of N_a particles in different a orbits are explicitly specified, and the distributions of angular momenta are actually calculated. We show in Secs. II C and II D that the distributions of angular momenta in the $\mathcal{IS}$'s of just the a particles are similar to the distribution of angular momenta in the $\mathcal{IS}$'s belonging to appropriate SU(3) representations. A quantitative measure of this similarity is obtained in Sec. II E. Another aspect of the collectivity of the $\mathcal{IS}$ is the relationship between its quadrupole moment and the maximum angular momentum $J_{\max}$ contained in it. This connection is examined in Sec. II F.

In Sec. III, we use the results of Sec. II to obtain a measure of the quadrupole collectivity of the $\mathcal{IS}$ of N particles in a large single-j shell. We had used such $\mathcal{IS}$'s in our previous works [1,13] to reproduce the trend of the quadrupole moments of N particles in a major shell.

In Sec. IV, we examine quantitatively the changes in some properties of the $\mathcal{IS}$ $\mathcal{F}_K(j_a,N_a)$ when it is subjected to perturbations resulting from the pairing interaction and from the so-called $0\hbar\omega$ mixing caused by the deformation of the mean field. These two are the most important of the perturbations of this $\mathcal{IS}$ in the configuration space of one major shell.

In Sec. V, we move on to determine the collective properties of the yrast band projected from the $\mathcal{IS}$ $\mathcal{F}_K(j_a,N_a)$. We first calculate, with high accuracy, the complete set of reduced quadrupole matrix elements $(J_f\|Q\|J_i)$ for all possible transitions between the states $|J_a\rangle$ of the projected band. The numerical accuracy of the calculated reduced matrix elements is tested in Sec. V C by a consistency check. This check is then used as a tool for comparing the scaling behavior of the quadrupole collectivity of different $\mathcal{IS}$'s. In Sec. V D, we consider the relationship between the $B(E2{:}2\rightarrow 0)$ value (calculated for the projected $J_a=2$ and $J_a=0$ states) and the square of the total quadrupole moment of the $\mathcal{IS}$. This consideration is followed in Sec. V E by a discussion of the trend of the $B(E2{:}J\rightarrow J-2)$ values for the entire band projected from each of the $\mathcal{IS}$'s. We present comparisons of these trends for the bands projected from the $(\frac{13}{2})^6$ and $(\frac{15}{2})^8$ $\mathcal{IS}$'s with trends obtained for bands belonging to SU(3) representations.

In cranking models [14], it is a common practice to regard the variation with J of the so-called transition moment $Q_t(J)$ derived from the $B(E2{:}J\rightarrow J-2)$ values as an indicator of the *change* in the deformation of the cranked $\mathcal{IS}$ with rotational frequency. On the other hand, the $Q_t(J)$ values calculated here for the states $|J\rangle$ projected from the *same* $\mathcal{IS}$ also vary with J. This variation is displayed in Sec. V F. The variation of the spectroscopic quadrupole moment $Q(J)$ with J of the projected states is illustrated in Sec. V G. These comparisons should prove helpful in understanding the relationships between the cranking model and projection model predictions of various physical properties.

In some algebraic models [15–17], rotationlike quadrupole collectivity is obtained not only with SU(3) symmetry but also with SO(6) symmetry. In Sec. V H, we demonstrate that the trend of the projected $B(E2{:}J\rightarrow J-2)$ values is more collective than the corresponding trend obtained for the yrast band containing the same set of angular momenta belonging to a representation of SO(6) symmetry. In the last part of Sec. V, we compare the collective properties of the band of projected states with properties of the band of states of the $j_a^{N_a}$ configuration belonging to the Sp$(2j_a+1)$ symmetry with seniorities $v=0$, 2, and 4.

After studying the collective properties of the bands $|J_a\rangle$ projected from the individual $\mathcal{IS}$'s, we next consider the simultaneous $\mathcal{IS}$ of both protons (π) and neutrons (ν) in the $j_{a\pi}^{N_{a\pi}}$ and $j_{a\nu}^{N_{a\nu}}$ configurations, respectively. We show in Sec. VI how the requirement that these nucleons share the same mean field induces a coupling between the projected states of protons and neutrons—a coupling that determines the structure of the yrast band of the $\pi\nu$ system. As an example, we consider the yrast band resulting from protons in the $0h_{11/2}$ state and neutrons in the $0i_{13/2}$ state. Such configurations

occur in the rare-earth nuclei. We calculate the $B(E2:J\rightarrow J-2)$, $Q_t(J)$, and $Q(J)$ values for the coupled projected band and compare them with the rotor and SU(3) model values. This exercise explores the enhancement of quadrupole collectivity in the coupled $\pi\nu$ system of *a* nucleons.

In Sec. VII, we bring the *n* and *a* nucleons together to share the common mean field. We determine the structure of the yrast band of the nucleus in terms of the states $|J_n\rangle$ and $|J_a\rangle$ of *n* and *a* nucleons projected from their respective $\mathcal{IS}$'s. We then calculate the relative contributions of *n* and *a* nucleons to the total *J* of an yrast state and to the $B(E2:J\rightarrow J-2)$ values. The procedure is illustrated by considering the nuclei $^{160-166}$Yb, ^{156,158}Dy, ^{232}Th, ^{234}U, and ^{236}U. A final discussion of the main results follows in Sec. VIII. A preliminary account of this work was presented [18] at the international conference held to commemorate the 40th anniversary of the introduction of SU(3) symmetry to describe collective nuclear phenomena.

II. COLLECTIVITY OF THE INTRINSIC STATE OF ABNORMAL-PARITY NUCLEONS

A. Distribution of angular momenta

The $\mathcal{IS}$ $\mathcal{F}_K$ of *N* valence particles, generated by a deformed axially symmetric mean-field potential, is a Slater determinant of the deformed single-particle states

$$\phi_k^\alpha=\sum_j c_{j,k}^\alpha \psi_k^j \tag{1}$$

occupied by the particles. Here, $k=\langle j_{z'}\rangle$ is the projection of the single-particle angular momentum along the symmetry axis, and $K=\Sigma_i k_i$ is the projection of the total angular momentum along the same axis with the sum running over the individual k_i of different occupied orbits labeled by *i*. The label α distinguishes different states ϕ_k^α with the same value of *k*. The states ψ_k^j with angular momenta *j* are the spherical states belonging to the major shell. The expansion coefficients $c_{j,k}^\alpha$ depend, in general, on the deformation of the potential representing the mean field of the nucleus.

In an axially symmetric potential, the states ϕ_k^α and ϕ_{-k}^α have the same energy. In the lowest-energy $\mathcal{IS}$'s (considered in this paper) of an even number of valence particles, if a state ϕ_k^α is occupied, ϕ_{-k}^α will also be occupied. Consequently, $K=0$ for such $\mathcal{IS}$'s.

The $\mathcal{IS}$ $\mathcal{F}_K$ is deformed and can be expanded in states of definite angular momenta Ψ_K^J contained in it as

$$\mathcal{F}_K=\sum_J C_{JK}\Psi_K^J. \tag{2}$$

The probability $P_1(J)$ that $\mathcal{F}_K$ contains an angular momentum *J* (in units of $\hbar$) is given by $|C_{JK}|^2$. The calculation of this quantity for a given $\mathcal{IS}$ is described in Sec. II B of Ref. [4] (see also Ref. [19]). The probability distribution $P_1(J)$ is a measure of the quadrupole collectivity; that is, a more collective $\mathcal{IS}$ will give rise to a broader distribution within the same range of *J* values.

An axially symmetric $\mathcal{IS}$ of an even-even nucleus with symmetry about the midplane contains only states with even values of angular momenta [20] up to the maximum angular momentum possible within the model valence space. If an $\mathcal{IS}$ belongs to an SU(3) representation $[\lambda,0]$, it has $K=0$, and it contains states with $J=0,2,4,\ldots,J_{\max}$, where $J_{\max}=\lambda$. The probability $P_1([\lambda,0];J)$ that the SU(3) $\mathcal{IS}$ contains an angular momentum *J* is given by [21]

$$P_1([\lambda,0];J)\equiv|C_{JK}(\lambda,0)|^2=\begin{cases}\dfrac{1}{\lambda+1} & \text{for } J=0,\\[2ex] (2J+1)\dfrac{\lambda(\lambda-1)(\lambda-2)\ldots(\lambda-J+1)}{(\lambda-J+1)(\lambda-J+3)\ldots(\lambda+J-1)(\lambda+J+1)} & \text{for } J\geqslant 1.\end{cases} \tag{3}$$

The distribution $P_1([\lambda,0];J)$ will be referred to as the SU(3) distribution.

The calculation of $P_1([\lambda,\mu];J\rangle$ for the more general triaxial $\mathcal{IS}$'s of SU(3) representations $[\lambda,\mu]$ is described in Sec. III of Ref. [4]. The $K=0$ band contains states with $J=0,2,4,\ldots,(\lambda+\mu)$. We found in Ref. [4] that $P_1([\lambda,\mu];J)$ normalized to unity for the $K=0$ band is nearly indistinguishable from $P_1([\lambda',0];J)$ for the axially symmetric representation $[\lambda',0]$, where $\lambda'=\lambda+\mu$ and $\lambda\gg\mu$. For this reason, we use in this paper the simpler SU(3) distributions $P_1([\lambda,0];J)$ for comparison with the distributions $P_1[(j_a,N_a);J]$, which are discussed in the next section.

B. Determinantal intrinsic states

Let $\psi_{k_a}^{j_a}$ with angular momenta j_a be the so-called abnormal-parity intruder states in a major shell. There is only one state $\psi_{k_a}^{j_a}$ of a given k_a in a major shell, and the axially symmetric quadrupole deformation cannot mix that state with other states $\psi_{k_n}^{j_n}$ of normal parity in the same shell. Hence, the deformed states ϕ_k^α of abnormal parity are just the states $\phi_{k_a}^\alpha=\psi_{k_a}^{j_a}$.

In an $\mathcal{IS}$ of *N* valence particles in a major shell, let N_a be the number of particles which occupy the states $\phi_{k_a}^\alpha=\psi_{k_a}^{j_a}$

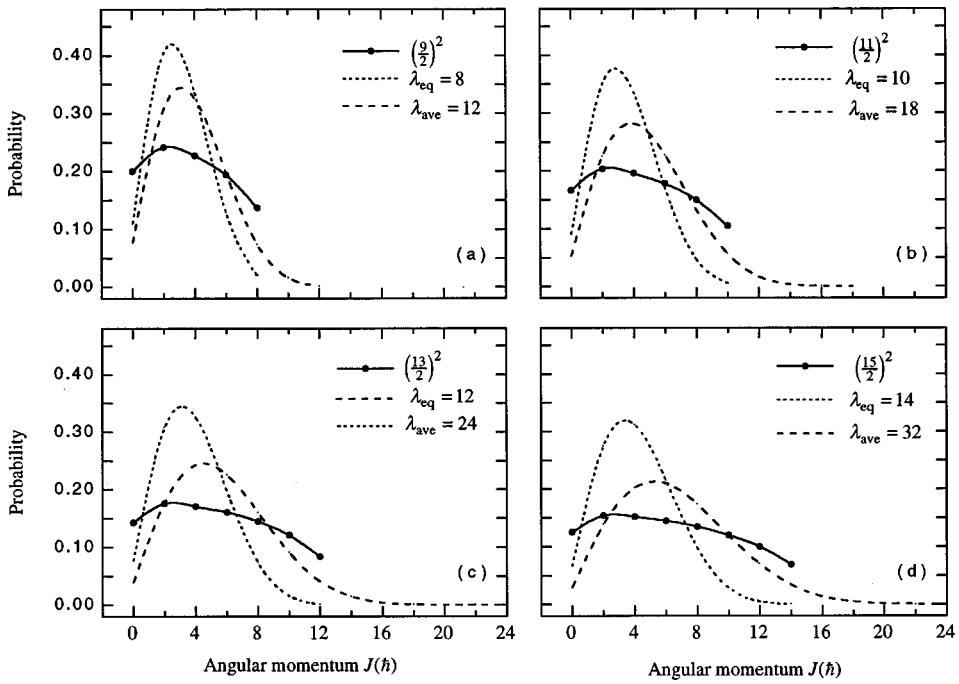

FIG. 1. The dots and connecting solid line show the probability distribution $P_1=|C_{JK}|^2$ [see Eq. (4)] that the $\mathcal{IS}$ $\mathcal{F}_K(j_a,N_a=2)$ of two particles contains a state with definite angular momentum J. The two particles are in the single-particle abnormal-parity states $0g_{9/2}$, $0h_{11/2}$, $0i_{13/2}$, and $0j_{15/2}$. The smooth curve represents what is actually a distribution restricted to even values of J (see Fig. 1 of Ref. [4]). The dotted and dashed curves show the probability distributions obtained for the SU(3) $\mathcal{IS}$'s $\mathcal{F}_K[\lambda_{eq},0]$ and $\mathcal{F}_K[\lambda_{ave},0]$, respectively, which are defined in Secs. II C and II D.

with different k_a values. We are interested in examining the collective properties of the $\mathcal{IS}$ $\mathcal{F}_{K_a}(j_a,N_a)$ of just the N_a particles in the state $|j_a\rangle$ embedded within the total $\mathcal{IS}$ of N particles. The $\mathcal{IS}$ $\mathcal{F}_{K_a}(j_a,N_a)$ are deformed and can be expanded in terms of the states $|(j_a,N_a);J_aK_a\rangle$ as

$$\mathcal{F}_{K_a}(j_a,N_a)=\sum_{J_a} C_{J_aK_a}(j_a,N_a)|(j_a,N_a);J_aK_a\rangle. \quad (4)$$

(Hereafter, we drop the subscript a in J_a and K_a if there is no confusion.) The states $|(j_a,N_a);JK\rangle$ can be projected from $\mathcal{F}_K(j_a,N_a)$ using the standard projection operator P^J_{MK} [14] and can be written as

$$|(j_a,N_a);J,K\rangle=\frac{P^J_{KK}\mathcal{F}_K(j_a,N_a)}{C_{JK}(j_a,N_a)}. \quad (5)$$

The distribution of J in $\mathcal{F}_K(j_a,N_a)$ is then given by the probabilities

$$P_1[(j_a,N_a);J]=|C_{JK}(j_a,N_a)|^2, \quad (6)$$

where

$$\sum_J P_1[(j_a,N_a);J]=1. \quad (7)$$

For N_a particles in the state $|j_a\rangle$, $J_{\max}$ is given by

$$J_{\max}=(N_a/2)[(2j_a+1)-N_a]; \quad N_a=0,2,\ldots,2j_a+1. \quad (8)$$

In this work, we consider only the prolate $\mathcal{IS}$'s of a nucleons because most nuclei are prolate. In a prolate mean-field potential, the orbits $\pm\psi^{j_a}_{k_a}$ are degenerate, and their energies increase with k_a.

Consider only two particles in the a state. In the prolate $\mathcal{IS}$, these two particles will occupy the states $\psi^{j_a}_{k_a}$ with $k_a=\pm\frac{1}{2}$. The $\mathcal{IS}$ is a Slater determinant with the structure

$$\mathcal{F}_K(j_a,2)=\frac{1}{\sqrt{2}}\begin{vmatrix}\psi^{j_a}_{1/2}(1) & \psi^{j_a}_{-1/2}(1)\\ \psi^{j_a}_{1/2}(2) & \psi^{j_a}_{-1/2}(2)\end{vmatrix}. \quad (9)$$

The state $\mathcal{F}_K(j_a,2)$ can be expanded in states of definite J of the two nucleons as

$$\mathcal{F}_K(j_a,2)=\sum_J \sqrt{2}\left(jj\frac{1}{2}-\frac{1}{2}\middle|J0\right)|(j_a,2);J\rangle$$
$$=\sum_J C_{JK}(j_a,2)|(j_a,2);J\rangle. \quad (10)$$

The probabilities $P_1[(j_a,2);J]\equiv|C_{JK}(j_a,2)|^2=2|(jj\frac{1}{2}-\frac{1}{2}|J0)|^2$ are plotted as solid lines in Fig. 1 for the $0g_{9/2}$, $0h_{11/2}$, $0i_{13/2}$, and $0j_{15/2}$ states. For two particles in these a states, $J_{\max}=8$, 10, 12, and 14, respectively.

If there are four particles in the high-j a state, the prolate $\mathcal{IS}$ has the structure

$$\mathcal{F}_K(j_a,4)$$
$$=\sqrt{\frac{1}{4!}}\begin{vmatrix}\psi^{j_a}_{1/2}(1) & \psi^{j_a}_{-1/2}(1) & \psi^{j_a}_{3/2}(1) & \psi^{j_a}_{-3/2}(1)\\ \psi^{j_a}_{1/2}(2) & \cdots & \cdots & \psi^{j_a}_{-3/2}(2)\\ \psi^{j_a}_{1/2}(3) & \cdots & \cdots & \psi^{j_a}_{-3/2}(3)\\ \psi^{j_a}_{1/2}(4) & \psi^{j_a}_{-1/2}(4) & \psi^{j_a}_{3/2}(4) & \psi^{j_a}_{-3/2}(4)\end{vmatrix}. \quad (11)$$

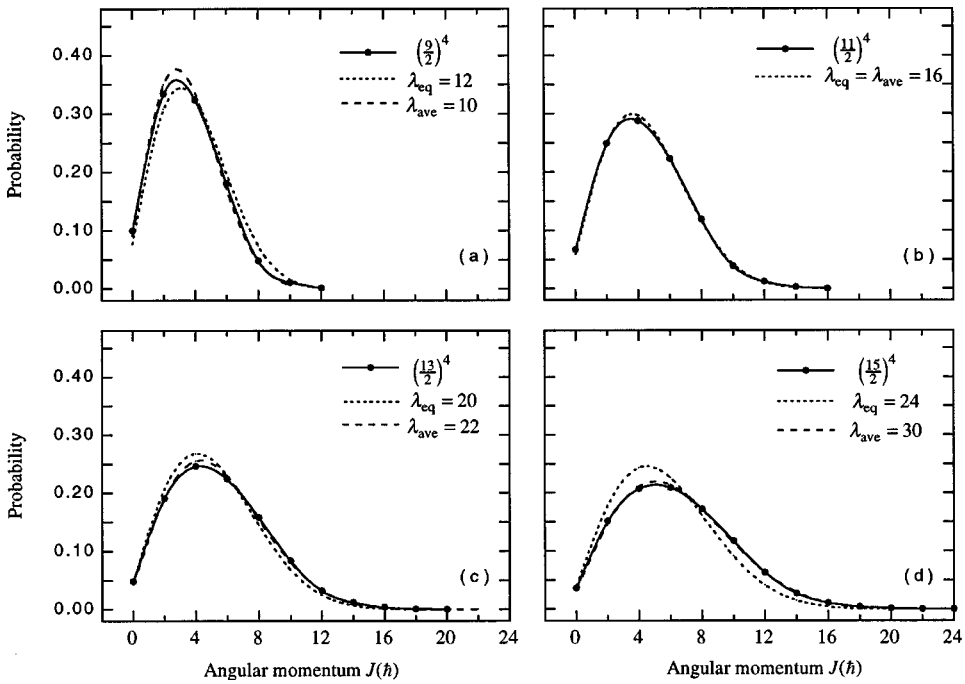

FIG. 2. See caption for Fig. 1. Considered here are the intrinsic states for four particles.

The $(\frac{9}{2})^4$, $(\frac{11}{2})^4$, $(\frac{13}{2})^4$, and $(\frac{15}{2})^4$ $\mathcal{IS}$'s contain even J values up to $J_{\max}=12$, 16, 20, and 24, respectively. The probabilities $P_1[(j_a,4);J]=|C_{JK}(j_a,4)|^2$ for the above four $\mathcal{IS}$'s are shown in Fig. 2.

For six a particles, the $\mathcal{IS}$ is a Slater determinant of particles occupying the states $\psi^{j_a}_{k_a}$ with $k_a=\pm\frac{1}{2}$, $\pm\frac{3}{2}$, and $\pm\frac{5}{2}$. For the $0g_{9/2}$, $0h_{11/2}$, $0i_{13/2}$, and $0j_{15/2}$ states, $J_{\max}=12$, 18, 24, and 30, respectively. Finally, the $\mathcal{IS}$ of eight a particles is a Slater determinant with the particles occupying the states $\psi^{j_a}_{k_a}$ with $k_a=\pm\frac{1}{2}$, $\pm\frac{3}{2}$, $\pm\frac{5}{2}$, and $\pm\frac{7}{2}$. The maximum angular momenta contained in these $\mathcal{IS}$'s are $J_{\max}=8$, 16, 24, and 32, respectively, for the $j_a=\frac{9}{2}$, $\frac{11}{2}$, $\frac{13}{2}$, and $\frac{15}{2}$ a particles. The probabilities $P_1[(j_a,6);J]$ and $P_1[(j_a,8);J]$ for the six- and eight-particle $\mathcal{IS}$'s are shown in Figs. 3 and 4, respectively. The *exact* values of $P_1[(j_a,N_a);J]$ for $j_a=\frac{9}{2}$, $\frac{11}{2}$, $\frac{13}{2}$, $\frac{15}{2}$, and $N_a=2$, 4, 6, 8 are given in Table II.

C. Equivalent SU(3) representations

The $\mathcal{IS}$ $\mathcal{F}_K(j_a,N_a)$ has no SU(3) symmetry. Nevertheless, we define an SU(3) $\mathcal{IS}$ $\mathcal{F}_K[\lambda_{eq},0]$ to be *equivalent* to

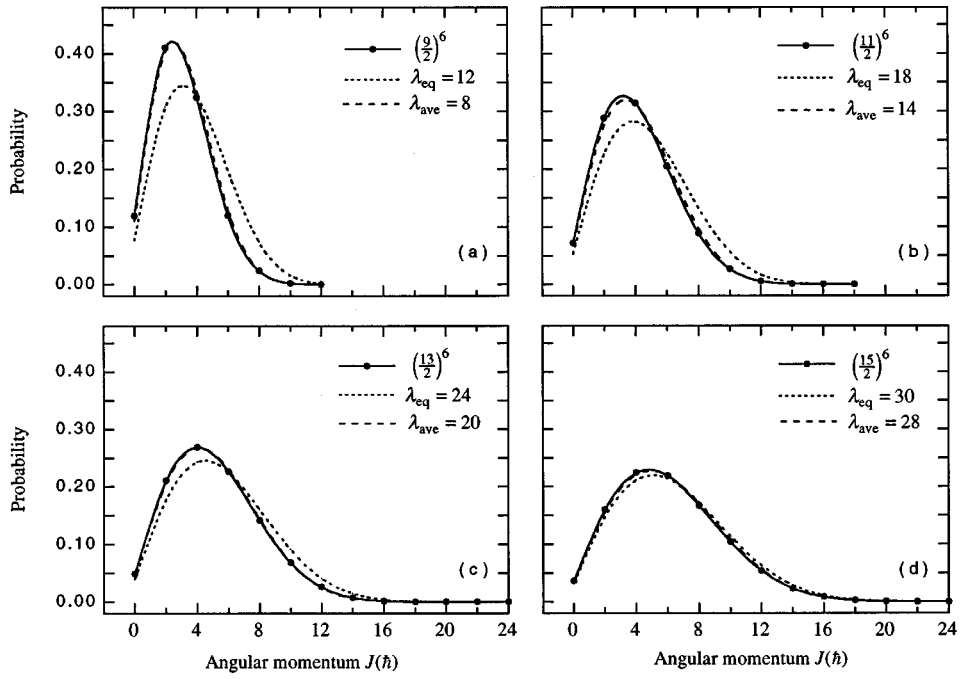

FIG. 3. See caption for Fig. 1. Considered here are the intrinsic states for six particles.

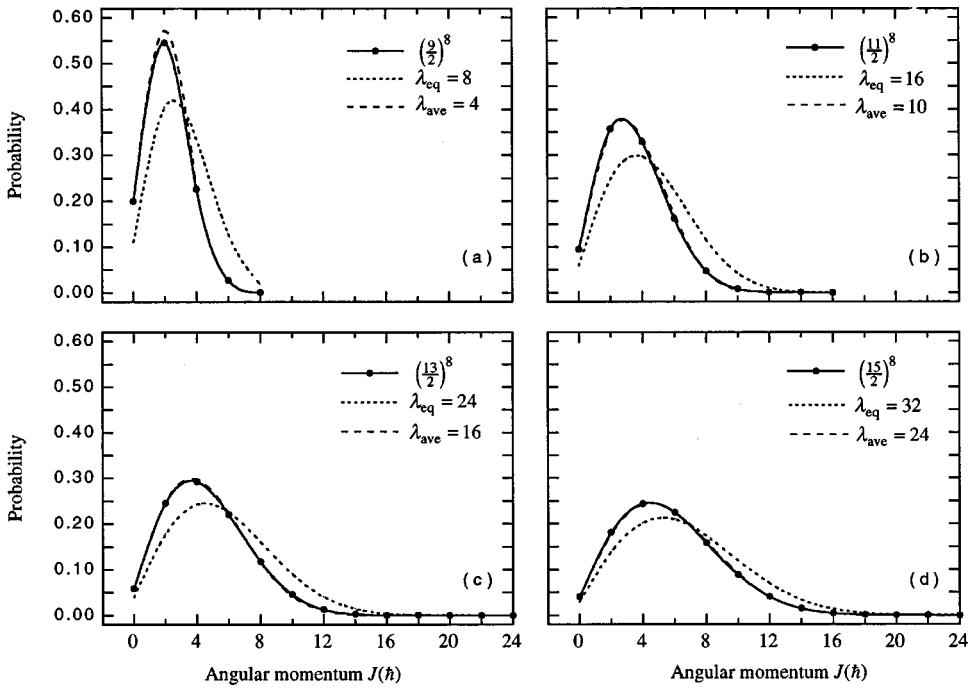

FIG. 4. See caption for Fig. 1. Considered here are the intrinsic states for eight particles.

the $\mathcal{IS}$ $\mathcal{F}_K(j_a,N_a)$ if the former corresponds to an SU(3) representation $[\lambda_{eq},0]$, which contains the same set of angular momenta as contained in the latter. The state $\mathcal{F}_K[\lambda_{eq},0]$ contains angular momenta $J'=0,2,4,\ldots,J'_{max}$, where $J'_{max}=\lambda_{eq}$. The state $\mathcal{F}_K(j_a,N_a)$ contains angular momenta $J=0,2,4,\ldots,J_{max}$. These two $\mathcal{IS}$'s will be equivalent if $\lambda_{eq}=J_{max}$.

With this definition, the λ_{eq} values are 8, 10, 12, and 14, respectively, for the $(\frac{9}{2})^2$, $(\frac{11}{2})^2$, $(\frac{13}{2})^2$, and $(\frac{15}{2})^2$ $\mathcal{IS}$'s. The $P_1([\lambda_{eq},0];J)$ distributions are calculated using Eq. (3) and plotted as dashed lines in Fig. 1. As one might expect, there is little resemblance between the $P_1([\lambda_{eq},0];J)$ and $P_1[(j_a,2);J]$ distributions.

For each of the four-particle $\mathcal{IS}$'s, we show in Fig. 2 the equivalent SU(3) probabilities $P_1([\lambda_{eq},0];J)$. For example, the $\lambda_{eq}=J_{max}$ values are 12 and 24, respectively, for the $(\frac{9}{2})^4$ and $(\frac{15}{2})^4$ $\mathcal{IS}$'s. Compared to the case of two particles, there is now considerable similarity between the $P_1[(j_a,4);J]$ and equivalent SU(3) distributions.

For six and eight particles (see Figs. 3 and 4), the distributions $P_1[(j_a,N_a);J]$ are similar to but narrower than the equivalent SU(3) distributions $P_1([\lambda_{eq},0];J)$. In other words, the $\mathcal{F}_K(j_a,N_a)$ $\mathcal{IS}$'s have a smaller probability of containing higher angular momentum states (that is, smaller quadrupole collectivity) than the corresponding equivalent SU(3) $\mathcal{IS}$'s.

D. Average SU(3) representations

In Ref. [4], we considered the *average* SU(3) representation $[\lambda_{ave},0]$ and determined λ_{ave} by requiring that the average value of $\hat{J}^2$,

$$\langle\hat{J}^2\rangle=\sum_J J(J+1)|C_{J0}|^2, \tag{12}$$

obtained for the SU(3) representation $[\lambda_{ave},0]$ is as close as possible to the average value obtained for $\mathcal{F}_K(j_a,N_a)$. The values of λ_{ave} obtained in this way are compared in Table III with the equivalent values $\lambda_{eq}=J_{max}$. In Figs. 1–4, we compare the distributions $P_1([\lambda_{ave},0];J)$ with $P_1[(j_a,N_a);J]$ for the various $\mathcal{IS}$'s. For two particles, the λ_{ave} values are significantly larger than the λ_{eq} values. Moreover, for these cases, the resemblance (see Fig. 1) of the distributions $P_1([\lambda_{ave},0];J)$ to the corresponding distributions $P_1[(j_a,2);J]$ is no better than that of $P_1([\lambda_{eq},0];J)$. However, for all other $\mathcal{IS}$'s with $N_a>2$ (see Figs. 2–4), there is a remarkable similarity between the $P_1([\lambda_{ave},0];J)$ and $P_1[(j_a,n);J]$ distributions, thus implying similarity in collectivity also.

Referring to Table III, for $N_a=4$, the λ_{ave} value is smaller than the λ_{eq} value in the case of the $(\frac{9}{2})^4$ state, equal for the $(\frac{11}{2})^4$ state, and larger for the $(\frac{13}{2})^4$ and $(\frac{15}{2})^4$ states. For $N_a>4$, the λ_{ave} values are uniformly smaller than the λ_{eq} values. In other words, when $N_a>4$, the collectivity of the $\mathcal{F}_K(j_a,N_a)$ $\mathcal{IS}$ (as implied by the λ_{ave} value) relative to that of the equivalent SU(3) state decreases with increasing N_a.

E. Overlaps of the $\mathcal{F}_K(j_a,N_a)$ and SU(3) intrinsic states

Similar to Eq. (4), the SU(3) $\mathcal{IS}$ may be expanded as

$$\mathcal{F}_K[\lambda,0]=\sum_J C_{JK}[\lambda,0]|JK\rangle_\lambda . \tag{13}$$

Although there is no connection between the states $|JK\rangle_\lambda$ and $|JK\rangle_a$, for this current discussion, we define the ''overlap'' ρ of these two states as

$$\rho=\langle\mathcal{F}_K[\lambda,0]|\mathcal{F}_K(j_a,N_a)\rangle=\sum_J C^*_{JK}(j_a,N_a)C_{JK}[\lambda,0]. \tag{14}$$

TABLE II. Probability $P_1[(j_a,N_a);J]=|C_{JK}(j_a,N_a)|^2$ of finding J in $\mathcal{F}_K(j_a,N_a)$.

J	$j_a=\frac{9}{2}$	$j_a=\frac{11}{2}$	$j_a=\frac{13}{2}$	$j_a=\frac{15}{2}$	$j_a=\frac{9}{2}$	$j_a=\frac{11}{2}$	$j_a=\frac{13}{2}$	$j_a=\frac{15}{2}$
			$N_a=2$ particles				$N_a=4$ particles	
0	$\frac{1}{5}$	$\frac{1}{6}$	$\frac{1}{7}$	$\frac{1}{8}$	$\frac{43}{429}$	$\frac{163}{2431}$	$\frac{1413}{29393}$	$\frac{69899}{1931540}$
2	$\frac{8}{33}$	$\frac{175}{858}$	$\frac{16}{91}$	$\frac{21}{136}$	$\frac{287}{858}$	$\frac{80576}{323323}$	$\frac{334575}{1749748}$	$\frac{305665}{2028117}$
4	$\frac{162}{715}$	$\frac{28}{143}$	$\frac{2916}{17017}$	$\frac{5103}{33592}$	$\frac{1575}{4862}$	$\frac{93248}{323323}$	$\frac{36537561}{148728580}$	$\frac{20324313}{98025655}$
6	$\frac{32}{165}$	$\frac{100}{561}$	$\frac{4000}{24871}$	$\frac{375}{2584}$	$\frac{1924}{10659}$	$\frac{54592}{245157}$	$\frac{1507}{67298}$	$\frac{4190875}{20036013}$
8	$\frac{98}{715}$	$\frac{1225}{8151}$	$\frac{250}{1729}$	$\frac{6125}{45448}$	$\frac{392}{8151}$	$\frac{111212}{937365}$	$\frac{572875}{3624478}$	$\frac{3513375}{20428876}$
10		$\frac{441}{4199}$	$\frac{11664}{96577}$	$\frac{35721}{297160}$	$\frac{11907}{1062347}$	$\frac{205824}{5311735}$	$\frac{8608059}{102144380}$	$\frac{10124544}{86822723}$
12			$\frac{4356}{52003}$	$\frac{5929}{59432}$	$\frac{147}{96577}$	$\frac{100976}{8402199}$	$\frac{11109725}{347290892}$	$\frac{3664739375}{57823933518}$
14				$\frac{20449}{297160}$		$\frac{9856}{3454485}$	$\frac{5654}{474145}$	$\frac{2071498}{76689567}$
16						$\frac{12936}{33393355}$	$\frac{6534000}{1729775789}$	$\frac{3255520125}{283683229396}$
18							$\frac{2475}{2750041}$	$\frac{21181875}{4848322283}$
20							$\frac{3267}{26776715}$	$\frac{457743}{328971070}$
22								$\frac{21023145}{63392725189}$
24								$\frac{2474329}{55124108860}$
			$N_a=6$ particles				$N_a=8$ particles	
0	$\frac{17}{143}$	$\frac{1789}{24871}$	$\frac{25489}{520030}$	$\frac{1742679863}{48620724880}$	$\frac{1}{5}$	$\frac{295}{3094}$	$\frac{10469}{177905}$	$\frac{171766229}{4207562730}$
2	$\frac{16}{39}$	$\frac{8451}{29393}$	$\frac{142360}{676039}$	$\frac{14044678615}{87517304784}$	$\frac{6}{11}$	$\frac{115550}{323323}$	$\frac{263087}{1067430}$	$\frac{379837096}{2103781365}$
4	$\frac{788}{2431}$	$\frac{9327555}{29745716}$	$\frac{289904987}{1078282205}$	$\frac{32745290633}{145862174640}$	$\frac{162}{715}$	$\frac{212427}{646646}$	$\frac{3384513}{11532430}$	$\frac{1614335628}{6613848605}$
6	$\frac{1280}{10659}$	$\frac{2346219}{11440660}$	$\frac{116726812}{514257667}$	$\frac{54525937499}{249087713616}$	$\frac{3}{110}$	$\frac{277960}{1716099}$	$\frac{3095256439}{14025209100}$	$\frac{87423542104}{389199552525}$
8	$\frac{6}{247}$	$\frac{70431}{795340}$	$\frac{5062487}{35750533}$	$\frac{10620510263}{63492946608}$	$\frac{1}{1430}$	$\frac{62455}{1312311}$	$\frac{420424983}{3575053300}$	$\frac{1933622928649}{12202550676225}$
10	$\frac{2352}{1062347}$	$\frac{16587423}{616161260}$	$\frac{29386716}{434113615}$	$\frac{3287391435161}{31610416989840}$		$\frac{12028}{1448655}$	$\frac{690006}{14969435}$	$\frac{194350327032}{2178281940005}$
12	$\frac{12}{96577}$	$\frac{521841}{93501394}$	$\frac{44256300}{1729775789}$	$\frac{34024771862675}{634315700929456}$		$\frac{100375}{117630786}$	$\frac{159651998}{11904927489}$	$\frac{21963208768}{538163773413}$
14		$\frac{1743}{2302990}$	$\frac{2262788}{298237205}$	$\frac{196400772139}{8412675078640}$		$\frac{154}{3454485}$	$\frac{7765043}{2684134845}$	$\frac{1132250049944}{7413669913051 5}$
16		$\frac{2673}{33393355}$	$\frac{245862683}{141841614698}$	$\frac{58880649949693}{6879885679311790}$		$\frac{55}{40072026}$	$\frac{43050711}{93316851775}$	$\frac{2398302482433}{511896255901175}$
18		$\frac{9}{1964315}$	$\frac{1500532}{4848322283}$	$\frac{28663099333}{10937815070448}$			$\frac{23199}{439956650}$	$\frac{1027275591368}{871607138426325}$
20			$\frac{53757}{1151398745}$	$\frac{88704996061}{132475334004720}$			$\frac{9801}{2302797490}$	$\frac{106432830244}{438824543890635}$
22			$\frac{319440}{63392725189}$	$\frac{19659224172445}{134338820369719000}$			$\frac{323433}{1267854503780}$	$\frac{565402571448}{13993627121845805}$
24			$\frac{3993}{13781027215}$	$\frac{50232218179}{178800559498296 0}$			$\frac{1331}{165372326580}$	$\frac{11497672043}{2123256644042265}$
26				$\frac{3008559125}{697959416741776}$				$\frac{68251043432}{1158176407155884 55}$
28				$\frac{1096577625}{2344274002310990}$				$\frac{2312491896}{4468772316905328 5}$
30				$\frac{289496493}{1075132559680550 0}$				$\frac{2126696}{671957849800349}$
32								$\frac{265837}{2644479279859438}$

TABLE III. Equivalent and average SU(3) representations $[\lambda_{eq},0]$ and $[\lambda_{ave},0]$ associated with the $\mathcal{IS}$'s of 2, 4, 6, and 8 particles in the a states. The quantities λ_{eq} and λ_{ave} are defined in Secs. II C and II D, respectively. The symbols $\langle\hat{J}^2\rangle_N$ and $\langle\hat{J}^2\rangle_S$ refer to the average values [see Eq. (12)] calculated for the $\mathcal{F}_K(j_a,N_a)$ and SU(3) $[\lambda_{ave},0]\mathcal{IS}$'s, respectively.

N_a	j_a	$\lambda_{eq}=J_{max}$	λ_{ave}	$\sqrt{\langle\hat{J}^2\rangle_N}$	$\sqrt{\langle\hat{J}^2\rangle_S}$
2	$\frac{9}{2}$	8	12	4.90	4.90
	$\frac{11}{2}$	10	18	5.90	6
	$\frac{13}{2}$	12	24	6.94	6.93
	$\frac{15}{2}$	14	32	7.94	8
4	$\frac{9}{2}$	12	10	4.58	4.47
	$\frac{11}{2}$	16	16	5.66	5.66
	$\frac{13}{2}$	20	22	6.71	6.63
	$\frac{15}{2}$	24	30	7.74	7.75
6	$\frac{9}{2}$	12	8	4	4
	$\frac{11}{2}$	18	14	5.20	5.29
	$\frac{13}{2}$	24	20	6.34	6.32
	$\frac{15}{2}$	30	28	7.41	7.48
8	$\frac{9}{2}$	8	4	3	2.83
	$\frac{11}{2}$	16	10	4.47	4.47
	$\frac{13}{2}$	24	16	5.74	5.66
	$\frac{15}{2}$	32	24	6.92	6.93

If this overlap is large, we may regard the angular momentum structure of the $\mathcal{F}_K(j_a,N_a)$ $\mathcal{IS}$ to be similar to that of the SU(3) $\mathcal{IS}$. The numerical values of these overlaps are listed in Table IV. The total number N_J of different J values (the number of components) contained in $\mathcal{F}_K(j_a,N_a)$ is also listed in the table. For a given $\mathcal{F}_K(j_a,N_a)$ $\mathcal{IS}$, the overlap with the average SU(3) $\mathcal{IS}$ is larger than with the equivalent one. Except for the $\mathcal{IS}$'s of two particles, the ρ_{ave} values are >0.98.

Finally, we obtain an objective measure of how ''good'' these overlaps are. Such a measure is given by the probability $\mathcal{P}(N,\rho)$ of randomly finding an N component $\mathcal{IS}$ having an overlap with $\mathcal{F}_K(j_a,N_a)$ greater than ρ. This probability has been derived as [11]

$$\mathcal{P}(N,\rho)\approx\sqrt{\frac{N}{2\pi}}\int_\rho^1 e^{-(1/2)Nx^2}dx. \tag{15}$$

In Table IV, these probabilities are listed in columns labeled by $\mathcal{P}_{eq}$ and $\mathcal{P}_{ave}$ for the overlaps obtained with the SU(3) $\mathcal{IS}$'s of representations $[\lambda_{eq},0]$ and $[\lambda_{ave},0]$, respectively. The probabilities are appreciably smaller for the representation $[\lambda_{ave},0]$. This result means that the distributions of J in the $\mathcal{F}_K(j_a,N_a)$ and SU(3) $\mathcal{F}_K[\lambda_{ave},0]$ are very similar. It is this surprising similarity which was noted in an earlier paper [4].

We recall that for two particles the SU(3) distributions $P_1([\lambda_{eq},0];J)$ and $P_1([\lambda_{ave},0];J)$ looked very different from the distributions $P_1[(j_a,2);J]$ (see Fig. 1). On the other hand, the corresponding probabilities $\mathcal{P}_{eq}$ and $\mathcal{P}_{ave}$ are $\sim10^{-3}$ (see Table IV). Therefore, we have arbitrarily defined the overlaps ρ as *poor* if $\mathcal{P}\sim10^{-3}$ and as *good* if $\mathcal{P}\ll10^{-3}$. According to this criterion, the overlaps of the $\mathcal{F}_K(j_a,N_a)$ $\mathcal{IS}$'s for 4, 6, and 8 particles in the $\frac{11}{2}$, $\frac{13}{2}$, and $\frac{15}{2}$ a states with the appropriate SU(3) $\mathcal{IS}$'s are very good indeed (see Table IV).

F. Quadrupole moments of the intrinsic states

The mass quadrupole moment Q_0 provides another measure of the collectivity of an $\mathcal{IS}$—a larger value of Q_0 implies more collectivity. In a particular model, the quadrupole moment is usually made up of two parts: (i) a calculated quantity, which depends on the specific structure of the model $\mathcal{IS}$ and (ii) its unit, which is determined by the size of the wave functions used in the calculations. In this section, we want to compare the $Q_0(j_a,N_a)$ value of the $\mathcal{IS}$ $\mathcal{F}_K(j_a,N_a)$ with the $Q_0[\lambda_{eq},0]$ value of the equivalent SU(3) $\mathcal{IS}$ $\mathcal{F}_K[\lambda_{eq},0]$.

The maximum J contained in an $\mathcal{IS}$ is also an indicator of its collectivity. There should therefore be a relation between Q_0 and J_{max}. If the $\mathcal{IS}$ belongs to a harmonic-oscillator SU(3) representation $[\lambda,0]$, Q_0 is given by $Q_0=2\lambda$ in units of the harmonic oscillator size parameter, which we label as $\alpha^2(\lambda)$. The value of J_{max} contained in the representation $[\lambda,0]$ is $J_{max}=\lambda$. Hence, in this case, $Q_0[\lambda,0]=2J_{max}$ in units of $\alpha^2(\lambda)$. The factor $2J_{max}$ is characteristic of the SU(3) structure of the $\mathcal{IS}$, and the unit $\alpha^2(\lambda)$ reflects the geometric size of the underlying single-particle oscillator wave functions. (We will establish this unit later.) We pose the following question: Is there a simple relationship between $Q_0(j_a,N_a)$ and J_{max} in the $\mathcal{IS}$ $\mathcal{F}_K(j_a,N_a)$ case also?

1. Comparison of $Q_0(j_a,N_a)$ and $Q_0[\lambda_{eq},0]$ values

The $Q_0(j_a,N_a)$ value of an $\mathcal{IS}$,

$$Q_0(j_a,N_a)=\sum_{k_i} q_{k_{ai}}(j_a), \tag{16}$$

is the sum of the single-particle mass quadrupole moments

$$q_{k_{ai}}(j_a)\equiv\langle j_a k_{ai}|\sqrt{(16\pi/5)}r^2Y_0^2|j_a k_{ai}\rangle \tag{17}$$

of the N_a states $|j_a k_{ai}\rangle(i=1,2,\ldots,N_a)$ occupied in $\mathcal{F}_K(j_a,N_a)$. For any state $|j_a k_a\rangle$, Eq. (17) can be rewritten using Eq. (1A-60) of Ref. [20] as

$$q_{k_a}(j_a)=\sqrt{(16\pi/5)}(j_a 2k_a 0|j_a k_a)\langle j_a\|r^2\|j_a\rangle\frac{\langle j_a\|Y^2\|j_a\rangle}{\sqrt{2j_a+1}}. \tag{18}$$

TABLE IV. Overlap ρ [see Eq. (14)] of the $\mathcal{F}_K(j_a,N_a)$ and SU(3) $\mathcal{IS}$'s and the probability $\mathcal{P}$ [see Eq. (15)] of randomly finding an SU(3) $\mathcal{IS}$ having an overlap greater than ρ with $\mathcal{F}_K(j_a,N_a)$.

N_a	j_a	N_J	$\lambda_{\rm eq}$	$\lambda_{\rm ave}$	$\rho_{\rm eq}$	$\rho_{\rm ave}$	$\mathcal{P}_{\rm eq}$	$\mathcal{P}_{\rm ave}$
2	$\frac{9}{2}$	5	8	12	0.948	0.966	4.3×10^{-3}	2.7×10^{-3}
	$\frac{11}{2}$	6	10	18	0.929	0.963	4.3×10^{-3}	2.0×10^{-3}
	$\frac{13}{2}$	7	12	24	0.911	0.963	3.9×10^{-3}	1.3×10^{-3}
	$\frac{15}{2}$	8	14	30	0.893	0.964	3.4×10^{-3}	0.9×10^{-3}
4	$\frac{9}{2}$	7	12	10	0.997	0.998	9.2×10^{-5}	7.7×10^{-5}
	$\frac{11}{2}$	9	16	16	>0.999	>0.999	5.2×10^{-6}	5.2×10^{-6}
	$\frac{13}{2}$	11	20	22	0.998	>0.999	1.1×10^{-5}	1.7×10^{-6}
	$\frac{15}{2}$	15	24	30	0.993	>0.999	1.5×10^{-5}	3.7×10^{-7}
6	$\frac{9}{2}$	7	12	8	0.979	0.999	7.2×10^{-4}	1.1×10^{-4}
	$\frac{11}{2}$	10	18	14	0.989	>0.999	9.5×10^{-5}	8.0×10^{-6}
	$\frac{13}{2}$	13	24	20	0.996	>0.999	9.5×10^{-6}	5.3×10^{-7}
	$\frac{15}{2}$	16	30	28	0.999	>0.999	5.3×10^{-7}	7.2×10^{-8}
8	$\frac{9}{2}$	5	8	4	0.957	0.986	3.5×10^{-3}	2.2×10^{-3}
	$\frac{11}{2}$	9	16	10	0.972	>0.999	4.2×10^{-4}	3.5×10^{-5}
	$\frac{13}{2}$	13	24	16	0.982	>0.999	4.3×10^{-5}	4.2×10^{-6}
	$\frac{15}{2}$	17	32	24	0.990	>0.999	3.8×10^{-6}	1.2×10^{-7}

The a states with $j_a=\frac{9}{2}$, $\frac{11}{2}$, $\frac{13}{2}$, and $\frac{15}{2}$ belong to the $\mathcal{N}=4$, 5, 6, and 7 harmonic oscillator shells, respectively. For these states, $j_a=\mathcal{N}+\frac{1}{2}$. The reduced matrix elements $\langle j_a\|r^2\|j_a\rangle$ [in units of the oscillator size parameter $\alpha^2(j_a)$] and $\langle j_a\|Y^2\|j_a\rangle$ are given by [22,23]

$$\langle j_a\|r^2\|j_a\rangle=\mathcal{N}+\frac{3}{2}=j_a+1 \tag{19}$$

and

$$\langle j_a\|Y^2\|j_a\rangle=\left[\frac{5(2j_a+1)}{4\pi}\right]^{1/2}\left(j_a 2\frac{1}{2}0\middle|j_a\frac{1}{2}\right). \tag{20}$$

With these reduced matrix elements, the resulting values of $q_k(j_a)$ are listed in Table V. To calculate the total moment $Q_0(j_a,N_a)$ of a prolate $\mathcal{IS}$ $\mathcal{F}_K(j_a,N_a)$, we recall that the N_a particles occupy sequentially the intruder orbits $|j_ak_a\rangle$ with $k_a=\pm\frac{1}{2},\pm\frac{3}{2},\ldots,\pm j_a$. The $Q_0(j_a,N_a)$ values obtained by adding the individual q_k values are listed in Table VI for $N_a=2$, 4, 6, and 8 particles. Once again, the listed quantities depend on the specific structure of $\mathcal{F}_K(j_a,N_a)$ and the units $\alpha^2(j_a)$ on the sizes of the oscillator wave functions.

We also list, in Table VI, the $Q_0[\lambda_{\rm eq},0]$ values for the equivalent SU(3) $\mathcal{IS}$ $\mathcal{F}_K[\lambda_{\rm eq},0]$. Recall that this $\mathcal{IS}$ was defined to have the same set of J values as the $\mathcal{IS}\mathcal{F}_K(j_a,N_a)$. Hence, both $\mathcal{IS}$'s have the same $J_{\max}$. We now wish to compare their Q_0 values. A quantitative measure of the difference in the quadrupole collectivity of $\mathcal{F}_K(j_a,N_a)$ and $\mathcal{F}_K[\lambda_{\rm eq},0]$, arising from the essential difference in the structures of these $\mathcal{IS}$'s independent of their geometric sizes, can be obtained by equating the two oscillator size parameters. With $\alpha^2(j_a)=\alpha^2(\lambda_{\rm eq})$, the Q_0 values listed in columns 3 and 4 of Table VI can now be directly compared. From this comparison, we conclude that the $\mathcal{IS}$ $\mathcal{F}_K(j_a,N_a)$ is less collective than the equivalent SU(3) $\mathcal{IS}$ $\mathcal{F}_K[\lambda_{\rm eq},0]$ by a factor of 2 to 3 (see last column of Table VI). This result gives a

TABLE V. Single-particle mass quadrupole moments $q_{k_a}(j_a)$ [see Eq. (18)] of the states $|j_ak_a\rangle$ in units of $\alpha^2(j_a)=\hbar/M\omega=0.0101A^{1/3}$ b.

k_a	$j_a=\frac{9}{2}$	$j_a=\frac{11}{2}$	$j_a=\frac{13}{2}$	$j_a=\frac{15}{2}$
$\frac{1}{2}$	$\frac{24}{9}$	$\frac{35}{11}$	$\frac{48}{13}$	$\frac{63}{15}$
$\frac{3}{2}$	$\frac{18}{9}$	$\frac{29}{11}$	$\frac{42}{13}$	$\frac{57}{15}$
$\frac{5}{2}$	$\frac{6}{9}$	$\frac{17}{11}$	$\frac{30}{13}$	$\frac{45}{15}$
$\frac{7}{2}$	$-\frac{12}{9}$	$-\frac{1}{11}$	$\frac{12}{13}$	$\frac{27}{15}$
$\frac{9}{2}$	-4	$-\frac{25}{11}$	$-\frac{12}{13}$	$\frac{3}{15}$
$\frac{11}{2}$	...	-5	$-\frac{42}{13}$	$-\frac{27}{15}$
$\frac{13}{2}$	...	...	-6	$-\frac{63}{15}$
$\frac{15}{2}$	...	...	...	-7

TABLE VI. Total mass quadrupole moments Q_0 (see Sec. II F 1) of the prolate $\mathcal{IS}$'s of the number N_a of particles in the a states with the listed j_a values. The ratios of the quadrupole moments given in the last column are in units of $\alpha^2(\lambda)/\alpha^2(j_a)$.

N_a	j_a	$Q_0(j_a,N_a)$ $[\alpha^2(j_a)]$	$Q_0[\lambda_{eq},0]$ $[\alpha^2(\lambda)]$	$\frac{Q_0[\lambda_{eq},0]}{Q_0(j_a,N_a)}$
2	$\frac{9}{2}$	5.33	16	3
	$\frac{11}{2}$	6.36	20	3.14
	$\frac{13}{2}$	7.38	24	3.25
	$\frac{15}{2}$	8.40	28	3.33
4	$\frac{9}{2}$	9.33	24	2.57
	$\frac{11}{2}$	11.64	32	2.75
	$\frac{13}{2}$	13.85	40	2.89
	$\frac{15}{2}$	16	48	3
6	$\frac{9}{2}$	10.67	24	2.25
	$\frac{11}{2}$	14.73	36	2.44
	$\frac{13}{2}$	18.46	48	2.60
	$\frac{15}{2}$	22	60	2.73
8	$\frac{9}{2}$	8	16	2
	$\frac{11}{2}$	14.55	32	2.20
	$\frac{13}{2}$	20.31	48	2.36
	$\frac{15}{2}$	25.60	64	2.50
10	$\frac{11}{2}$	10	20	2
	$\frac{13}{2}$	18.46	40	2.17
	$\frac{15}{2}$	26.13	60	2.30
12	$\frac{13}{2}$	12	24	2
	$\frac{15}{2}$	22.40	48	2.14
14	$\frac{15}{2}$	14	28	2

quantitative measure to the qualitative conclusion arrived at in Sec. II D from a comparison of the P_1 distributions.

2. Variation of $Q_0(j_a,N_a)$ with J_{max}

For N_a particles in the state $|j_a\rangle$, the maximum J contained in the $\mathcal{IS}$ $\mathcal{F}_K(j_a,N_a)$ is given by Eq. (8). The same $J_{\max}$ is obtained for N_a particles and for N_a holes [or $(2j_a+1-N_a)$ particles]. For prolate $\mathcal{IS}$'s, the variation of $Q_0(j_a,N_a)$ with $J_{\max}$ is shown in Fig. 5(a) for $j_a=\frac{9}{2},\frac{11}{2},\frac{13}{2}$, and $\frac{15}{2}$. While $Q_0(j_a,N_a)$ does increase with $J_{\max}$, the relation between the two quantities is not strictly linear as it is for the corresponding quantities in the equivalent SU(3) model. Instead, we have four nested loops in the $\mathcal{IS}$ $\mathcal{F}_K(j_a,N_a)$ case. [The loop becomes a straight line in the

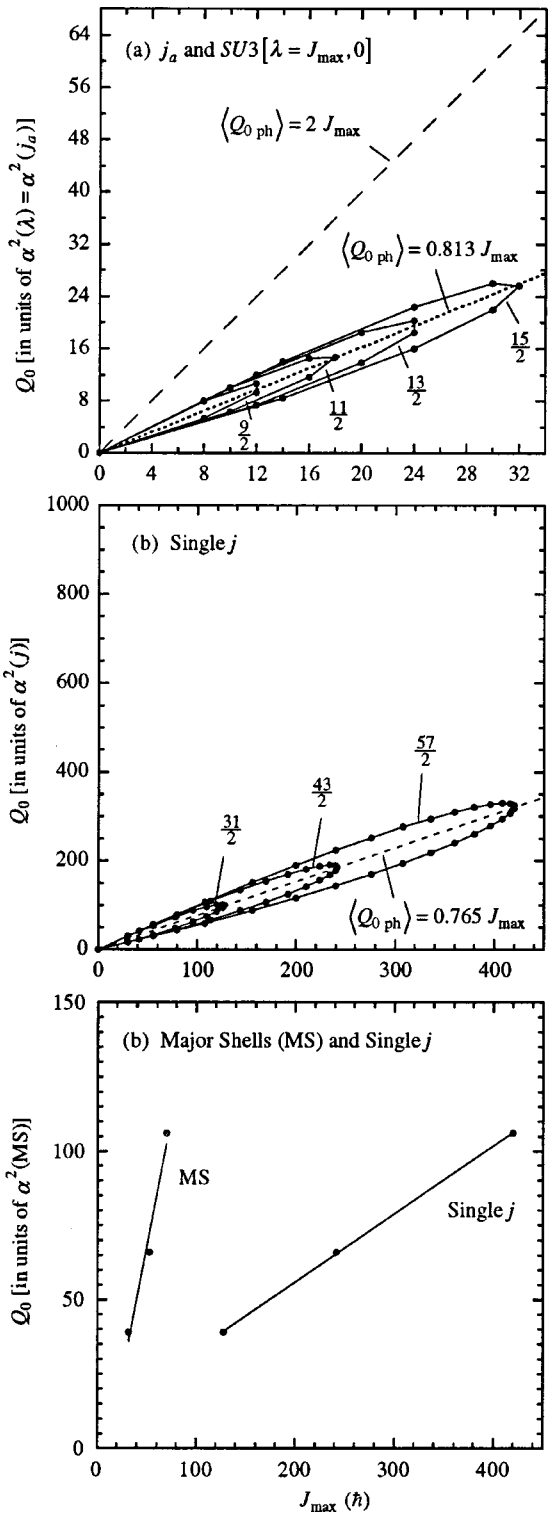

FIG. 5. Mass quadrupole moments Q_0 (in appropriate α^2 units) as a function of $J_{\max}$ for different $\mathcal{IS}$'s. See related discussion in Secs. II F and III. (a) The four loops correspond to $\mathcal{F}_K(j_a,N_a)$ for four different values of j_a and the dashed curve to the SU(3) $\mathcal{IS}$ (see Sec. II F 2). (b) The three loops correspond to $\mathcal{F}_K(j,N)$ for three different values of j (see Sec. III). (c) The Q_0 values at midshell for the 50–82, 82–126, and 126–184 major shells (MS) are compared with the Q_0 values at midshell for the $j=\frac{31}{2}$, $\frac{43}{2}$, $\frac{57}{2}$ (single-j) shells (see Sec. III).

TABLE VII. Single-j simulation of the intrinsic mass quadrupole moment in three major shells. The listed quantities are explained in Sec. III.

Shell	N	N_n	N_a	Model Q_0	Q_0(norm)	$J_{\max}$	$\left[\frac{Q_0(\text{norm})}{J_{\max}}\right]$ [a]
50–82	16	10	6	$39\alpha^2$(MS)	$39\alpha^2$(MS)	32	1.22
$j=\frac{31}{2}$	16			$102\alpha^2(j)$	$39\alpha^2$(MS)	128	0.30
82–126	22	14	8	$66\alpha^2$(MS)	$66\alpha^2$(MS)	50	1.32
$j=\frac{43}{2}$	22			$190\alpha^2(j)$	$66\alpha^2$(MS)	242	0.27
126–184	30	20	10	$106\alpha^2$(MS)	$106\alpha^2$(MS)	70	1.51
$j=\frac{57}{2}$	30			$330\alpha^2(j)$	$106\alpha^2$(MS)	420	0.25

[a] In units of $\alpha^2(\text{MS})/\hbar$.

SU(3) case because $J_{\max}(=\lambda)$ has the same value for $\mathcal{IS}$'s with a particular number of particles and the same number of holes and $Q_0=2\lambda=2J_{\max}$.]

In the $\mathcal{F}_K(j_a,N_a)$ case, for a given $J_{\max}$, there are two values of Q_0. The smaller value $Q_{0\ \text{particle}}^{N_a}$ corresponds to N_a particles, and the larger value $Q_{0\ \text{hole}}^{N_a}$ corresponds to N_a holes. We find that for each j_a, the average of these two values

$$\langle Q_{0\ \text{ph}}^{N_a}\rangle=\frac{Q_{0\ \text{particle}}^{N_a}+Q_{0\ \text{hole}}^{N_a}}{2} \tag{21}$$

varies linearly with $J_{\max}$. We can write

$$\langle Q_{0\ \text{ph}}^{N_a}\rangle=b(j_a)J_{\max}. \tag{22}$$

The coefficient $b(j_a)$ is independent of N_a, and its value can be determined easily from the value of $\langle Q_{0\ \text{ph}}^{N_a}\rangle$ for $N_a=2$ particles. In a two-particle prolate $\mathcal{IS}$, the particles occupy the $k=\pm\frac{1}{2}$ orbits with a total quadrupole moment $Q_{0\ \text{particle}}^{N_a=2}=2q_{1/2}(j_a)$. In a two-hole $\mathcal{IS}$, the holes occupy the $k=j_a$ orbits with a total moment $Q_{0\ \text{hole}}^{N_a=2}=-2q_{j_a}(j_a)$. The average of these two moments is then given by

$$\langle Q_{0\text{ph}}^{N_a=2}\rangle=q_{1/2}(j_a)-q_{j_a}(j_a). \tag{23}$$

Using Eqs. (18)–(20), we obtain

$$q_{1/2}(j_a)=2\left(j_a 2\frac{1}{2}0\middle|j_a\frac{1}{2}\right)^2(j_a+1) \tag{24}$$

and

$$q_{j_a}(j_a)=-\left(j_a-\frac{1}{2}\right). \tag{25}$$

The algebraic expression for the Clebsch-Gordan coefficients $(j_a 2\frac{1}{2}0|j_a\frac{1}{2})$ given in Table 3 of Ref. [24] can be used to write

$$q_{1/2}(j_a)=\frac{2\left[\frac{3}{4}-j_a(j_a+1)\right]^2}{j_a(2j_a+3)(2j_a-1)}. \tag{26}$$

For two particles, the slope $b(j_a)$ is obtained from $b(j_a)=\langle Q_{0\ \text{ph}}^{N_a=2}\rangle/J_{\max}$, where $J_{\max}=2j_a-1$. It follows that

$$b(j_a)=\frac{[4j_a(j_a+1)-3]^2}{8j_a(2j_a+3)(2j_a-1)^2}+\frac{1}{2}. \tag{27}$$

The function $b(j_a)$ varies slowly with j_a, and the numerical values of $b(j_a)$ range from 1 for $j_a=\frac{3}{2}$ to 0.75 for $j_a\to\infty$. For the $0g_{9/2}$, $0h_{11/2}$, $0i_{13/2}$, and $0j_{15/2}$ states, Eq. (27) gives $b(j_a)=\frac{5}{6}$, $\frac{9}{11}$, $\frac{21}{26}$, and $\frac{4}{5}$, respectively. These values are all close to 0.8. Consequently, we find that the $\langle Q_{0\ \text{ph}}\rangle$ values for the $\mathcal{F}_K(j_a,N_a)$ $\mathcal{IS}$'s of the above four $|j_a\rangle$ states are related to a very good approximation to the $J_{\max}$ values by $\langle Q_{0\ \text{ph}}\rangle\approx b^{\text{ave}}J_{\max}$. Here, $b^{\text{ave}}=\frac{1}{16}[3b(\frac{9}{2})+4b(\frac{11}{2})+4b(\frac{13}{2})+5b(\frac{15}{2})]$ is the average of the $b(j_a)$ values weighted by the number of different even values of N_a for each j_a. For example, for the $0h_{11/2}$ state, there are four values of $N_a(N_a=0,2,4,\text{and }6)$. Therefore, while calculating b^{ave}, the value of $b(\frac{11}{2})$ is weighted by a factor of 4. Similarly the weights for the $0g_{9/2}$, $0i_{13/2}$, and $0j_{15/2}$ states are 3, 4, and 5, respectively. With these weights and the numerical values for $b(j_a)$, we find $b^{\text{ave}}=\frac{3719}{4576}=0.813$ as the average slope of the $\langle Q_{0\text{ph}}\rangle$ values vs $J_{\max}$ for the $j_a=\frac{9}{2}$, $\frac{11}{2}$, $\frac{13}{2}$, and $\frac{15}{2}$ states. This line is also shown in Fig. 5(a). By comparing this line with the $Q_0[\lambda,0]=2J_{\max}$ line, we conclude that for a given value of $J_{\max}$ (of the $\mathcal{IS}$), the mass quadrupole moment $Q_0(j_a,N_a)$ is smaller than the equivalent SU(3) value by a factor of about 2.5. Conversely, for a given value of $Q_0(j_a,N_a)$, the $\mathcal{IS}$ of N particles in state $|j_a\rangle$ has a $J_{\max}$ value, which is about 2.5 times larger than that of a similarly deformed SU(3) $\mathcal{IS}$.

III. SINGLE-j SIMULATION OF MAJOR SHELLS

Different aspects of the quadrupole collectivity of heavy nuclei have been studied by Otsuka, Arima, and Iachello [25]

and by Bohr and Mottelson [26] in terms of collective states of nucleons in j^N configurations with large j values (Otsuka *et al.* used $j=\frac{23}{2}$ and $\frac{29}{2}$). In a similar spirit, we wish to simulate the quadrupole moments $Q_0(\mathrm{MS},N)$ of N identical valence particles in the $\mathcal{IS}$'s of the 50–82, 82–126, and 126–184 major shells (MS's) by the quadrupole moments $Q_0(j,N)$ of the same number of particles in the $\mathcal{IS}$'s of single-j shells with $j=\frac{31}{2}$, $\frac{43}{2}$, and $\frac{57}{2}$, respectively, having degeneracies equal to those of the corresponding major shells. Our aim here is to compare the quadrupole collectivities for corresponding $\mathcal{IS}$'s given by these two models.

One aspect of the quadrupole collectivity of an $\mathcal{IS}$ can be quantitatively specified by the ratio $Q_0(\mathrm{model})/J_{\max}$. We wish to emphasize again that the quadrupole moment Q_0 is made up of two parts: a quantity that depends on the structure of the $\mathcal{IS}$ and a unit that depends on the size of the wave functions used in the calculations. If a harmonic oscillator is used to generate the wave functions, the unit is the oscillator size parameter α defined by $\alpha^2=\hbar/M\omega$, where ω is the oscillator frequency.

As an illustration of the single-j simulation, we considered the $\mathcal{IS}$'s for the half-filled major shells. The $Q_0(\mathrm{MS},N)$ values close to the midshell were obtained as follows: We used Table VIII of Ref. [3] to obtain the numbers N_n and N_a of particles occupying the n and a states when $N=16$, 22, and 30 particles are in the 50–82, 82–126, and 126–184 shells, respectively. For these N values and shells, the same table lists the appropriate SU(3) representations $[\lambda,\mu]$ which yield the $J_{n\ \max}$ $(=\lambda+\mu)$ and Q_{0n} values. We then used Eq. (8) and Table VI of this paper to obtain the $J_{a\ \max}$ and Q_{0a} values for N_a particles in the state $|j_a\rangle$ appropriate for each major shell. With this information, we obtained $J_{\max}=J_{n\ \max}+J_{a\ \max}$ and $Q_0=Q_{0n}+Q_{0a}$. These Q_0 and $J_{\max}$ values are given in Table VII. For the 50–82 major shell, the quantity $Q_0(\mathrm{MS},N)$ is 39, and the unit is $\alpha^2(\mathrm{MS})$. The harmonic oscillator frequency ω is customarily adjusted to reproduce the observed nuclear mean-square radius; that is, $\hbar\omega\approx 40A^{-1/3}$ MeV. Using $Mc^2=939$ MeV, we obtain $\alpha^2(\mathrm{MS})=0.0101A^{1/3}$ b. The average midshell value of $Q_0(\mathrm{MS})/J_{\max}$ for the three major shells considered here is 1.35.

We now return to the simulation of the quadrupole moments in the 50–82, 82–126, and 126–184 major shells by those in the $j=\frac{31}{2}$, $\frac{43}{2}$, and $\frac{57}{2}$ shells, respectively. We consider these three j shells to be the highest j subshells in the harmonic oscillator shells with principle quantum numbers $\mathcal{N}=15$, 21, and 28, respectively, and with $j=\mathcal{N}+\frac{1}{2}$. We can therefore use Eqs. (16)–(18) to obtain the $Q_0(j,N)$ values for the different prolate $\mathcal{IS}$'s of the j^N configurations. These values are calculated in units of oscillator size parameter labeled as $\alpha^2(j)$ to distinguish this parameter from $\alpha^2(j_a)$ and $\alpha^2(\lambda_{\mathrm{eq}})$, used in Sec. II F, and from $\alpha^2(\mathrm{MS})$, used in the previous paragraph. For the $j=\frac{31}{2}$ shell, the model Q_0 value is $102\alpha^2(j)$ (see Table VII) for $N=16$. For each $\mathcal{IS}$, the $J_{\max}$ value is given by Eq. (8). In Fig. 5(b), we have plotted the nested loops of $Q_0(j,N)$ vs $J_{\max}$ for the three j cases. The particle-hole averaged values of these quadrupole moments fall on a straight line given by $\langle Q_0^{j,N}{}_{\mathrm{ph}}\rangle=0.765J_{\max}$. In Table VII we have listed the $Q_0(j,N)$ and $J_{\max}$ values for $N=16$, 22, and 30 particles in the $j=\frac{31}{2}$, $\frac{43}{2}$, and $\frac{57}{2}$ shells, respectively.

A successful simulation requires that the quadrupole moments given by the two models (single-j and MS) are similar for all numbers N of valence particles. To achieve this similarity, we know from previous work [1] that it is sufficient to normalize the quadrupole moments for an N value close to midshell. The remaining Q_0 values will then track well. Therefore, we want to set $Q_0(j,N)$ equal to $Q_0(\mathrm{MS},N)$ for $N=16$, 22, and 30. Referring to Table VII, $Q_0(j=\frac{31}{2},N=16)=102\alpha^2(j)$, and $Q_0(\mathrm{MS},N=16)=39\alpha^2(\mathrm{MS})$. The former value can be made equal to the latter by choosing $\alpha^2(j)=\frac{39}{102}\alpha^2(\mathrm{MS})$. In other words, the size of the harmonic oscillator wave functions used in the single-j simulation needs to be adjusted accordingly. The normalization factors are slightly different for the three different single-j shells considered here; the average normalization is $\alpha^2(j)\approx 0.35\alpha^2(\mathrm{MS})$. The normalized $Q_0(\mathrm{norm})$ values are given in column 6 of Table VII. This normalization, however, will in no way affect either the numerical quantities in Q_0 or the $J_{\max}$ values for different j shells.

We made Q_0 of $\mathcal{F}_K(j,N)$ equal to Q_0 of $\mathcal{F}_K(\mathrm{MS},N)$. However, the $J_{\max}$ in $\mathcal{F}_K(j,N)$ is different from the $J_{\max}$ in $\mathcal{F}_K(\mathrm{MS},N)$. Hence, the collectivities of $\mathcal{F}_K(j,N)$ and $\mathcal{F}_K(\mathrm{MS},N)$ will also be different. This situation should be contrasted with Sec. II F, in which we compared the collectivities of $\mathcal{F}_K(j_a,N_a)$ and $\mathcal{F}_K[\lambda_{\mathrm{eq}},0]$. In that case, the $J_{\max}$ values for both $\mathcal{IS}$'s were equal, but the Q_0 values were different.

The values of $Q_0(\mathrm{norm})/J_{\max}$ for the j^N and major-shell $\mathcal{IS}$'s are given in the last column of Table VII. The latter ratio is, on average, five times larger than the former. This result implies that in the j^N simulation, the quadrupole collectivity of the simulated major shell is underestimated by a factor of ~ 5. These differences in the collectivities of the two $\mathcal{IS}$'s are illustrated by the $Q_0(\mathrm{norm})$ vs $J_{\max}$ trends, which are shown in Fig. 5(c).

IV. PERTURBATIONS OF THE INTRINSIC STATE

The study of the properties of the $\mathcal{IS}$ $\mathcal{F}_K(j_a,N_a)$ and of the states with definite angular momenta projected from it would be useful only if the perturbations of this $\mathcal{IS}$ by the pairing interaction and by the $0\hbar\omega$-mixing component of the mean field are not very large. In this section, we examine the effects of these perturbations.

A. Effect of the pairing interaction

The pairing interaction within a major shell can modify $\mathcal{F}_K(j_a,N_a)$ [see Eqs. (9)–(11)] by scattering a pair of particles from an occupied single-particle a state $|j_a,\pm k_a\rangle$ to other unoccupied a states $|j_a,\pm k_a'\rangle$ or n states $|j_n,\pm k_n'\rangle$. We consider here scattering only among the a states. The modification of $\mathcal{F}_K(j_a,N_a)$ produced by the pairing interaction of strength G in a mean field of deformation β gives rise to the

correlated $\mathcal{IS}$ $\mathcal{F}^c_K(j_a,N_a;\beta,G)$. In the following, we shall also refer to the uncorrelated and correlated $\mathcal{IS}$'s as $\mathcal{F}_K$ and $\mathcal{F}^c_K$, respectively.

We calculate three quantities to illustrate the effect of pairing on $\mathcal{F}_K$.

(i) The first quantity is

$$P(\Delta\mathcal{F})=1-|\langle\mathcal{F}^c_K(j_a,N_a;\beta,G)|\mathcal{F}_K(j_a,N_a)\rangle|^2, \quad (28)$$

where $P(\Delta\mathcal{F})$ is the probability of *change* in the $\mathcal{F}_K$ induced by the pairing interaction. If the effect of pairing is large, $\mathcal{F}^c_K$ will be very different from $\mathcal{F}_K$, and $P(\Delta\mathcal{F})$ will be large.

(ii) In the absence of deformation ($\beta=0$), the lowest-energy state of the $j_a^{N_a}$ configuration generated by the pairing interaction is the completely correlated state $|j_a^{N_a};v=0\rangle$ with seniority $v=0$ (and, hence, $J=0$) for any nonzero value of the pairing strength G. In the absence of pairing ($G=0$), the uncorrelated $\mathcal{IS}$ $\mathcal{F}_K$ has some probability

$$P(v=0)=|\langle j_a^{N_a};v=0|\mathcal{F}_K(j_a,N_a)\rangle|^2 \quad (29)$$

of containing the state $|j_a^{N_a};v=0\rangle$. When pairing is present ($G>0$), the correlated $\mathcal{IS}$ $\mathcal{F}^c_K$ has the probability

$$P_c(v=0)=|\langle j_a^{N_a};v=0|\mathcal{F}^c_K(j_a,N_a;\beta,G)\rangle|^2 \quad (30)$$

of containing the $v=0$ state. One expects $P_c(v=0)$ to be greater than $P(v=0)$. As a second measure of the influence of the pairing interaction on $\mathcal{F}_K$, we calculate the increase

$$\Delta P(v=0)=P_c(v=0)-P(v=0) \quad (31)$$

in the probability of the $v=0$ state in $\mathcal{F}^c_K$ compared with that in $\mathcal{F}_K$. The $\Delta P(v=0)$ value will depend on the values of both β and G.

(iii) In view of the tendency of the pairing interaction to make the nucleus spherical, the quadrupole moment of $\mathcal{F}^c_K$,

$$Q_c=\langle\mathcal{F}^c_K(j_a,N_a;\beta,G)|Q_0^2|\mathcal{F}^c_K(j_a,N_a;\beta,G)\rangle, \quad (32)$$

is expected to be smaller than the quadrupole moment of $\mathcal{F}_K$,

$$Q=\langle\mathcal{F}_K(j_a,N_a)|Q_0^2|\mathcal{F}_K(j_a,N_a)\rangle. \quad (33)$$

The difference

$$\Delta Q=Q_c-Q \quad (34)$$

is taken as the third measure of the influence of pairing on $\mathcal{F}_K$. Note that Q_c tends to zero for $\beta>0$ if G becomes large and $Q_c=0$ at $\beta=0$ for any $G>0$.

We now describe how the quantities $P(\Delta\mathcal{F})$, $\Delta P(v=0)$, and ΔQ are calculated for the state $\mathcal{F}_K$ with two values of j_a ($\frac{11}{2}$ and $\frac{13}{2}$) and three values of N_a (2, 4, and 6 particles). The Hamiltonian for N_a particles in a mean field with deformation β can be written as

$$\mathcal{H}(\beta,G)=h(\beta)+H_{\rm pair}(G). \quad (35)$$

TABLE VIII. Single-particle eigenvalues $\epsilon(j_a,k_\alpha;\beta)$ (in MeV relative to the energy of the $k_\alpha=\frac{1}{2}$ state) obtained from the Nilsson-model calculations [see Eq. (37)].

	$\lvert j_a\rangle=0h_{11/2}$ state		$\lvert j_a\rangle=0i_{13/2}$ state	
k_α	$\beta=0.21$	$\beta=0.32$	$\beta=0.21$	$\beta=0.32$
$\frac{1}{2}$	0	0	0	0
$\frac{3}{2}$	0.27	0.41	0.23	0.35
$\frac{5}{2}$	0.82	1.24	0.70	1.05
$\frac{7}{2}$	1.65	2.47	1.39	2.09
$\frac{9}{2}$	2.75	4.12	2.37	3.49
$\frac{11}{2}$	4.12	6.18	3.44	5.23
$\frac{13}{2}$			4.38	7.32

Here,

$$h(\beta)=\sum_{i=1}^{N_a} h_i(\beta) \quad (36)$$

is the one-body Hamiltonian characterizing the mean field. The intruder single-particle states $|j_a,k\rangle$ are the eigenstates of $h(\beta)$ in the space of *one major shell*, with eigenvalues $\epsilon(j_a,k;\beta)$. Thus

$$h(\beta)|j_a,k\rangle=\epsilon(j_a,k;\beta)|j_a,k\rangle. \quad (37)$$

We calculated the eigenvalues for the $|\frac{11}{2},k\rangle$ and $|\frac{13}{2},k\rangle$ states at both $\beta=0.21$ and 0.32, with $h(\beta)$ taken to be the Nilsson Hamiltonian. The Hamiltonian parameters [27] are $\hbar\omega_0=7.55$ MeV, $\kappa=0.05$, and $\mu=0.63$, respectively, which are all appropriate for the rare-earth region. The single-particle eigenvalues $\epsilon(j_a,k;\beta)$ are listed in Table VIII. The prolate $\mathcal{IS}$ $\mathcal{F}_K$ is obtained by sequentially occupying the states $|j_a,\pm k\rangle$ with $k=\frac{1}{2}$, $\frac{3}{2}$, $\frac{5}{2}$, etc.

The pairing Hamiltonian $H_{\rm pair}(G)$ of Eq. (35) is specified by the two-body matrix elements

$$\langle j_a k';j_a-k'|H_{\rm pair}|j_a k;j_a-k\rangle=-G. \quad (38)$$

The usual value of the pairing strength G is 0.12 MeV for rare-earth nuclei [14].

The three $\mathcal{IS}$'s (a) $\mathcal{F}_K(j_a,N_a)$, (b) $|j_a^{N_a};v=0\rangle$, and (c) $\mathcal{F}^c_K(j_a,N_a;\beta,G)$ are, respectively, the lowest-energy eigenstates of $\mathcal{H}(\beta,G)$ with the presence of (a) no pairing (that is, $G=0$), (b) no deformation ($\beta=0$), and (c) both pairing and deformation ($G\neq0,\beta\neq0$).

The state $\mathcal{F}^c_K$ is obtained by diagonalizing $\mathcal{H}(\beta,G)$ in the space of the basis states consisting of a complete set of determinantal eigenstates $\Phi_\alpha(j_a,N_a)$ of $h(\beta)$ with eigenvalues $E(\alpha,\beta;j_a,N_a)$. These states can be coupled by the pairing interaction. The structure of the basis states $\Phi_\alpha(j_a,N_a)$ is described below.

(i) For $N_a=2$ particles, the basis states are

$$\Phi_\alpha(j_a,N_a=2)=|j_a;k_\alpha,-k_\alpha| \quad (39)$$

TABLE IX. Expansion coefficients $A_\alpha(\beta,G)$ and B_α [see Eqs. (49) and (50)] for the states $\mathcal{F}_K^c(j_a,N_a)$, $\mathcal{F}_K^c(j_a,N_a)$, and $\mathcal{F}_K^{cc}(j_a,N_a)$ for $N_a=2$ and $j_a=\frac{11}{2}$ and $\frac{13}{2}$. For $\beta\neq 0$, $G=0.12$ MeV and for $\beta=0$, the coefficients B_α are independent of the values of G.

		Two particles in the $0h_{11/2}$ orbit				Two particles in the $0i_{13/2}$ orbit			
		$\mathcal{F}_K$	$\mathcal{F}_K^c$	$\mathcal{F}_K^c$	$\mathcal{F}_K^{cc}$	$\mathcal{F}_K$	$\mathcal{F}_K^c$	$\mathcal{F}_K^c$	$\mathcal{F}_K^{cc}$
		A	A	A	B	A	A	A	B
		$G=0$	$G=0.12$	$G=0.12$	$\beta=0$, $G>0$ or	$G=0$	$G=0.12$	$G=0.12$	$\beta=0$, $G>0$ or
α	k_α	$\beta>0$	$\beta=0.21$	$\beta=0.32$	$\beta\neq 0$, $G\to\infty$	$\beta>0$	$\beta=0.21$	$\beta=0.32$	$\beta\neq 0$, $G\to\infty$
0	$\frac{1}{2}$	1	0.967	0.986	0.408	1	0.953	0.979	0.378
1	$\frac{3}{2}$	0	0.231	0.154	0.408	0	0.272	0.184	0.378
2	$\frac{5}{2}$	0	0.091	0.057	0.408	0	0.112	0.070	0.378
3	$\frac{7}{2}$	0	0.042	0.030	0.408	0	0.060	0.036	0.378
4	$\frac{9}{2}$	0	0.029	0.018	0.408	0	0.037	0.022	0.378
5	$\frac{11}{2}$	0	0.020	0.012	0.408	0	0.025	0.015	0.378
6	$\frac{13}{2}$	0			0.408	0	0.018	0.011	0.378

with unperturbed eigenvalues

$$E(\alpha,\beta;j_a,N_a=2)=2\epsilon(j_a,k_\alpha;\beta). \tag{40}$$

The index $\alpha=0,1,2,\ldots j_a-\frac{1}{2}$ and $k_\alpha=\alpha+\frac{1}{2}$. The number of such basis states are $\mathcal{N}^\alpha=6$ and 7 for the $(0h_{11/2})^2$ and $(0i_{13/2})^2$ states, respectively.

(ii) For $N_a=4$ particles, we need two labels α_1 and α_2 to specify the four-particle determinants

$$\Phi_\alpha(j_a,N_a=4)\equiv\Phi_{\alpha_1,\alpha_2}(j_a,N_a=4) =|j_a;k_{\alpha_1},-k_{\alpha_1};k_{\alpha_2},-k_{\alpha_2}|, \tag{41}$$

where $k_i=\alpha_i+\frac{1}{2}$, $\alpha_i=0,1,2,\ldots,j_a-\frac{1}{2}$, and $\alpha_2>\alpha_1$. The unperturbed eigenvalues are

$$E(\alpha_1,\alpha_2,\beta;j_a,N_a=4)=2[\epsilon(j_a,k_{\alpha_1};\beta)+\epsilon(j_a,k_{\alpha_2};\beta)]. \tag{42}$$

The number of such basis states are $\mathcal{N}^\alpha=15$ and 21 for the $(0h_{11/2})^4$ and $(0i_{13/2})^4$ states, respectively.

(iii) For $N_a=6$ particles, three labels α_1, α_2, and α_3 are required to specify the basis states

$$\Phi_\alpha(j_a,N_a=6)\equiv\Phi_{\alpha_1,\alpha_2,\alpha_3}(j_a,N_a=6) =|j_a;k_{\alpha_1},-k_{\alpha_1};k_{\alpha_2},-k_{\alpha_2};k_{\alpha_3},-k_{\alpha_3}|. \tag{43}$$

In this case, $\alpha_i=0,1,2,\ldots,j_a-\frac{1}{2}$ for $i=1,2,3$ and $\alpha_3>\alpha_2>\alpha_1$. The unperturbed eigenvalues are

$$E(\alpha_1,\alpha_2,\alpha_3,\beta;j_a,N_a=6) =2[\epsilon(j_a,k_{\alpha_1};\beta)+\epsilon(j_a,k_{\alpha_2};\beta)+\epsilon(j_a,k_{\alpha_3};\beta)]. \tag{44}$$

For the $(0h_{11/2})^6$ and $(0i_{13/2})^6$ states, $\mathcal{N}^\alpha=20$ and 25, respectively.

For all the basis states $\Phi_\alpha(j_a,N_a)$, the lowest state $\Phi_{\alpha=0}(j_a,N_a)$ is the state $\mathcal{F}_K$. With these basis states, the Hamiltonian matrices

$$\mathcal{H}_{\alpha',\alpha}(\beta,G)=\langle\Phi_{\alpha'}(j_a,N_a)|\mathcal{H}(\beta,G)|\Phi_\alpha(j_a,N_a)\rangle \tag{45}$$

are given by

(i) For $N_a=2$ particles,

$$\mathcal{H}_{\alpha',\alpha}(\beta,G)=E(\alpha,\beta;j_a,N_a=2)\delta_{\alpha'\alpha}-G. \tag{46}$$

(ii) For $N_a=4$ particles,

$$\mathcal{H}_{\alpha',\alpha}(\beta,G)=E(\alpha_1,\alpha_2,\beta;j_a,N_a=4)\delta_{\alpha_1'\alpha_1}\delta_{\alpha_2'\alpha_2} -[\delta_{\alpha_1'\alpha_1}+\delta_{\alpha_2'\alpha_2}]G. \tag{47}$$

(iii) For $N_a=6$ particles,

$$\mathcal{H}_{\alpha',\alpha}(\beta,G)=E(\alpha_1,\alpha_2,\alpha_3,\beta;j_a,N_a=6) \times\delta_{\alpha_1'\alpha_1}\delta_{\alpha_2'\alpha_2}\delta_{\alpha_3'\alpha_3} +\langle\Phi_{\alpha_1',\alpha_2',\alpha_3'}|H_{\text{pair}}|\Phi_{\alpha_1,\alpha_2,\alpha_3}\rangle. \tag{48}$$

In the $N_a=6$ case, the pairing matrix element is zero unless at least two of the α' labels are equal to two of the α labels. The nonzero, off-diagonal matrix elements are all equal to $-G$, and the diagonal pairing matrix elements are equal to $-3G$.

We diagonalized the matrices $\mathcal{H}_{\alpha',\alpha}(\beta,G)$ of Eqs. (46)–(48) and determined the lowest-energy eigenstates, which are the states $\mathcal{F}_K^c(j_a,N_a;\beta,G)$ obtained as linear combinations of the basis states Φ_α. Thus

$$\mathcal{F}_K^c(j_a,N_a;\beta,G)=\sum_\alpha A_\alpha(\beta,G)\Phi_\alpha(j_a,N_a). \tag{49}$$

To illustrate the calculation, we consider the effect of pairing on the $\mathcal{IS}$ $\mathcal{F}_K$ of two particles with $j_a=\frac{11}{2}$ and $\frac{13}{2}$. The ex-

TABLE X. Calculated values of three quantities, $P(\Delta\mathcal{F})$ [Eq. (51)], $\Delta P(v=0)$ [Eq. (54)], and $\Delta Q = Q_c - Q$ [Eqs. (55) and (56c)] that illustrate the effect of pairing on the $\mathcal{IS}$ $\mathcal{F}_K$.

N_a	j_a	β	$P(\Delta\mathcal{F})$	$P_c(v=0)$	$P(v=0)$	$\Delta P(v=0)$	Q	Q_c	ΔQ
2	$\frac{11}{2}$	0.21	0.065	0.320	0.167	0.153	6.36	6.24	−0.12
	$\frac{11}{2}$	0.32	0.028	0.263	0.167	0.096	6.36	6.32	−0.04
6	$\frac{13}{2}$	0.21	0.023	0.061	0.029	0.032	18.46	18.34	−0.12
	$\frac{13}{2}$	0.32	0.009	0.047	0.029	0.018	18.46	18.41	−0.05

pansion coefficients for $\mathcal{F}_K$ are listed in columns 3 and 7 of Table IX. These coefficients are independent of β. The coefficients $A_\alpha(\beta,G)$ for the correlated $\mathcal{IS}$ $\mathcal{F}_K^c$, obtained with the normal value of $G=0.12$ MeV for the pairing strength, are listed in columns 4 and 5 of Table IX for the $(\frac{11}{2})^2$ state and in columns 8 and 9 for the $(\frac{13}{2})^2$ state]. For both cases, the coefficients A_0 are greater than 0.95, implying that these correlated states $\mathcal{F}_K^c$ are very similar to the uncorrelated states $\mathcal{F}_K$. The change in $\mathcal{F}_K$ produced by the pairing interaction of normal strength is small.

We now define the completely correlated $\mathcal{IS}$ $\mathcal{F}_K^{cc}$ to be the state produced by the Hamiltonian when the pairing interaction dominates the effect of deformation as would happen under two circumstances: (i) $\beta=0$, any $G>0$, and (ii) $\beta>0$, $G\to\infty$. Under these conditions, the state $\mathcal{F}_K^{cc}$ is just the seniority $v=0$ state of the $j_a^{N_a}$ configuration. The structure of $\mathcal{F}_K^{cc}$ is given by

$$\mathcal{F}_K^{cc}(j_a,N_a)\equiv|j_a^{N_a};v=0\rangle=\sum_\alpha B_\alpha\Phi_\alpha(j_a,N_a), \quad (50)$$

where the coefficients are all equal and given by $B_\alpha=1/\sqrt{N^\alpha}$. The values of B_α for the $(\frac{11}{2})^2$ and $(\frac{13}{2})^2$ states are given in columns 6 and 10, respectively, of Table IX. Note that for a normal pairing strength, $\mathcal{F}_K^{cc}$ is significantly different from $\mathcal{F}_K^c$ even at $\beta=0.21$.

With the aid of Eqs. (49) and (50), we can calculate the probabilities $P(\Delta\mathcal{F})$, $P_c(v=0)$, and $P(v=0)$. They are given by

$$P(\Delta\mathcal{F})=1-|A_\alpha(\beta,G)|^2, \quad (51)$$

$$P_c(v=0)=\left|\sum_\alpha A_\alpha(\beta,G)B_\alpha\right|^2=\frac{1}{N^\alpha}\left|\sum_\alpha A_\alpha(\beta,G)\right|^2, \quad (52)$$

and

$$P(v=0)=|B_\alpha|^2=1/N^\alpha. \quad (53)$$

The increase ΔP [see Eq. (31)] is given by

$$\Delta P(v=0)=\frac{1}{N^\alpha}\left[\left|\sum_\alpha A_\alpha(\beta,G)\right|^2-1\right]. \quad (54)$$

The numerical values [using the values of $A_\alpha(\beta,G)$ and B_α coefficients listed in Table IX] are given in Table X. The results show the following: (i) Pairing interaction [see the $P(\Delta\mathcal{F})$ column] changes the $\mathcal{IS}$ of a nucleons by less than 7% in well-deformed nuclei. (ii) While the increase in the $v=0$ component [see the $\Delta P(v=0)$ column] of the $\mathcal{IS}$ produced by the pairing interaction is about 15% at $\beta=0.21$ for the $(\frac{11}{2})^2$ state, it reduces to only 3% for the $(\frac{13}{2})^6$ state. The smallness of these changes casts doubt on the validity of the simplifying assumption made in the pseudo-SU(3) [12,28,29] and fermion dynamic symmetry [17] models that the pairing interaction causes the a nucleons in spherical as well as deformed nuclei to couple to a seniority-zero state. Our calculations indicate that a pairing strength that is at least ten times stronger than the normal $G=0.12$ MeV is required to change the $\mathcal{IS}$ at $\beta>0.2$ sufficiently such that its overlap with the $v=0$ state is >0.95.

Finally, the quadrupole moments Q_c and Q are given by

$$Q_c=2\sum_\alpha |A_\alpha(\beta,G)|^2 q_{k_\alpha} \quad (55)$$

and

$$Q=2q_{k=1/2} \quad \text{for} \quad N_a=2, \quad (56a)$$

$$Q=2(q_{k=1/2}+q_{k=3/2}) \quad \text{for} \quad N_a=4, \quad (56b)$$

$$Q=2(q_{k=1/2}+q_{k=3/2}+q_{k=5/2}) \quad \text{for} \quad N_a=6. \quad (56c)$$

The values of the single-particle quadrupole moments q_k for the $0h_{11/2}$ and $0i_{13/2}$ states are listed in Table V. The values of Q, Q_c, and $\Delta Q=Q_c-Q$ are listed in the last three columns of Table X. The change in the quadrupole moment of $\mathcal{F}_K$ induced by the pairing interaction of normal strength is also negligibly small.

B. Effect of $0\hbar\omega$ mixing

The quadrupole collective states of heavy nuclei are well described in terms of shell models in which the nucleons are confined to single-particle states ψ_{jk} in a major shell (MS). The deformation of the nucleus mixes the n spherical states $\psi_{j_nk_n}$ to produce the deformed single-particle states $\phi_{k_n}^{\alpha_n}$, where α_n labels different n states with the same value of $k_n=\langle j'_{nz}\rangle$. The a orbitals $\psi_{j_ak_a}$ are not mixed by the quadrupole deformation with the n orbitals of a given major shell because they have opposite parities. Hence, in this descrip-

TABLE XI. The probabilities $P_k^\alpha(\delta)$ [see Eq. (61)] that a major shell abnormal-parity deformed orbit $\phi_k^\alpha(\mathrm{MS},\delta)$ is not modified by $0\hbar\omega$ mixing caused by deformation. Only probabilities less than 0.90 are listed. The Nilsson Hamiltonian parameters used in these calculations are $\mu=0.630$ for the 50–82 major shell and $\mu=0.448$ for the 82–126 major shell. The parameter χ is kept at a value of 0.05 throughout.

Type of orbit	α	k	Probability $P_k^\alpha(\delta)$ $\delta=0.20$	$\delta=0.30$	$\delta=0.35$	Probability $P_k^\alpha(\delta)$ $\delta=0.20$	$\delta=0.30$	$\delta=0.35$
			(a) 50–82 major shell (protons)			(a) 50–82 major shell (neutrons)		
a	1	$\frac{1}{2}$	0.89	0.76	0.70	0.82	0.65	0.57
a	1	$\frac{3}{2}$		0.83	0.79	0.87	0.67	0.72
a	1	$\frac{5}{2}$		0.90	0.88		0.87	0.85
			(c) 82–126 major shell (protons)			(c) 82–126 major shell (neutrons)		
a	1	$\frac{1}{2}$		0.79	0.73	0.84	0.67	0.59
a	1	$\frac{3}{2}$		0.83	0.79	0.87	0.76	0.70
a	1	$\frac{5}{2}$		0.89	0.86		0.84	0.81
a	1	$\frac{7}{2}$						0.90

tion of the deformed nucleus, the deformed a states $\phi_{k_a}^{\alpha_a}$ are the unmixed states $\phi_{k_a}^{\alpha_a}\equiv\psi_{j_a k_a}$.

The quadrupole deformation can, to a first approximation, affect the structure of the deformed orbitals of a major shell in the following two ways by a process known as $0\hbar\omega$ mixing. (i) It can modify the n orbitals by mixing them with the a state belonging to the lower major shell. Such an a state belongs to the same harmonic oscillator shell (OS) as the n states of the major shell under consideration. (ii) It can also modify the a orbitals of a major shell by mixing them with the n orbitals belonging to the next higher major shell. In this section, we make a quantitative estimate of the modification of the a orbits within a major shell produced by the latter mixing. This estimate is obtained by comparing the orbitals $\phi_k^\alpha(\mathrm{MS},\delta)$ at a deformation δ obtained within a single major shell space with the corresponding orbitals $\phi_k^\alpha(\mathrm{OS},\delta)$ obtained within the space of a single harmonic-oscillator shell $\mathcal{N}$. The latter orbitals contain the modification to the $\phi_k^\alpha(\mathrm{MS})$ orbitals resulting from the $0\hbar\omega$ mixing induced by the deformation.

The orbitals $\phi_k^\alpha(\mathrm{MS},\delta)$ are obtained by diagonalizing the Nilsson Hamiltonian

$$\mathcal{H}_{\mathrm{Nilsson}}=\hbar\omega_0\left[\frac{1}{2}(-\nabla^2+\rho^2)-\frac{4}{3}\sqrt{\frac{\pi}{5}}\delta\rho^2Y_{20}(\theta,\phi)-2\kappa\bar{l}\cdot\bar{s}-\mu\kappa\bar{l}\cdot\bar{l}\right] \tag{57}$$

in the space of the single-particle states of a major shell for different values of the deformation parameter δ. The strengths κ and μ for the spin-orbit and l^2 interactions are taken from Ref. [27] for different shells. The orbitals $\phi_k^\alpha(\mathrm{MS},\delta)$ for the a states in the 50–82 major shell are just the states $\psi_{j_a=11/2,k}$ belonging to the $0h_{11/2}$ intruder level, independent of the deformation. The orbitals $\phi_k^\alpha(\mathrm{OS},\delta)$ in the $\mathcal{N}=5$ oscillator shell can be expressed as

$$\phi_k^\alpha(\mathrm{OS},\delta)=\sum_j c_{jk}(\delta)\psi_{jk}, \tag{58}$$

where the sum is over all the $j=0h_{11/2}$, $0h_{9/2}$, $1f_{7/2}$, $1f_{5/2}$, $2p_{3/2}$, and $2p_{1/2}$ states of the $\mathcal{N}=5$ shell allowed by the value of k. The lowest-energy orbital $\phi_k^{\alpha=1}(\mathrm{OS},\delta)$ of the $\mathcal{N}=5$ shell is the intruder orbit $\psi_{j_a=11/2,k}$ of the 50–82 shell as modified by the $0\hbar\omega$ mixing. For example, the lowest $k=\frac{1}{2}$ orbital of the $\mathcal{N}=5$ shell obtained by diagonalizing Eq. (57) at a deformation of $\delta=0.30$ ($\beta=0.32$) is

$$\begin{aligned}\left|\mathrm{OS}:\alpha=1,k=\frac{1}{2};\delta=0.30\right\rangle &= 0.874\left|0h_{11/2}\frac{1}{2}\right\rangle-0.06\left|0h_{9/2}\frac{1}{2}\right\rangle-0.445\left|1f_{7/2}\frac{1}{2}\right\rangle\\ &\quad+0.061\left|1f_{5/2}\frac{1}{2}\right\rangle+0.165\left|2p_{3/2}\frac{1}{2}\right\rangle-0.05\left|2p_{1/2}\frac{1}{2}\right\rangle.\end{aligned} \tag{59}$$

The square of the overlap of this state with the $|0h_{11/2},k=\frac{1}{2}\rangle$ state of the major shell is obtained as

$$\left\langle 0h_{11/2},k=\frac{1}{2}\middle|\mathrm{OS}:\alpha=1,k=\frac{1}{2};\delta=0.30\right\rangle^2=0.76. \tag{60}$$

This value gives the probability that the $|0h_{11/2},k=\frac{1}{2}\rangle$ intruder level of the major shell remains unmodified by $0\hbar\omega$ mixing. In Table XI, we have listed the probabilities

$$P_k^\alpha(\delta)=|\langle j_a k|\mathrm{OS}:\alpha=1,k,\delta\rangle|^2 \tag{61}$$

TABLE XII. Changes in the quadrupole moments q_k^α(MS) [see Eq. (62)] of the deformed abnormal-parity orbits ϕ_k^α(MS) as a result of $0\hbar\omega$ mixing. The q_k^α values are in units of α^2. The Nilsson Hamiltonian parameters used in these calculations are $\mu=0.630$ for the 50–82 major shell and $\mu=0.448$ for the 82–126 major shell. The parameter χ is kept at a value of 0.05 throughout.

Type of				50–82 shell with $j_a=h_{11/2}$			82–126 shell with $j_a=i_{13/2}$		
orbit	α	k	δ	q_k^α(MS)	$q_k^{\alpha+1}$(OS)	Δq_k^α	q_k^α(MS)	$q_k^{\alpha+1}$(OS)	Δq_k^α
a	1	$\frac{1}{2}$	0.20	3.18	5.57	+2.39	3.69	6.87	+3.18
a	1	$\frac{1}{2}$	0.30	3.18	6.67	+3.49	3.69	8.31	+4.62
a	1	$\frac{1}{2}$	0.35	3.18	7.17	+3.99	3.69	8.94	+5.24
a	1	$\frac{3}{2}$	0.20	2.64	4.48	+1.84	3.23	5.81	+2.58
a	1	$\frac{3}{2}$	0.30	2.64	5.15	+2.51	3.23	6.73	+3.50
a	1	$\frac{3}{2}$	0.35	2.64	5.42	+2.78	3.23	7.09	+3.86
a	1	$\frac{5}{2}$	0.20	1.55	2.69	+1.14	2.31	4.10	+1.79
a	1	$\frac{5}{2}$	0.30	1.55	3.03	+1.48	2.31	4.63	+2.32
a	1	$\frac{5}{2}$	0.35	1.55	3.16	+1.61	2.31	4.83	+2.52
a	1	$\frac{7}{2}$	0.20	–0.091	0.44	+0.53	0.92	1.97	+1.04
a	1	$\frac{7}{2}$	0.30	–0.091	0.58	+0.67	0.92	2.24	+1.32
a	1	$\frac{7}{2}$	0.35	–0.091	0.63	+0.72	0.92	2.34	+1.42

that the intruder states $|j_a k\rangle$ of protons and neutrons with $j_a=\frac{11}{2}$ and $\frac{13}{2}$ remain unchanged by $0\hbar\omega$ mixing. The results show that the modification of the intruder orbits decreases with increasing k and increases with deformation. At $\beta=0.32$, the $k=\frac{1}{2}$ proton intruder orbits change by about 25%, while the neutron $k=\frac{1}{2}$ orbits change by 35%.

We next consider the change in the value of the quadrupole moment $q_k(\mathrm{MS})=\langle j_a k|q_0^2|j_a k\rangle$ of an intruder orbit caused by $0\hbar\omega$ mixing. The modified quadrupole moment is given by

$$q_k^\alpha(\mathrm{OS},\delta)=\langle \phi_k^{\alpha=1}(\mathrm{OS},\delta)|q_0^2|\phi_k^{\alpha=1}(\mathrm{OS},\delta)\rangle,$$

$$=\sum_{j'j} c_{j'k}^{\alpha=1}(\delta)c_{jk}^{\alpha=1}(\delta)\langle j'k|q_0^2|jk\rangle, \tag{62}$$

where $q_0^2=\sqrt{(16\pi/5)}r^2Y_0^2$. The values of q_k(MS) and q_k(OS) and the change $\Delta q_k=q_k(\mathrm{OS})-q_k(\mathrm{MS})$ resulting from $0\hbar\omega$ mixing are listed in Table XII. These results show that this mixing almost doubles the quadrupole moments of the orbits $|j_a k\rangle$ with $k=\frac{1}{2}$, $\frac{3}{2}$, and $\frac{5}{2}$. This conclusion is consistent with the suggestion made by Ahalpara, Abzouzi, and Bhatt [30] (in a projected Hartree-Fock study of deformed nuclei in the Ge-Sr region within the space of the $f_{5/2}p_{1/2}p_{3/2};g_{9/2}$ single-particle states) that the quadrupole moments q_k of the $k=\frac{1}{2}$, $\frac{3}{2}$, and $\frac{5}{2}$ orbits of the $0g_{9/2}$ state should be renormalized to twice their single-shell values as a result of $0\hbar\omega$ mixing.

Compared to this large increase in the quadrupole moments of the occupied a orbits, the quadrupole moments of the occupied n orbits of a major shell are reduced as a result of $0\hbar\omega$ mixing with the a orbits of the lower major shell. This reduction is by a smaller amount, but the number of valence particles in the n orbits is larger than the number in the a orbits. The net result is that the total quadrupole moment of the valence nucleons in a major shell does not change very much as a result of this $0\hbar\omega$ mixing process.

In this work, we will ignore the influences of pairing and $0\hbar\omega$ mixing and assume that the collectivity of a particular nucleus is described to a good approximation by the asymptotically deformed $\mathcal{IS}$ of its valence particles in a major shell.

V. COLLECTIVITY OF THE PROJECTED STATES OF ABNORMAL-PARITY NUCLEONS

Our main interest in this section is to examine the quadrupole collective properties of the band of states $|\mathrm{proj}:(j_a,N_a);J\rangle$ projected from the $\mathcal{IS}$'s $\mathcal{F}_K(j_a,N_a)$. We compare the collectivity of such a band with (i) the collectivity of the band of states $|\mathrm{rot};J\rangle$ belonging to a rigid rotor with an intrinsic quadrupole moment equal to the intrinsic quadrupole moment $Q_0(j_a,N_a)$ of $\mathcal{F}_K(j_a,N_a)$ and (ii) the collectivity of the band of states $|\mathrm{SU3}[\lambda_{\mathrm{eq}},0];J\rangle$ belonging to the equivalent SU(3) representation $[\lambda_{\mathrm{eq}},0]$. We also compare the collectivity of the projected states with that of the yrast band of the same size having SO(6) symmetry. This symmetry arises in the interacting boson [15,16] and fermion dynamic symmetry [17] models.

The natural symmetry of identical nucleons in the configuration $j_a^{N_a}$ is the symplectic $\mathrm{Sp}(2j_a+1)$ symmetry. The

bands $|j_a^{N_a};J,v\rangle$ of states with this symmetry are labeled by the seniority number v. In the pseudo-SU(3) [12,28,29] and fermion dynamic symmetry [17] models, this symmetry is imposed on the a nucleons. Therefore, we wish to compare the quadrupole collectivity of the band $|\text{proj:}(j_a,N_a);J\rangle$ with those of the low-lying states of the same J value belonging to the seniority band $|j_a^{N_a};J,v\rangle$.

A. Measures of collectivity

Because they can be measured, three quantities, (i) reduced quadrupole transition probability $B(E2:\alpha_i J_i\rightarrow\alpha_f J_f)$, (ii) transition moment $Q_t(J)$ of the state $|J\rangle$, and (iii) spectroscopic quadrupole moment $Q(J)$ of the state $|J\rangle$, are generally used to describe the quadrupole collectivity of a rotational band of states $|\alpha J\rangle$, where the label α denotes properties of the band other than J. These quantities are also related to the reduced matrix elements $(\alpha_f J_f\|Q\|\alpha_i J_i)$ as follows:

$$B(E2:\alpha_i J_i\rightarrow\alpha_f J_f)=\frac{5}{16\pi}\frac{(\alpha_f J_f\|Q\|\alpha_i J_i)^2}{2J_i+1}, \tag{63}$$

$$Q_t(J)=\left[\frac{16\pi}{5}\frac{B(E2:J\rightarrow J-2)}{(J200|J-2\,0)^2}\right]^{1/2}, \tag{64a}$$

$$=\frac{1}{(J200|J-2\,0)}\frac{(J-2||Q||J)}{\sqrt{2J+1}} \tag{64b}$$

and

$$Q(J)=\frac{(J2J0|JJ)}{\sqrt{2J+1}}(\alpha J\|Q\|\alpha J). \tag{65}$$

In the rigid-rotor model, the reduced matrix elements [see Eq. (4-68a) of Ref. [20]] are

$$(\text{rot};J'||Q||\text{rot};J)=\sqrt{2J+1}(J200|J'0)\tilde{Q}_0, \tag{66}$$

where $\tilde{Q}_0$ is the quadrupole moment of the rigid $\mathcal{IS}$. (The value of $\tilde{Q}_0$ is arbitrary.) When these reduced matrix elements are substituted into Eqs. (63), (64), and (65), one has [20]

$$B(E2:\text{rot};J_i\rightarrow J_f)=\frac{5}{16\pi}(J_i200|J_f0)^2\tilde{Q}_0^2, \tag{67}$$

$$Q_t(\text{rot};J)=\tilde{Q}_0, \tag{68}$$

and

$$Q(\text{rot};J)=-\frac{J}{2J+3}\tilde{Q}_0. \tag{69}$$

In the SU(3) model, the reduced matrix elements can be evaluated by noting that the single-particle states $|\mathcal{N}l\rangle$ with oscillator quantum number $\mathcal{N}$ and angular momenta $l=\mathcal{N},\mathcal{N}-2,\mathcal{N}-4,\ldots,1$ or 0 belong to an SU(3) representation $[\lambda=\mathcal{N},0]$. With $J_i=l_i$ and $J_f=l_f$, the reduced matrix elements are given by

$$\begin{aligned}&\langle[\lambda,0];J_f\|Q\|[\lambda,0];J_i\rangle\\&\quad=\langle\lambda=\mathcal{N}l_f\|Q\|\lambda=\mathcal{N}l_i\rangle\\&\quad=\sqrt{(16\pi/5)}\langle\mathcal{N}l_f\|r^2\|\mathcal{N}l_i\rangle\langle l_f\|Y^2\|l_i\rangle.\end{aligned} \tag{70}$$

The formulas for evaluating the reduced matrix elements of r^2 and Y^2 are listed in Ref. [31]. Once they are calculated, the quantities $B(E2:\text{SU3}[\lambda,0];J_i\rightarrow J_f)$, $Q_t(\text{SU3}[\lambda,0];J)$, and $Q(\text{SU3}[\lambda,0];J)$ can be obtained for the SU(3) band $|[\lambda,0];J\rangle$ using Eqs. (63), (64), and (65). It can be further shown [9,32] that

$$\begin{aligned}&\frac{B(E2:\text{SU3}[\lambda,0];J\rightarrow J-2)}{B(E2:\text{SU3}[\lambda,0];2\rightarrow 0)}\\&\quad=\frac{3\times 5}{4\lambda(\lambda+3)}\frac{2J(J-1)(\lambda-J+2)(\lambda+J+1)}{(2J-1)(2J+1)}\end{aligned} \tag{71}$$

and

$$\frac{Q(\text{SU3}[\lambda,0];J)}{Q(\text{SU3}[\lambda;0],2)}=-\frac{7}{2}\frac{J}{2J+3}=\frac{Q(\text{rot};J)}{Q(\text{rot};2)}\quad(J\leqslant\lambda). \tag{72}$$

The remainder of this section is organized as follows. In Sec. V B, we summarize the calculation of the projected reduced matrix elements. In Sec. V C, we describe a consistency check which tests the accuracy of these matrix elements. This check also provides a criterion for comparing the quadrupole collectivity of the state $\mathcal{F}_K(j_a,N_a)$ with that of the equivalent SU(3) $\mathcal{IS}$ $\mathcal{F}_K[\lambda_{\text{eq}},0]$. In Sec. V D, we examine the variation of the $B(E2:2\rightarrow 0)$ values with the intrinsic quadrupole moments $Q_0(j_a,N_a)$. The trend of the $B(E2:J\rightarrow J-2)/B(E2:2\rightarrow 0)$ values as a function of J obtained for the projected band is compared in Sec. V E with the corresponding trends for a rigid-rotor band and for bands belonging to selected SU(3) representations. In Secs. V F and V G, we display the variations of the transitions moments $Q_t(J)$ and the spectroscopic quadrupole moments $Q(J)$, respectively, with J for the projected states. In Sec. V H, we compare the projected $B(E2:J\rightarrow J-2)$ trend with the corresponding trend obtained for an yrast band having SO(6) symmetry. Finally, in Sec. V I, we present a comparison of the projected $B(E2)$ values with those obtained for the low-lying states with definite seniority.

B. Projected reduced matrix elements

In Sec. II B, the state $\mathcal{F}_K(j_a,N_a)$ was expanded in terms of the projected states $|(j_a,N_a);JK\rangle$ [see Eq. (5)]. We want to next calculate the reduced $E2$ matrix elements $[(j_a,N_a);J'K\|Q\|(j_a,N_a);JK]$ between the projected states J and J'. The reduced matrix elements are defined by the Wigner-Eckhart theorem in the form [20]

$$(\alpha' J' M' | T^{\lambda}_{\mu} | \alpha J M) = (J \lambda M \mu | J' M') \frac{(\alpha' J' \| T^{\lambda} \| \alpha J)}{\sqrt{2J'+1}}. \tag{73}$$

With this definition,

$$(\alpha' J' \| T^{\lambda} \| \alpha J) = (\alpha J \| T^{\lambda} \| \alpha' J'). \tag{74}$$

The procedure for calculating the reduced matrix elements for an arbitrary one-body operator T^{λ}_{μ} between states $|J'K'\rangle$ and $|JK\rangle$ projected from general determinantal $\mathcal{IS}$'s $\Phi_{K'}$ and Φ_K has been discussed by Gunye and Warke [33] and by Hara and Sun [34]. (In our case, $\Phi_{K'} = \Phi_K$). We adopt their general procedure to express the reduced matrix elements as a sum of contributions from each of the nucleons in the $\mathcal{IS}$ $\mathcal{F}_K(j_a, N_a)$. The reduced matrix element is then given by

$$\begin{aligned}
&[(j_a, N_a); J', K \| Q \| (j_a, N_a); JK] \\
&\quad = \sqrt{\frac{(2J'+1)(2J+1)}{C_{J'K} C_{JK}}} \\
&\qquad \times \sum_{i=1}^{N_a} \sum_{m=1}^{N_a} \sum_{I} (-1)^{i+m+j_i+J'+I+2} \\
&\qquad \times c_{j_m \Omega_m}(K) c_{j_i \Omega_i}(K) p^{I}_{K-\Omega_m, K-\Omega_i}(N_a - 1) \\
&\qquad \times (I, j_m; K-\Omega_m, \Omega_m | J' K) (I, j_i; K-\Omega_i, \Omega_i | JK) \\
&\qquad \times \begin{Bmatrix} J & j_i & I \\ j_m & J' & 2 \end{Bmatrix} (n_m l_m j_m \| q \| n_i l_i j_i).
\end{aligned} \tag{75}$$

This equation is a modified version of Eq. (5) in Ref. [33]. There are two modifications. The first is the factor $\sqrt{2J'+1}$, which arises because of the difference in the definition of the reduced matrix elements in the Wigner-Eckart theorem. We use the definition given in Eq. (73). The definition used by Warke and Gunye [33] does not have this factor. The second modification is the factor $1/\sqrt{C_{J'K} C_{JK}}$ which does not appear in Eq. (5) of Ref. [33], but should be there.

In Eq. (75), the sums over i and m run over the nucleons in the initial and final $\mathcal{IS}$'s. The index I is the angular momentum of the $N_a - 1$ spectator nucleons in the $\mathcal{IS}$ when one of the nucleons is contributing to the reduced matrix element. The quantity $c_{j_i \Omega_i}(K)$ is the amplitude that the contributing nucleon in the initial state has an angular momentum j_i and projection Ω_i. Similarly, $c_{j_m \Omega_m}(K)$ is the corresponding amplitude for the nucleon in the final $\mathcal{IS}$. The quantity $p^{I}_{K-\Omega_m, K-\Omega_i}(N_a - 1)$ is the probability amplitude that the $N_a - 1$ spectator nucleons in the initial and final $\mathcal{IS}$'s are coupled to a total angular momentum I. The Clebsch-Gordan coefficient on the right in Eq. (75) gives the amplitude (in the initial state) that the spectator nucleons in the state $|I, K-\Omega_i\rangle$ are coupled to the contributing nucleon in the state $|j_i \Omega_i\rangle$ resulting in a total initial angular momentum state $|JK\rangle$. The Clebsh-Gordan coefficient on the left is the corresponding amplitude for the final state. The last two terms in the sum are, respectively, the $6j$ symbol and the reduced matrix elements of the single-particle quadrupole operator $q_{\mu} = \sqrt{(16\pi/5)} r^2 Y^2_{\mu}$.

In our calculations, $K=0$ and $j_i = j_m = j_a$. The coefficients are $c_{j_i, |\Omega_i|} = 1$ and $c_{j_i, -|\Omega_i|} = (-1)^{j_i - |\Omega_i|} c_{j_i |\Omega_i|}$. The radial quantum numbers and the orbital angular momenta are given by $n_i = n_m = 0$ and $l_i = l_m = j_a - \frac{1}{2}$, respectively. The probability amplitude p^I is given by

$$\begin{aligned}
&p^{I}_{K-\Omega_m, K-\Omega_i}(N_a - 1) \\
&\quad = \langle \mathcal{F}_{K-\Omega_m}(j_a, N_a - 1) | P^{I}_{K-\Omega_m, K-\Omega_i} \\
&\qquad \times (N_a - 1) | \mathcal{F}_{K-\Omega_i}(j_a, N_a - 1) \rangle.
\end{aligned} \tag{76}$$

The reduced matrix elements $[(j_a, N_a); J'K \| Q \| (j_a, N_a); JK]$ between the various projected states are listed in Table XIII for $J = J'$ and $J = J' + 2$. Because the values of C_{JK} and p^I become very small for large values of J and I, considerable care is required in the calculation of $(J' \| Q \| J)$, especially for higher values of J. Fortunately, we can derive a consistency check that can monitor the numerical accuracy of the calculated reduced matrix elements.

C. Consistency check

The quadrupole moment $Q_0(j_a, N_a)$ of an $\mathcal{IS}$ $\mathcal{F}_K(j_a, N_a)$ is given by

$$\begin{aligned}
Q_0(j_a, N_a) &= \langle \mathcal{F}_K(j_a, N_a) | Q_0 | \mathcal{F}_K(j_a, N_a) \rangle, \\
&= \sum_{i=1}^{N_a} q_{k_i}(j_a),
\end{aligned} \tag{77}$$

where the sum is over all the occupied a orbits and q_{k_i} are the quadrupole moments of the occupied orbits (see Table V). The values of $Q_0(j_a, N_a)$ are listed in Table VI.

We now obtain an alternative expression for $Q_0(j_a, N_a)$. The states $\mathcal{F}_K(j_a, N_a)$ can be expanded as

$$|\mathcal{F}_{K=0}(j_a, N_a)\rangle = \sum_{J} C_{JK=0}(j_a, N_a) | \text{proj:}(j_a, N_a); JK \rangle. \tag{78}$$

Substituting into Eq. (77), we get the sum rule

$$\begin{aligned}
Q_0(j_a, N_a) = \sum_{J'} \sum_{J} &C_{J'K=0}(j_a, N_a) C_{JK=0} \\
&\times [(j_a, N_a); J'K | Q_0 | (j_a, N_a); JK]
\end{aligned} \tag{79}$$

or

TABLE XIII. Reduced matrix elements $[(j_a,N_a);J',J\|Q\|(j_a,N_a);JK]$[see Eq. (75)] for $J=J'$ and $J=J'+2$. The reduced matrix elements $(J\|Q\|J')$ are not listed because $(J\|Q\|J')=(J'\|Q\|J)$ for each (j_a,N_a). The units are α^2.

	$j_a=g_{9/2}$		$j_a=h_{11/2}$		$j_a=i_{13/2}$		$j_a=j_{15/2}$	
J	$J\to J$	$J+2\to J$	$J\to J$	$J+2\to J$	$J\to J$	$J+2\to J$	$J\to J$	$J+2\to J$
$N_a=2$ particles								
0	0	10.832	0	12.863	0	14.884	0	16.900
2	11.155	15.578	−13.908	19.163	16.550	22.631	19.124	26.029
4	7.135	15.570	11.954	20.845	16.230	25.735	20.182	30.398
6	−4.851	11.266	3.307	18.755	10.075	25.357	16.008	31.452
8	−26.250		−13.188	12.758	−2.869	21.545	5.803	29.361
10			−38.457		−23.346	14.095	−11.036	24.052
12					−52.051		−35.085	15.317
14							−66.900	
$N_a=4$ particles								
0	0	11.424	0	13.497	0	15.524	0	17.531
2	−10.378	17.241	−13.018	20.975	−15.606	24.486	−18.157	27.883
4	−13.887	19.962	−16.596	25.294	−19.413	30.154	−22.321	34.745
6	−18.100	21.910	−21.678	27.712	−24.487	33.765	−27.359	39.514
8	−6.735	25.779	−25.576	30.694	−30.418	36.304	−33.569	42.792
10	−6.761	22.532	−13.718	35.891	−33.305	40.377	−39.743	45.732
12	−15.135		−13.562	35.112	−20.964	46.516	−41.240	50.875
14			−21.302	28.224	−20.741	47.137	−28.514	57.722
16			−36.774		−27.942	43.169	−28.148	59.335
18					−42.038	33.220	−34.953	57.017
20					−63.192		−48.362	50.318
22							−67.992	37.582
24							−94.318	
$N_a=6$ particles								
0	0	12.839	0	16.472	0	19.916	0	23.249
2	−14.198	19.681	−19.053	25.990	−23.416	31.717	−27.528	37.158
4	−16.088	23.203	−23.259	31.921	−29.221	39.505	−34.687	46.561
6	−12.705	24.595	−25.514	36.101	−33.665	45.423	−40.573	53.940
8	−8.077	22.942	−24.229	38.934	−36.192	50.186	−45.088	60.060
10	6.924	22.537	−22.294	39.886	−36.319	53.925	−47.924	65.332
12	14.386		−17.785	39.842	−36.016	56.279	−49.084	69.731
14			−5.181	40.990	−34.619	57.676	−49.948	73.043
16			0	33.998	−29.527	59.267	−50.255	75.513
18			0		−19.473	60.938	−48.555	77.829
20					−17.017	56.390	−43.074	80.581
22					−19.717	44.258	−35.748	82.316
24					−27.478		−35.751	78.913
26							−40.796	70.241
28							−50.715	53.535
30							−65.633	
$N_a=8$ particles								
0	0	10.832	0	16.800	0	22.188	0	27.220
2	−11.155	15.578	−19.403	26.296	−26.188	35.265	−32.341	43.465
4	−7.135	15.570	−22.466	31.777	−32.283	43.773	−40.643	54.406
6	4.851	11.266	−21.995	34.833	−36.123	50.036	−47.011	62.954
8	26.250		−18.145	35.711	−37.505	54.624	−51.437	69.888
10			−9.654	34.752	−36.639	57.732	−54.061	75.532
12			1.703	30.930	−33.288	59.527	−55.033	80.041
14			21.299	28.251	−27.204	60.052	−54.310	83.534
16			36.607		−19.238	58.953	−51.753	86.095
18					−7.836	57.056	−47.472	87.671
20					8.545	55.208	−41.803	88.165
22					19.717	44.258	−33.951	87.980
24					27.496		−22.950	87.572
26							−10.609	85.555
28							−3.504	76.857
30							0	59.113
32							0	

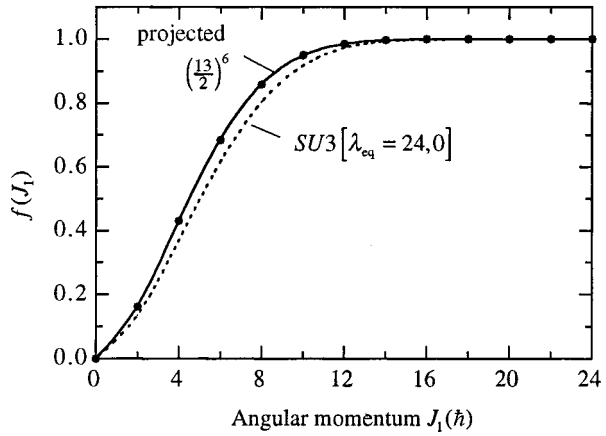

FIG. 6. Variation of $f(J_1)$ with J_1 [see Eq. (81)] for the $\mathcal{F}_K(j_a=\frac{13}{2},N_a=6)$ and SU(3) $\mathcal{F}_K[\lambda_{eq}=24,0]$ $\mathcal{IS}$'s. See also Sec. V C.

$$\sum_i q_{k_i}(j_a,N_a)=\sum_{J'}\sum_J C_{J'K=0}C_{JK=0}\frac{(J200|J'0)}{\sqrt{2J+1}} \times[(j_a,N_a);J'K\|Q\|(j_a,N_a);JK]. \tag{80}$$

Here, the sums run over all the states $|J\rangle$ contained in the $\mathcal{IS}$ $\mathcal{F}_K(j_a,N_a)$. We verified that Eq. (80) is satisfied by the calculated reduced matrix elements.

We now use this sum rule for comparing the collectivity of the $\mathcal{IS}$ $\mathcal{F}_K(j_a,N_a)$ with that of the corresponding equivalent SU(3) $\mathcal{IS}$ $\mathcal{F}_K[\lambda_{eq},0]$. Let $Q(J_1)$ be the value of the sum on the right-hand side of Eq. (80) obtained up to the contribution from the states with $J'=J=J_1$ contained in the $\mathcal{IS}$. The quantity

$$f(J_1)=\frac{Q(J_1)}{Q_0(j_a,N_a)} \tag{81}$$

represents the fraction of the quadrupole moment exhausted up to the projected state $|J_1\rangle$. The variation of $f(J_1)$ with J_1 is characteristic of the collectivity of the yrast band. As an illustration, we show, by a solid line in Fig. 6, the variation of $f(J_1)$ with J_1 calculated for the $\mathcal{IS}$ of $N_a=6$ particles in the state with $j_a=\frac{13}{2}$. For comparison, we also show the similar variation for the equivalent SU(3) $\mathcal{IS}$ $\mathcal{F}_K[\lambda_{eq}=24,0]$. From this comparison, we conclude that the $\mathcal{F}_K(j_a,N_a)$ and the equivalent SU(3) $\mathcal{IS}$'s have similar collectivities. For both of these $\mathcal{IS}$'s, 90% of the quadrupole moment sum is exhausted within the first 40% of the band which extends up to $J=24$. Similar results were obtained for a few other $\mathcal{IS}$'s $\mathcal{F}_K(j_a,N_a)$, and the conclusions are expected to be valid for all the $\mathcal{IS}$'s considered here.

D. $B(E2;2\rightarrow0)$ values

In the rotor model, the $B(E2{:}\text{rot};2\rightarrow0)$ values are related to the quadrupole moment Q_0 of the $\mathcal{IS}$ by

$$B(E2{:}\text{rot};2\rightarrow0)=\frac{1}{16\pi}(Q_0)^2\approx0.0199(Q_0)^2. \tag{82}$$

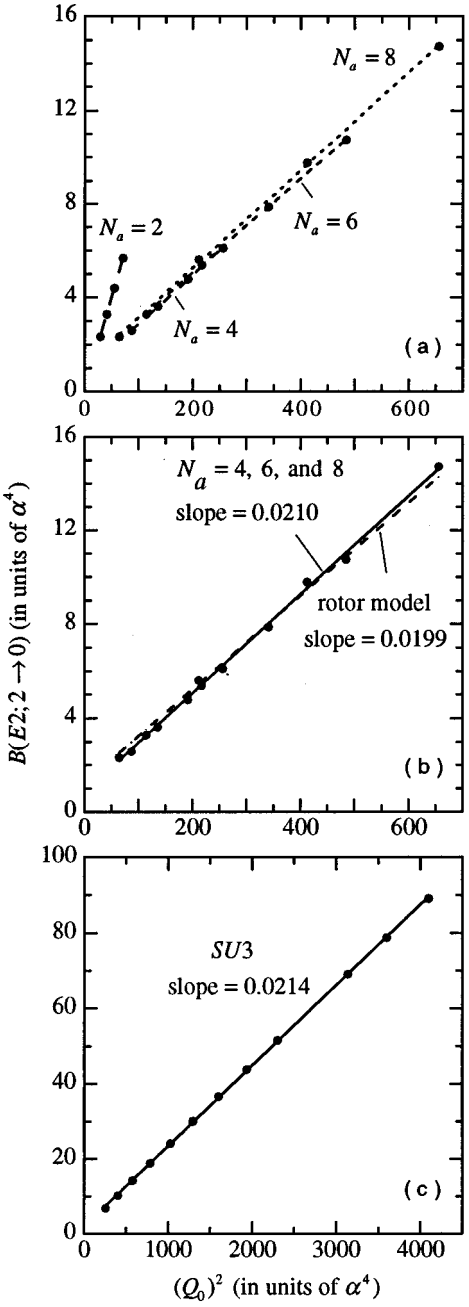

FIG. 7. Variation of $B(E2{:}2\rightarrow0)$ with $(Q_0)^2$ for the $|J=2\rangle$ and $|J=0\rangle$ states projected from different $\mathcal{IS}$'s (see Sec. V D). (a) The four straight lines correspond to $\mathcal{F}_K(j_a,N_a)$ for four different values of N_a. (b) Simultaneous fit to the $N_a=4$, 6, and 8 trends (solid line) and forced fit (dashed line) to the same data with the rotor-model slope. (c) The straight line corresponds to the SU(3) $\mathcal{F}_K[\lambda=Q_0/2,0]$.

The values of the quadrupole moments $Q_0(j_a,N_a)$ of the $\mathcal{IS}$ $\mathcal{F}_k(j_a,N_a)$ are listed in Table VI. The $B(E2{:}\text{proj};2\rightarrow0)$ values calculated for the $J=2$ and $J=0$ states projected from the $\mathcal{IS}$ are plotted in Fig. 7(a) as a function of $[Q_0(j_a,N_a)]^2$. The overall trend of these $B(E2)$ values is described by

$$B(E2{:}\text{proj};2\rightarrow0)\approx c(N_a)+m(N_a)[Q_0(j_a,N_a)]^2. \tag{83}$$

The $B(E2)$ trend for the two-particle case [see Fig. 7(a)] is markedly different from those for four, six, and eight particles. The latter have similar slopes, and these $B(E2)$ values can be fitted by a single line, as shown in Fig. 7(b). This line has a slope $m=0.0210$ and an intercept $c=0.86$. If we fix the slope as $m=m(\mathrm{rot})=0.0199$, the best fit to the $B(E2{:}\mathrm{proj};2\rightarrow 0)$ values for $N_a=4$, 6, and 8 particles is obtained with an intercept of 1.25. This fit, shown by a dashed line in Fig. 7(b), demonstrates that the projected and rotor-model values are very similar. This similarity is expected because for a well-deformed $\mathcal{IS}$, the projection formula for the $B(E2{:}2\rightarrow 0)$ values reduces to the rotor-model formula to a good approximation for small values of J [14,35].

The $B(E2{:}\mathrm{SU3}[\lambda,0];2\rightarrow 0)$ values also depend on the quadrupole moment $Q_0(\lambda)=2\lambda$ of the $\mathcal{IS}$ of representation $[\lambda,0]$ in the same way; namely,

$$B(E2{:}\mathrm{SU3}[\lambda,0],2\rightarrow 0)\approx c(\lambda)+m(\lambda)[Q_0(\lambda)]^2. \quad (84)$$

The $B(E2{:}\mathrm{SU3}[\lambda,0];2\rightarrow 0)$ values for $8\leqslant\lambda\leqslant 34$, plotted against $[Q_0(\lambda)]^2=4\lambda^2$ [see Fig. 7(c)], can be described by

$$B(E2{:}\mathrm{SU3}[\lambda,0];2\rightarrow 0)\approx 2.11+0.0214[Q_0(\lambda)]^2. \quad (85)$$

The rotor-model, projected, and SU(3) $B(E2{:}\mathrm{model};2\rightarrow 0)$ values have almost identical dependence on $[Q_0(\mathrm{model})]^2$. Both the projected and the SU(3) $B(E2{:}2\rightarrow 0)$ trends have a small, constant intercept value independent of Q_0. When Q_0 is sufficiently large, the constant addition to the $B(E2)$ value becomes negligible compared to the direct contribution from Q_0, which is in agreement with the rotor-model result.

E. $B(E2{:}J\rightarrow J-2)$ values

We adopt a criterion that the closer the trend of the ratio $B(E2{:}J\rightarrow J-2)/B(E2{:}2\rightarrow 0)$ for a model yrast band is to the rotor trend, the greater is the collectivity of the model band. The rotor $B(E2)$ values are given by

$$B(E2{:}\mathrm{rot};J\rightarrow J-2)=\frac{5}{16\pi}[J200|(J-2)0]^2(\tilde{Q}_0)^2. \quad (86)$$

In the next step, we calculated the $B(E2{:}\mathrm{proj};J\rightarrow J-2)$ values for the $\mathcal{IS}$'s $\mathcal{F}_K(j_a,N_a)$ of $N_a=2$, 4, 6, and 8 particles in the $j_a=\frac{9}{2}$, $\frac{11}{2}$, $\frac{13}{2}$, and $\frac{15}{2}$ single-particle orbits using Eq. (63) and the appropriate projected reduced matrix elements from Table XIII. [The care taken in these calculations is illustrated in Table XIV by reproducing the *exact* calculated values for the $(j_a=\frac{13}{2},N_a=8)$ case.] The calculated $B(E2)$ values are plotted as a function of J in Fig. 8. For $N_a>2$, there is a double-humped structure in the $B(E2{:}\mathrm{proj};J\rightarrow J-2)$ vs J trend. This feature is most pronounced for the j_a^4 configurations. The second maximum is significantly smaller for the j_a^6 configuration and almost disappears for the j_a^8 configuration. Selection rules governing the $E2$ transition probabilities between $|(j_a,N_a);J\rangle$ projected states imposed by the residual seniority properties of these states are probably responsible for the double-humped structure.

TABLE XIV. Calculated $B(E2{:}\mathrm{proj};J\rightarrow J-2)$ values (in units of α^4) for states $|J\rangle$ projected from $\mathcal{F}_K(j_a,N_a)$. See Sec. V E.

J	$B(E2{:}\ \mathrm{proj}\ (j_a=\frac{13}{2},N_a=8);J\rightarrow J-2)$
2	$\frac{124371720}{4041973}\frac{1}{\pi}$
4	$\frac{710066872090650}{16443768783169}\frac{1}{\pi}$
6	$\frac{16548971043390192000}{359288999835417587}\frac{1}{\pi}$
8	$\frac{157998970259336078901}{3433150935722452009}\frac{1}{\pi}$
10	$\frac{14134586635496318750}{318340050610297261}\frac{1}{\pi}$
12	$\frac{48456692009845060887}{1163086609359337832}\frac{1}{\pi}$
14	$\frac{2963172000492259325}{77602156736697398}\frac{1}{\pi}$
16	$\frac{13180904782081031 25}{38597213645370952}\frac{1}{\pi}$
18	$\frac{3106532246177574}{105831145034069}\frac{1}{\pi}$
20	$\frac{5122788000}{206459149}\frac{1}{\pi}$
22	$\frac{4152920}{196209}\frac{1}{\pi}$
24	$\frac{99225}{7943}\frac{1}{\pi}$

In Fig. 9, we show the rotor-model $B(E2{:}\mathrm{rot};J\rightarrow J-2)$ values normalized to the projected $B(E2{:}\mathrm{proj};2\rightarrow 0)$ value for the $(\frac{11}{2})^6$, $(\frac{13}{2})^6$, and $(\frac{15}{2})^8$ states. As expected, the projected bands are less collective than the rigid-rotor band. We next compare the $B(E2{:}\mathrm{proj};J\rightarrow J-2)$ values with the $B(E2{:}\mathrm{SU3}[\lambda_{\mathrm{eq}},0];J\rightarrow J-2)$ values obtained for the SU(3) band belonging to the equivalent representations [18,0], [24,0], and [32,0] appropriate for the three $\mathcal{IS}$'s $\mathcal{F}_K(\frac{11}{2},6)$, $\mathcal{F}_K(\frac{13}{2},6)$, and $\mathcal{F}_K(\frac{15}{2},8)$, respectively. They are also shown in Fig. 9. It is clear from this figure that the projected $B(E2)$ trends are slightly more collective than the equivalent SU(3) $B(E2)$ trends. This result is suprising because the distribution of angular momenta in the $\mathcal{IS}$ $\mathcal{F}_K(j_a,N_a)$ was found (in Sec. II C) to be less collective than the distribution in the equivalent SU(3) $\mathcal{IS}$ belonging to the representation $[\lambda_{\mathrm{eq}},0]$.

We also determined the SU(3) representation $[\lambda_{B(E2)},0]$ such that the $B(E2{:}[\lambda_{B(E2)},0];J\rightarrow J-2)$ values normalized to the projected $B(E2{:}\mathrm{proj};2\rightarrow 0)$ value agree with the similarly normalized $B(E2{:}\mathrm{proj};J\rightarrow J-2)$ values over as large a range of J as possible. The results for the $(\frac{11}{2})^6$, $(\frac{13}{2})^6$, and

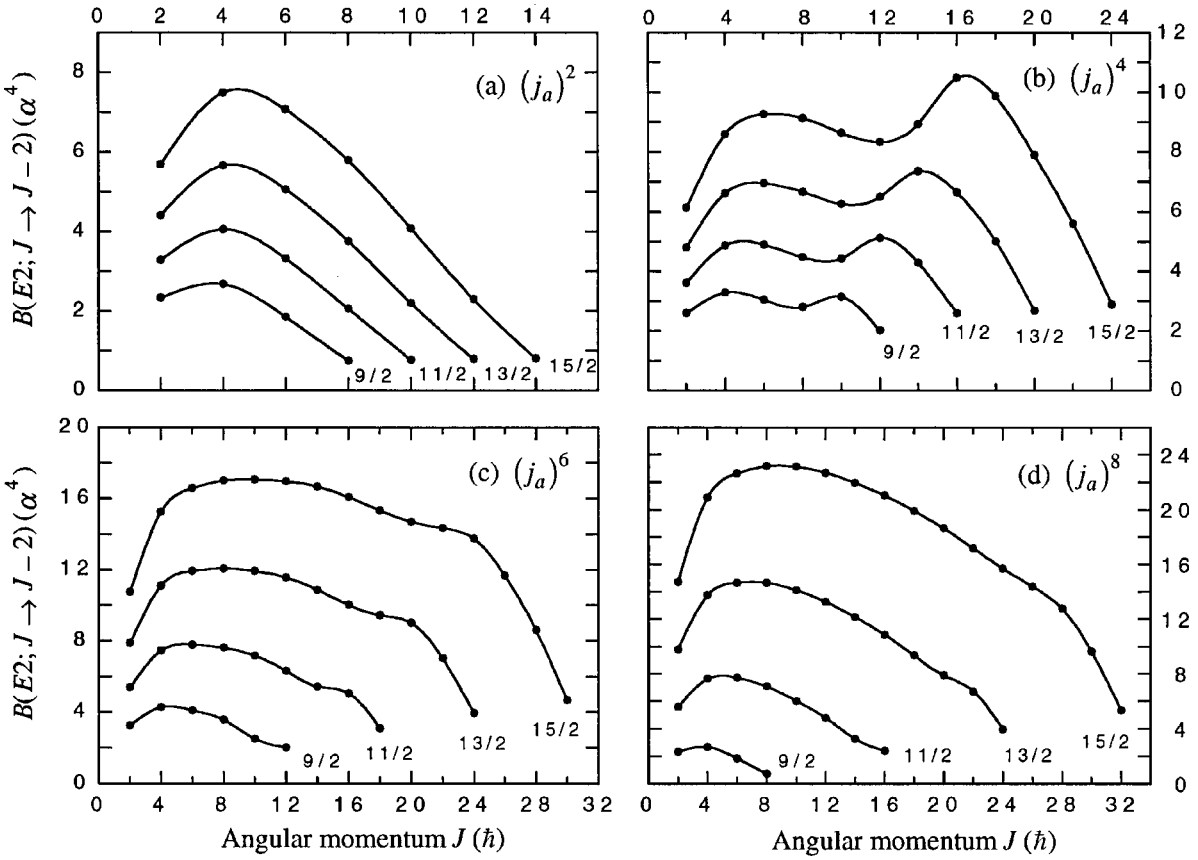

FIG. 8. $B(E2{:}J\rightarrow J-2)$ values for the states $|\text{proj}{:}(j_a,N_a);J\rangle$ projected from each of the $\mathcal{IS}$'s $\mathcal{F}_K(j_a,N_a)$ (see Sec. V E). The calculated values are connected by smooth lines for easy visualization.

$(\frac{15}{2})^8$ $\mathcal{IS}$'s are shown in Fig. 9 [see the curves labeled by $\lambda_{B(E2)}$]. The $\lambda_{B(E2)}$ values are larger than the λ_{eq} values by 2–4 units.

F. Transition moments $Q_t(J)$

The transition probabilities $B(E2{:}J\rightarrow J-2)$ are often expressed in terms of the transition moments $Q_t(J)$ of a state [see Eq. (64)]. We calculated the $Q_t(\text{proj};J)$ values for the band of states $|\text{proj}{:}(j_a,N_a);J\rangle$ using Eq. (64) and the $B(E2{:}\text{proj};J\rightarrow J-2)$ values obtained in Sec. V E. The resulting $Q_t(\text{proj};J)$ values plotted in Fig. 10 show a significant variation with J. For the bands with $N_a=6$ and 8 particles, these values decrease with J [see Figs. 10(b) and 10(c)], while for $N_a=4$ particles, they have a second maximum [see Fig. 10(a)] at $J=10$, 12, 14, and 16, respectively, for $j_a=\frac{9}{2}$, $\frac{11}{2}$, $\frac{13}{2}$, and $\frac{15}{2}$. Also plotted in Fig. 10 by means of horizontal lines are the quadrupole moments $Q_0(j_a,N_a)$ for each of the $\mathcal{IS}$'s $\mathcal{F}_K(j_a,N_a)$. These lines represent the rigid rotor values; that is, $Q_t(\text{rot};J)=\tilde{Q}_0=Q_0(j_a,N_a)$. The projected values are slightly larger(smaller) than the rotor values for small(large) J values.

The variation of $Q_t(\text{proj};J)$ with J is interesting from the point of view of the cranking model in which the yrast band is obtained while the $\mathcal{IS}$ rotates with different angular momenta. The structure of the $\mathcal{IS}$ changes in response to the increase in the angular momentum J, and the transition moment $Q_t(\text{crank};J)$ is expected to be the quadrupole moment of the $\mathcal{IS}$ when it is rotating with angular momentum J along an axis perpendicular to the symmetry axis. Hence, in the cranking model, the variation of $Q_t(J)$ with J gives a measure of the change in the deformation of the $\mathcal{IS}$ as a function of its rotational frequency.

In our calculations, all the states $|\text{proj}{:}(j_a,N_a);J\rangle$ are projected from the same $\mathcal{IS}$. In other words, the structure of the $\mathcal{IS}$ does not change with the J of the projected state. Hence, the variation of $Q_t(\text{proj};J)$ with J cannot be considered as a measure of the change of the deformation of the $\mathcal{IS}$. The exact relationship between $Q_t(J)$ vs J in the cranking model and in the projection approach (in the $j_a^{N_a}$ configuration space) needs to be explored further, possibly along the lines followed by Hara, Hayashi, and Ring [36].

G. Spectroscopic quadrupole moments $Q(J)$

We calculated the values of the spectroscopic quadrupole moments $Q(\text{proj};J)$ of the states $|\text{proj}{:}(j_a,N_a);J\rangle$ using Eq. (65) and the reduced matrix elements given in Table XIII. The variations of $Q(\text{proj};J)$ vs J are shown in Fig. 11 for the projected bands of $N_a=4$, 6, and 8 particles. We note the general absence of particle-hole symmetry in the $Q(\text{proj};J)$ values. For example, the values for the $(\frac{11}{2})^4$ band are not equal in magnitude to those for the $(\frac{11}{2})^8$ band, nor are the

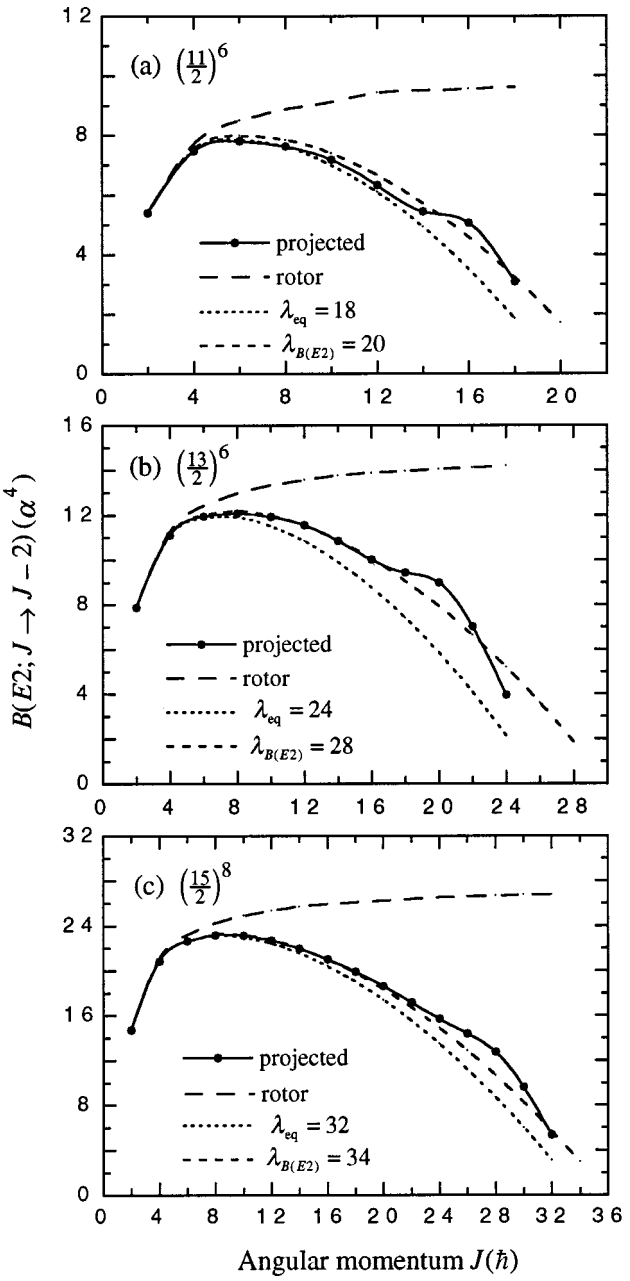

FIG. 9. Comparison of the $B(E2{:}J\rightarrow J-2)$ values for the states projected from the $\mathcal{IS}$'s $\mathcal{F}_K(j_a,N_a)$ and SU(3) $\mathcal{F}_K[\lambda,0]$. The $B(E2{:}\mathrm{rot};J\rightarrow J-2)$ values from the rotor model are normalized to the $B(E2{:}\mathrm{proj};2\rightarrow 0)$ values. See also Sec. V E.

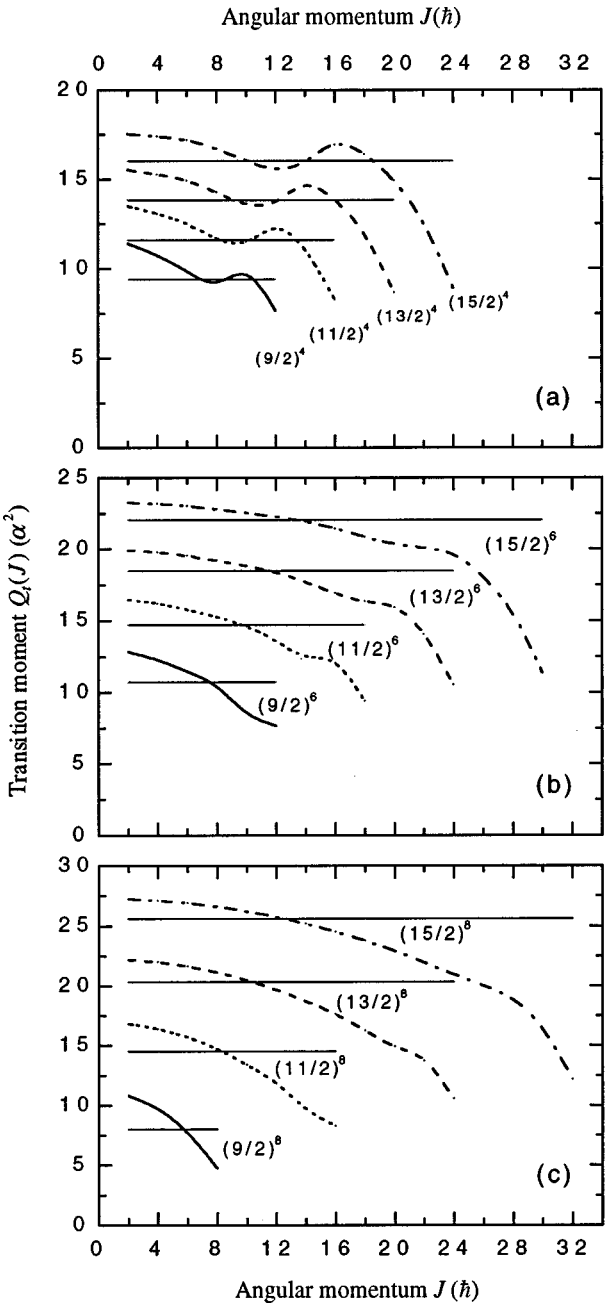

FIG. 10. Transition moments $Q_t(J)$ for the yrast band of states $|\mathrm{proj}{:}(j_a,N_a);J\rangle$ projected from the $\mathcal{IS}$'s $\mathcal{F}_K(j_a,N_a)$. For each band, the constant rotor-model $Q_t(\mathrm{rot};J)$ value, chosen to be equal to the corresponding intrinsic quadrupole moment $Q_0(j_a,N_a)$, is shown as a horizontal line. See related discussion in Sec. V F.

values for the $(\frac{13}{2})^6$ band equal in magnitude to those for the $(\frac{13}{2})^8$ band. However, for the projected states with $J=J_{\max}$, the $Q(\mathrm{proj};J)$ values do exhibit particle-hole symmetry; that is, $Q[(\frac{9}{2})^4,12]=-Q[(\frac{9}{2})^6,12]$, $Q[(\frac{11}{2})^4,16]=-Q[(\frac{11}{2})^8,16]$, and $Q[(\frac{13}{2})^6,24]=-Q[(\frac{13}{2})^8,24]$. The reason for this behavior is that there is only one state of the $j_a^{N_a}$ configuration with $J=J_{\max}$, and this state has a definite seniority $v=v_{\max}=N_a$. Another consequence of the particle-hole symmetry is that $Q[(\frac{11}{2})^6,18]=Q[(\frac{15}{2})^8,32]=0$.

The $Q(\mathrm{rot};J)$ values for the states $|\mathrm{rot},J\rangle$ of an axially symmetric rigid rotor (with an $\mathcal{IS}$ having $K=0$ and an intrinsic quadrupole moment $\tilde{Q}_0$) are given by Eq. (69). For a prolate $\mathcal{IS}$, $\tilde{Q}_0>0$, and $Q(\mathrm{rot};J)<0$ for all J values. The rotor $Q(\mathrm{rot};J)$ values decrease smoothly from $-\frac{2}{7}\tilde{Q}_0$ to $-\frac{1}{2}\tilde{Q}_0$ as J increases from $J=2$ to $J=\infty$. If $\tilde{Q}_0$ is chosen to be equal to $Q_0(j_a,N_a)$, the rotor-model spectroscopic quadrupole moment $Q(\mathrm{rot};2)$ for the $J=2$ state is quite close to the projected value $Q(\mathrm{proj};2)$ for the $j_a^{N_a}$ band. Because the $\mathcal{IS}$'s $\mathcal{F}_K(j_a,N_a)$ are far from being rigid, the overall trend of the corresponding $Q(\mathrm{proj};J)$ values is significantly different

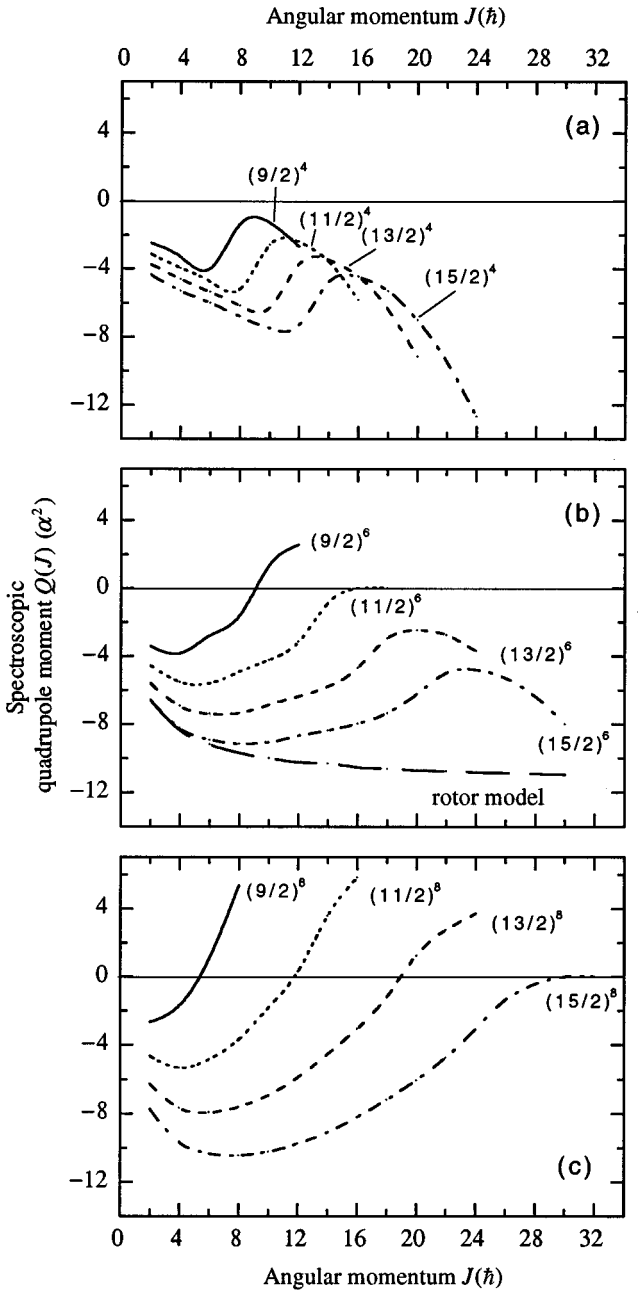

FIG. 11. Spectroscopic quadrupole moments $Q(J)$ for the yrast band of states $|\text{proj}:(j_a,N_a);J\rangle$ projected from the $\mathcal{IS}$'s $\mathcal{F}_K(j_a,N_a)$. For the $(\frac{15}{2})^6$ band, we show in (b) the rotor-model $Q(J)$ values normalized to the $Q(J=2)$ value. See related discussion in Sec. V G.

from the trend of the $Q(\text{rot};J)$ values. We illustrate this difference in Fig. 11(b), where we have plotted the $Q(\text{rot};J)$ values such that $Q(\text{rot};2)=Q(\text{proj};2)$ for the $(\frac{15}{2})^6$ configuration. The projected $Q(\text{proj};J)$ values resemble the rotor values only for the first few J states.

H. Comparison with $B(E2)$ values in the SO(6) scheme

In the interacting boson model [15,16], rotation-like quadrupole collectivity is described in terms of the SO(6) symmetry in addition to the SU(3) symmetry. For the SO(6) symmetry, the trend of the $B(E2{:}J\rightarrow J-2)$ values for the yrast states of N_b bosons coupled strongly by $E2$ transitions are given by [9]

$$R^{N_b}_{\text{SO(6)}}(J)=\frac{B(E2{:}\text{SO6};J\rightarrow J-2)}{B(E2{:}\text{SO6};2\rightarrow 0)}$$
$$=\frac{5}{2(2N_b)(2N_b+4)}\frac{J}{J+3}$$
$$\times(2N_b+2-J)(2N_b+6-J). \qquad (87)$$

The highest angular momentum $J_{\max}$ for N_b bosons is $J_{\max}=2N_b$. We also define

$$R_{\text{proj}}(J)=\frac{B(E2{:}\text{proj};J\rightarrow J-2)}{B(E2{:}\text{proj};2\rightarrow 0)}. \qquad (88)$$

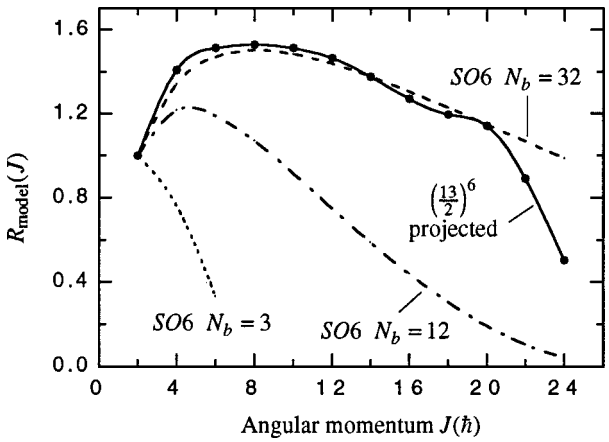

FIG. 12. Trends of the $R_{\text{model}}(J)$ values [see Eqs. (87) and (88)]. The $R_{\text{proj}}(J)$ trend is more collective than the $R^{N_b}_{\text{SO(6)}}(J)$ trend for the equivalent SO(6) band with $N_{b\ \text{eq}}=12$. See related discussion in Sec. V H.

In Fig. 12, we compare the $R^{N_b}_{\text{SO(6)}}(J)$ values (for different N_b) with the $R_{\text{proj}}(J)$ values, the latter projected from the $\mathcal{IS}$ of six particles in the $i_{13/2}$ state. In the interacting boson model, the boson number N_b is three for a six-particle state, and the maximum angular momentum of the yrast band is $J_{\max}=2N_b=6$. The $R^{N_b}_{\text{SO(6)}}(J)$ values for $N_{b\text{IBA}}=3$, shown in Fig. 12, are significantly smaller than the projected values. We next consider an SO(6) band with an equivalent boson number $N_{b\text{eq}}=12$ for which $J_{\max}=24$. This $J_{\max}$ value is equal to the $J_{\max}$ for the $(\frac{13}{2})^6$ configuration. The $R^{N_b}_{\text{SO(6)}}(J)$ values for $N_{b\text{eq}}=12$ are still less collective than the projected values. The boson number for which the SO(6) $B(E2)$ trend best fits the trend of the projected values is $N_{bB(E2)}=32$.

I. Comparison with $B(E2)$ values in the seniority scheme

In the seniority scheme, the states $|j_a^{N_a};J\nu,\alpha\rangle$ of the $j_a^{N_a}$ configuration may be classified in terms of ''bands'' of different angular momenta J having the same seniority quantum number ν. The label α distinguishes between orthogonal

TABLE XV. Comparison between $R_1(N_a)_{\rm proj}$ [see Eq. (92)] and $R_1(N_a)_{\rm sen}$ [see Eq. (90)] values for $N_a=4$, 6, and 8 particles in different j_a orbits. The $B(E2)$ values are in units of α^4.

	$B(E2)$ proj $(j_a,N_a=2)$	$B(E2)$ proj $(j_a,N_a=4)$			$B(E2)$ proj $(j_a,N_a=6)$			$B(E2)$ proj $(j_a,N_a=8)$		
j_a	$2\rightarrow 0$	$2\rightarrow 0$	$R_1(4)_{\rm proj}$	$R_1(4)_{\rm sen}$	$2\rightarrow 0$	$R_1(6)_{\rm proj}$	$R_1(6)_{\rm sen}$	$2\rightarrow 0$	$R_1(8)_{\rm proj}$	$R_1(8)_{\rm sen}$
$\frac{9}{2}$	2.33	2.60	1.12	1.50	3.28	1.41	1.50	2.33	1	1
$\frac{11}{2}$	3.29	3.62	1.10	1.60	5.40	1.64	1.80	5.62	1.71	1.60
$\frac{13}{2}$	4.41	4.79	1.09	1.67	7.89	1.79	2.00	9.79	2.22	2
$\frac{15}{2}$	5.68	6.11	1.08	1.71	10.75	1.89	2.14	14.74	2.60	2.29

states with the same values of J and v. When the pairing interaction is dominant, the ground state has $J=0$ and $v=0$. The first excited ''band'' of states has $v=2$ and $J=2,4,6,\ldots,2j_a-1$. The states with $v=4,6,8,\ldots,n$ lie at higher energies.

The states $|(j_a,N_a);JK\rangle$ projected from the $\mathcal{IS}$ $\mathcal{F}^a_K(j_a,N_a)$ do not, in general, have a definite seniority for $N_a>2$ and $j_a>\frac{7}{2}$ (see p. 324 of Ref. [8]). The projected state for each J can, in principle, be expressed as a linear combination of different seniority states. Thus

$$|\text{proj:}(j_a,N_a);JK\rangle=\sum_{\alpha v} A(Jv,\alpha)||\text{sen:}j_a^{N_a};Jv,\alpha\rangle. \tag{89}$$

We do not attempt such an explicit expansion of the projected states here.

The projected states are likely to be the low-lying states of the a nucleons embedded in the mean field of deformed nuclei in which the quadrupole-quadrupole interaction dominates. Because the seniority states and projected states are generally likely to be important in very different physical situations, there is ordinarily no need to compare their quadrupole collectivities. However, both the pseudo-SU(3) model (with its symplectic extension) [12,28,29] and the fermion dynamic symmetry model [17] successfully describe deformed nuclei, assuming that for the $j_a^{N_a}$ configuration the pairing interaction is dominant even in deformed nuclei. In view of this success, a comparison of the $B[E2\text{:proj }(j_a,N_a);J\rightarrow J-2]$ and $B(E2\text{:sen }j_a^{N_a};J\rightarrow J-2)$ values for transitions between the low-lying projected and seniority states, respectively, is of interest. Such a comparison will display the influence of the deformation-induced seniority mixing on the $B(E2)$ values as one goes from the $j_a^{N_a}$ states of definite seniority to the states projected from a deformed $\mathcal{IS}$.

1. B(E2:2→0) values

We want to compare the variation of the $B(E2\text{:}2\rightarrow 0)$ values as a function of the number of particles for the projected states with the corresponding variation for the seniority states. In the seniority scheme, the lowest $J=2$ state has $v=2$, and the ground state has $v=0$. In this scheme, the $B(E2\text{:sen }j_a^{N_a};J=2,v=2\rightarrow J=0,v=0)$ value for N_a particles in $|j_a\rangle$ is related to the $B(E2\text{:sen }j_a^2;J=2,v=2\rightarrow J=0,v=0)$ value for two particles. The ratio

$$R_1(N_a)_{\rm sen}=\frac{B(E2\text{:sen }j_a^{N_a};J=2,v=2\rightarrow J=0,v=0)}{B(E2\text{:sen }j_a^2;J=2,v=2\rightarrow J=0,v=0)} \tag{90}$$

is given by [8]

$$R_1(N_a)_{\rm sen}=\frac{N_a(2j_a+1-N_a)}{2(2j_a-1)}. \tag{91}$$

We have also calculated the corresponding ratios

$$R_1(N_a)_{\rm proj}=\frac{B[E2\text{:proj }(j_a,N_a);2\rightarrow 0]}{B[E2\text{:proj }(j_a,2);2\rightarrow 0]} \tag{92}$$

for the $J=2$ and $J=0$ states projected from the $\mathcal{IS}$ $\mathcal{F}(j_a,N_a)$. While the $B(E2\text{:}J\rightarrow J-2)$ values for the $j_a^{N_a}$ configuration with $N_a>2$ and $j_a>\frac{7}{2}$ are different in the seniority and projection models, these values are the same for the j_a^2 configuration because there is only one state of each J in the latter configuration. [In particular, the $B(E2\text{:}2\rightarrow 0)$ values are the same in both models.] In Table XV, we have compared the $R_1(N_a)_{\rm proj}$ and $R_1(N_a)_{\rm sen}$ values for $N_a=4$, 6, and 8 particles in the $j_a=\frac{9}{2}$, $\frac{11}{2}$, $\frac{13}{2}$, and $\frac{15}{2}$ orbits. From this comparison we conclude that the projected states are (i) significantly less collective than the seniority j_a^4 states, (ii) slightly less collective than the seniority j_a^6 states, and (iii) slightly more collective than the seniority j_a^8 states.

2. B(E2:J→J−2) values for 4≤J≤2j_a−1

In the seniority scheme, the lowest states with $4\leq J\leq 2j_a-1$ have $v=2$. The $B(E2)$ values for the $J\rightarrow J-2$

TABLE XVI. Comparison of $R_2(N_a)_{\rm proj}$ [see Eq. (95)] values with $R_2(N_a)_{\rm sen}$ [see Eq. (93)] and $R_2(N_a)_{\rm SU3}$ [see Eq. (96)] values for $N_a=4$ particles in different j_a orbits. The $B(E2)$ values are in units of α^4.

		$B(E2:\text{proj}\,(j_a,N_a);$ $J\rightarrow J-2)$		$R_2(4)$	$R_2(4)$	$R_2(4)$
j_a	J	$N_a=2$	$N_a=4$	proj	sen	$SU(3)$
$\frac{9}{2}$	4	2.68	3.29	1.23	0.11	2.17
	6	1.86	3.05	1.64	0.11	2.53
	8	0.74	2.81	3.78	0.11	3.67
$\frac{11}{2}$	4	4.06	4.86	1.20	0.25	2.45
	6	3.33	4.90	1.47	0.25	2.70
	8	2.06	4.49	2.18	0.25	3.28
	10	0.77	4.46	5.76	0.25	5.11
$\frac{13}{2}$	4	5.66	6.63	1.17	0.36	2.65
	6	5.07	6.96	1.37	0.36	2.85
	8	3.76	6.67	1.77	0.36	3.22
	10	2.20	6.24	2.85	0.36	4.04
	12	0.79	6.49	8.23	0.36	6.55
$\frac{15}{2}$	4	7.49	8.59	1.15	0.44	2.80
	6	7.07	9.24	1.31	0.44	2.95
	8	5.79	9.14	1.58	0.44	3.23
	10	4.08	8.67	2.12	0.44	3.73
	12	2.30	8.32	3.63	0.44	4.79
	14	0.81	8.88	11.10	0.44	8.11

TABLE XVII. Comparison of $R_2(N_a)_{\rm proj}$ [see Eq. (95)] values with $R_2(N_a)_{\rm sen}$ [see Eq. (93)] and $R_2(N_a)_{\rm SU3}$ [see Eq. (96)] values for $N_a=6$ particles in different j_a orbits. The $B(E2)$ values are in units of α^4.

		$B(E2:\text{proj}\,(j_a,N_a);$ $J\rightarrow J-2)$		$R_2(6)$	$R_2(6)$	$R_2(6)$
j_a	J	$N_a=2$	$N_a=6$	proj	sen	$SU(3)$
$\frac{9}{2}$	4	2.68	3.28	1.22	0.11	2.17
	6	1.86	4.28	2.30	0.11	2.53
	8	0.74	4.12	5.56	0.11	3.67
$\frac{11}{2}$	4	4.06	7.47	1.83	0	1.90
	6	3.33	7.80	2.34	0	2.05
	8	2.06	7.63	3.68	0	2.41
	10	0.77	7.18	9.25	0	3.54
$\frac{13}{2}$	4	5.66	11.12	1.96	0.04	2.65
	6	5.07	11.94	2.35	0.04	2.85
	8	3.76	12.07	3.20	0.04	3.22
	10	2.20	11.93	5.38	0.04	4.04
	12	0.79	11.57	14.34	0.04	6.55
$\frac{15}{2}$	4	7.49	15.26	2.05	0.11	3.76
	6	7.07	16.59	2.35	0.11	4.00
	8	5.79	17.02	2.94	0.11	4.43
	10	4.08	17.09	4.13	0.11	5.20
	12	2.30	16.97	7.31	0.11	6.83
	14	0.81	16.68	20.14	0.11	11.92

transitions between the $v=2$ states of the $j_a^{N_a}$ configuration are related to the $B(E2)$ values for the transitions between the corresponding states of the j_a^2 configuration. The ratio of these two values

$$R_2(N_a)_{\rm sen}=\frac{B(E2{:}\,\text{sen}\;\; j_a^{N_a};J=2,v=2\rightarrow J-2,v=2)}{B(E2{:}\,\text{sen}\;\; j_a^2;J=2,v=2\rightarrow J-2,v=2)} \tag{93}$$

is independent of J and is given by [8]

$$R_2(N_a)_{\rm sen}=\left[\frac{2j_a+1-2N_a}{2j_a+1-2v}\right]^2. \tag{94}$$

In Tables XVI, XVII, and XVIII, we list the ratios $R_2(N_a)_{\rm sen}$ and compare them with the ratios

$$R_2(N_a)_{\rm proj}=\frac{B(E2{:}\,\text{proj}\;\; (j_a,N_a);J\rightarrow J-2)}{B(E2{:}\,\text{proj}\;\; (j_a,2);J\rightarrow J-2)} \tag{95}$$

calculated for the projected states (with $4\leqslant J\leqslant 2j_a-1$). We also include in these tables the corresponding ratios

$$R_2(N_a)_{\rm SU(3)}=\frac{B(E2{:}\,\text{SU3}[\lambda_{\rm eq}^{N_a},0];J\rightarrow J-2)}{B(E2{:}\,\text{SU3}[\lambda_{\rm eq}^{2},0];J\rightarrow J-2)} \tag{96}$$

for the SU(3) states belonging to the equivalent representation $[\lambda_{\rm eq},0]$. The values of $\lambda_{\rm eq}$ for the $(j_a,N_a)\mathcal{IS}$'s are listed in Table IV. The $R_2(N_a)$ values show that the $B(E2)$ values for the transitions between the (j_a,N_a) projected states are similar in collectivity to those between the SU(3) states and are significantly more collective than those for the transitions within the $v=2$ bands of the $j_a^{N_a}$ configurations. Note that $R_2(N_a)_{\rm sen}=0$ for the $(\frac{11}{2})^6$ and $(\frac{15}{2})^8$ states. These zero values reflect the seniority selection rule that even tensor elements between the states of the same seniority vanish at midshell.

3. B(E2:$J_i=2j_a+1\rightarrow J_f=2j_a-1$) values

The $R_2(N_a)_{\rm sen}$ values listed in Tables XVI, XVII, and XVIII are $\ll 1$ which implies that the $E2$ transitions within the $v=2$ band are weak. This band terminates at $J=2j_a-1$. The lowest state with $J=2j_a+1$ has $v=4$. We are interested in the $B(E2)$ values for transitions across this seniority gap. A general expression for the reduced $E2$ ma-

trix element for such transitions across a $v \rightarrow v-2$ seniority gap has been derived by Talmi [37] as

$$(j_a^{N_a}, v=N_a, J_i||T^{(2)}||j_a^{N_a}, v=N_a-2, J_f=J_i-2)^2 = (j_a||T^{(2)}||j_a)^2 \frac{4}{5} \frac{(N_a-2)(2j_a+3-N_a)+5}{2j_a+5-2N_a} \times [1-2(N_a-2)F_{j_a}(N_a)], \quad (97)$$

where

$$J_i=(N_a-2)j_a-\frac{1}{2}(N_a-2)(N_a-3)+2 \quad (98)$$

and the factor $F_{j_a}(N_a)$ is given by

$$F_{j_a}(N_a)=\frac{5\times 6}{(2j_a-1)(2j_a)(2j_a+1)(2j_a+2)(2j_a+3)} \times \left\{ 4j_a(2j_a-1)+(N_a-3)\left[6j_a^2-7j_a+1 + \frac{1}{6}(4j_a^2-14j_a+5)(2N_a-5)-(j_a-1) \times (N_a-2)(N_a-3)+\frac{1}{30}[6(N_a-3)^3 + 9(N_a-3)^2+N_a-4] \right] \right\}. \quad (99)$$

For the case $N_a=4$ particles, we consider the ratio

$$R_3(N_a=4)_{\rm sen}=\frac{B(E2{:}\,{\rm sen}\ \ j_a^4; v_i=4, J_i=2j_a+1 \rightarrow v_f=2, J_f=2j_a-1)}{B(E2{:}\,{\rm sen}\ \ j_a^2; v_i=2, J_i=2 \rightarrow v_f=0, J_f=0)}. \quad (100)$$

From Talmi's general formula and the definition of $B(E2)$ value, we obtain

$$R_3(N_a=4)_{\rm sen}=\frac{2j_a+1}{2j_a+3}[1-2F_{j_a}(4)]. \quad (101)$$

The factors $F_j(4)$ for the $j=\frac{9}{2}$, $\frac{11}{2}$, $\frac{13}{2}$, and $\frac{15}{2}$ states are 0.076, 0.047, 0.032, and 0.022, respectively. The values of $R_3(N_a=4)_{\rm sen}$, for the j_a^4 configurations, obtained from Eq. (100), are compared in Table XIX with the corresponding ratio

$$R_3(N_a=4)_{\rm proj}=\frac{B[E2{:}\,{\rm proj}\ \ (j_a,4); J_i=2j+1 \rightarrow J_f=2j-1]}{B[E2{:}\,{\rm proj}\ \ (j_a,2); J_i=2 \rightarrow J_f=0]} \quad (102)$$

of the $B(E2)$ values for the transitions between the projected states of the same J values considered in $R_3(N_a=4)_{\rm sen}$. On the average, the transitions between the projected states are stronger by about 80% than the transitions between the corresponding seniority states.

In Fig. 13, we summarize the qualitative differences between the quadrupole properties [spectroscopic quadrupole moments $Q(J)$ and $B(E2{:}J \rightarrow J-2)$ values] for the low-lying projected and seniority states. Both sets of states belong to the $j_a^{N_a}$ configuration, and this particular figure is for the $(\frac{13}{2})^6$ configuration. The projected states form a strongly coupled chain of quadrupole collectivity, whereas the $v=2$ part of the seniority band is totally devoid of such collectiv-

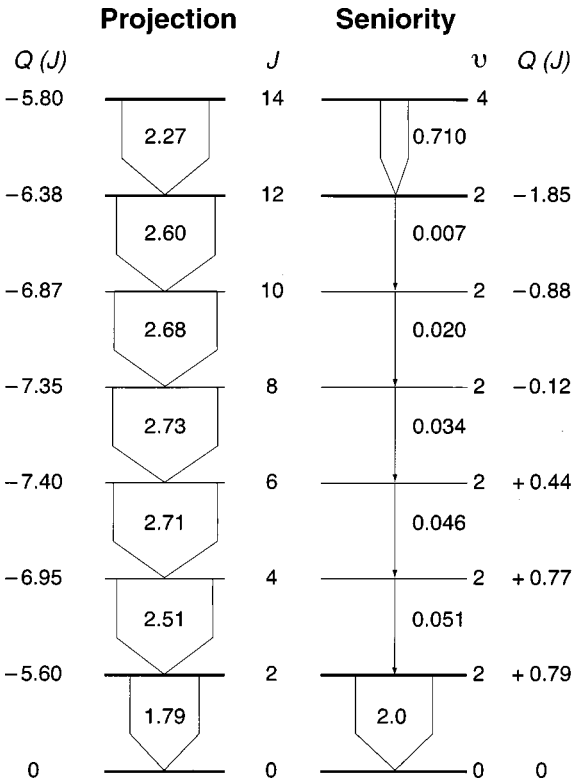

FIG. 13. Comparison between the spectroscopic quadrupole moments $Q(J)$ and the $B(E2{:}J \rightarrow J-2)$ values for the low-lying projected and seniority states of the $(\frac{13}{2})^6$ configuration. The $Q(J)$ values are in units of α^2 and the $B(E2{:}J \rightarrow J-2)$ values (associated with the downward arrows) in units of $B[E2{:}(\frac{13}{2})^2; 2 \rightarrow 0]$. The latter $B(E2)$ value is the same for the projected and seniority states. See related discussion in Sec. V I.

TABLE XVIII. Comparison of $R_{2(N_a)_{\rm proj}}$ [see Eq. (95)] values with $R_2(N_a)_{\rm sen}$ [see Eq. (93)] and $R_2(N_a)_{\rm SU3}$ [see Eq. (96)] values for $N_a=8$ particles in different j_a orbits. The $B(E2)$ values are in units of α^4.

		$B(E2:\text{proj}\,(j_a,N_a);$ $J\to J-2)$		$R_2(8)$	$R_2(8)$	$R_2(8)$
j_a	J	$N_a=2$	$N_a=8$	proj	sen	$SU(3)$
$\frac{9}{2}$	4	2.68	2.68	1	1	1
	6	1.86	1.86	1	1	1
	8	0.74	0.74	1	1	1
$\frac{11}{2}$	4	4.06	7.64	1.88	0.25	2.45
	6	3.33	7.73	2.32	0.25	2.70
	8	2.06	7.10	3.45	0.25	3.28
	10	0.77	6.04	7.84	0.25	5.11
$\frac{13}{2}$	4	5.66	13.75	2.43	0.04	3.76
	6	5.07	14.66	2.59	0.04	4.08
	8	3.76	14.65	3.90	0.04	4.72
	10	2.20	14.13	6.42	0.04	6.08
	12	0.79	13.26	16.78	0.04	10.29
$\frac{15}{2}$	4	7.49	20.88	2.79	0	4.87
	6	7.07	22.65	3.20	0	5.20
	8	5.79	23.19	4.01	0	5.80
	10	4.08	23.14	5.67	0	6.88
	12	2.30	22.70	9.87	0	9.16
	14	0.81	21.98	27.14	0	16.30

ity. It seems unlikely that such a seniority band can play any significant role in the structure of the yrast band of a deformed nucleus.

VI. YRAST BAND OF A SYSTEM OF ABNORMAL-PARITY NUCLEONS

A nucleus contains both protons and neutrons in abnormal-parity states. In this section, we calculate the collective properties of the yrast band projected from the $\mathcal{IS}$ of such protons and neutrons. We consider as an example a system of $n_\pi=4$ protons in the $j_\pi=0h_{11/2}$ state and $n_\nu=4$ neutrons in the $j_\nu=0i_{13/2}$ state in the mean field of a deformed nucleus. According to Table XX, such a configuration of the abnormal-parity nucleons should occur in a nucleus with at least $N_\pi=10$ protons in the 50–82 shell and $N_\nu=10$ neutrons in the 82–126 shell. Such a nucleus is $^{152}_{60}\mathrm{Nd}_{92}$. The total $\mathcal{IS}\mathcal{F}_{\pi\nu}(n_\pi=4,n_\nu=4)$ of the a nucleons is the product of the $\mathcal{IS}$'s of the protons and neutrons:

$$\mathcal{F}_{\pi\nu}(n_\pi=4,n_\nu=4)=\mathcal{F}_\pi\left(j_\pi=\frac{11}{2},n_\pi=4\right)\otimes\mathcal{F}_\nu\left(j_\nu=\frac{13}{2},n_\nu=4\right), \tag{103}$$

TABLE XIX. Comparison of $R_3(N_a)_{\rm proj}$ values [see Eq. (102)] with $R_3(N_a)_{\rm sen}$ values [see Eq. (101)] values for $N_a=4$ particles in different j_a orbits.

j_a	$R_3(4)_{\rm proj}$	$R_3(4)_{\rm sen}$
$\frac{9}{2}$	1.21	0.71
$\frac{11}{2}$	1.41	0.78
$\frac{13}{2}$	1.55	0.82
$\frac{15}{2}$	1.61	0.85

where $\mathcal{F}_\pi$ and $\mathcal{F}_\nu$ are four-particle Slater determinants in which the orbits $k_{\pi,\nu}=\pm\frac{1}{2}$ and $\pm\frac{3}{2}$ are occupied. The states $\mathcal{F}_\pi$ and $\mathcal{F}_\nu$ can be expanded as

$$\mathcal{F}_\pi\left(j_\pi=\frac{11}{2},n_\pi=4\right)=\sum_{J_\pi} C_{J_\pi K_\pi}\left|\left(\frac{11}{2}\right)^4;J_\pi\right\rangle \tag{104}$$

and

$$\mathcal{F}_\nu\left(j_\nu=\frac{13}{2},n_\nu=4\right)=\sum_{J_\nu} C_{J_\pi K_\nu}\left|\left(\frac{13}{2}\right)^4;J_\nu\right\rangle. \tag{105}$$

We have calculated the values of $|C_{J_\pi}|^2$ and $|C_{J_\nu}|^2$ for these $\mathcal{IS}$'s and listed them in Table II. The total $\mathcal{IS}$ $\mathcal{F}_{\pi\nu}$ can be expanded in terms of the states $|[J_\pi\otimes J_\nu]J\rangle$ of total angular momentum J as

$$\mathcal{F}_{\pi\nu}(n_\pi=4,n_\nu=4)=\sum_J\sum_{J_\pi}\sum_{J_\nu} C_{J_\pi}C_{J_\nu}(J_\pi J_\nu 00|J0)|[J_\pi\otimes J_\nu]J\rangle. \tag{106}$$

The state of angular momentum J projected from $\mathcal{F}_{\pi\nu}$ has the structure

$$|J\rangle=N_J\sum_{J_\pi}\sum_{J_\nu} C_{J_\pi}C_{J_\nu}(J_\pi J_\nu 00|J0)|[J_\pi\otimes J_\nu]J\rangle, \tag{107}$$

where N_J is a normalization constant given by

$$N_J=\left[\sum_{J_\pi}\sum_{J_\nu}|C_{J_\pi}C_{J_\nu}(J_\pi J_\nu 00|J0)^2\right]^{-1/2}. \tag{108}$$

We write the state $|J\rangle$ as

$$|J\rangle=\sum_{J_\pi}\sum_{J_\nu} A[J:J_\pi,J_\nu]|[J_\pi\otimes J_\nu]J\rangle, \tag{109}$$

where

$$A[J:J_\pi,J_\nu]=N_J C_{J_\pi}C_{J_\nu}(J_\pi J_\nu 00|J0). \tag{110}$$

A. Distribution of angular momenta in $\mathcal{F}_{\pi\nu}$

The state $\mathcal{F}_{\pi\nu}$ [see Eq. (106)] can be expanded in terms of the states $|J\rangle$ [see Eq. (109)] as

TABLE XX. Partition of N valence nucleons into N_n nucleons in the normal-parity and N_a nucleons in the abnormal-parity states and their average SU(3) representations for the yrast bands. See Sec. VII.

N	N_n	N_a	$[\widetilde{\lambda_n},\widetilde{\mu_n}]$	$[\lambda_{n_{\rm eff}},0]$	$[\lambda_{a_{\rm ave}},0]$	N	N_n	N_a	$[\widetilde{\lambda_n},\widetilde{\mu_n}]$	$[\lambda_{n_{\rm eff}},0]$	$[\lambda_{a_{\rm ave}},0]$
(a) 50–82 major shell with $j_a = h_{11/2}$ (neutrons and protons)						(c) 82–126 major shell with $j_a = i_{13/2}$ (protons)					
8	6	2	[12,0]	[12,0]		4	2 or 4	2 or 0	[8,0] or [12,2]	[8,0] or [14,0]	
10	6	4	[12,0]	[12,0]	[16,0]	6	4	2	[12,2]	[14,0]	
12	6 or 8	6 or 4	[12,0] or [10,4]	[12,0] or [14,0]	[14,0] or [16,0]	8	4	4	[12,2]	[14,0]	[22,0]
14	8	6	[10,4]	[14,0]	[14,0]	10	6	4	[18,0]	[18,0]	[22,0]
16	10	6	[10,4]	[14,0]	[14,0]	12	6	6	[18,0]	[18,0]	[20,0]
18	10	8	[10,4]	[14,0]	[10,0]	14	8	6	[18,4]	[22,0]	[20,0]
20	12	8	[12,0]	[12,0]	[10,0]	16	10	6	[20,4]	[24,0]	[20,0]
						18	10	8	[20,4]	[24,0]	[10,0]
(b) 82–126 major shell with $j_a = i_{13/2}$ (neutrons)						20	10	8	[24,0]	[24,0]	[10,0]
8	6	2	[18,0]	[18,0]							
10	6	4	[18,0]	[18,0]	[22,0]	(d) 126–184 major shell with $j_a = j_{15/2}$ (neutrons)					
12	8	4	[18,4]	[22,0]	[22,0]	8	6	2	[24,0]	[24,0]	
14	8	6	[18,4]	[22,0]	[14,0]	10	6	4	[24,0]	[24,0]	[30,0]
16	10	6	[20,4]	[24,0]	[14,0]	12	8	4	[26,4]	[30,0]	[30,0]
18	10	8	[20,4]	[24,0]	[16,0]	14	8	6	[26,4]	[30,0]	[28,0]
20	12	8	[24,0]	[24,0]	[16,0]	16	10	6	[30,4]	[34,0]	[28,0]
22	14	8	[20,6]	[26,0]	[16,0]	18	10	8	[30,4]	[34,0]	[28,0]
24	16	8	[18,8]	[26,0]	[16,0]	20	12	8	[36,0]	[36,0]	[28,0]
						22	14	8	[34,6]	[40,0]	[28,0]
						24	16	8	[34,8]	[42,0]	[28,0]

$$\mathcal{F}_{\pi\nu}=\sum_J C_J|J\rangle, \tag{111}$$

where $|C_J|^2=(1/N_J)^2$ is the probability that $\mathcal{F}_{\pi\nu}$ contains angular momentum J. The normalization constant N_J is given by Eq. (108). The distribution of $|C_J|^2$ vs J is shown in Fig. 14 for the coupled $\pi(\frac{11}{2})^4\otimes\nu(\frac{13}{2})^4$ system.

We recall that the distribution of the angular momenta J_π and J_ν in $\mathcal{F}_\pi$ and $\mathcal{F}_\nu$ [see Eqs. (104) and (105)] are well reproduced by the distributions of angular momenta in the SU(3) representations $\lambda_\pi=(\lambda_\pi)_{\rm eq}=(\lambda_\pi)_{\rm ave}=16$ and $\lambda_\nu=(\lambda_\nu)_{\rm ave}=22$ [see Figs. 2(b) and 2(c)]. [Note that the equivalent SU(3) representation for the neutrons is $(\lambda_\nu)_{\rm eq}=20$.] We find that the distribution of angular momenta in $\mathcal{F}_{\pi\nu}$ to be nearly indistinguishable from that in the average representation $[\lambda_{\pi\nu\ {\rm ave}},0]$ with $\lambda_{\pi\nu\ {\rm ave}}=\lambda_{\pi\ {\rm ave}}+\lambda_{\nu\ {\rm ave}}=38$. The equivalent representation for the $\pi(\frac{11}{2})^4\otimes\nu(\frac{13}{2})^4$ system is $[\lambda_{\rm eq},0]=[36,0]$. The distribution of angular momenta in the [36,0] representation is shown in Fig. 14. The distribution of angular momenta in the coupled $\pi\nu$ system of a nucleons follows to a good approximation the rules of coupling of SU(3) representations, namely

$$[\lambda_\pi,0]\otimes[\lambda_\nu,0]\rightarrow[\lambda_{\pi\nu}=\lambda_\pi+\lambda_\nu,0]. \tag{112}$$

B. Quadrupole properties of the $\pi\nu$ band

The electric quadrupole operator of the $\pi\nu$ system can be written as

$$Q_e=e_\pi Q_\pi+e_\nu Q_\nu, \tag{113}$$

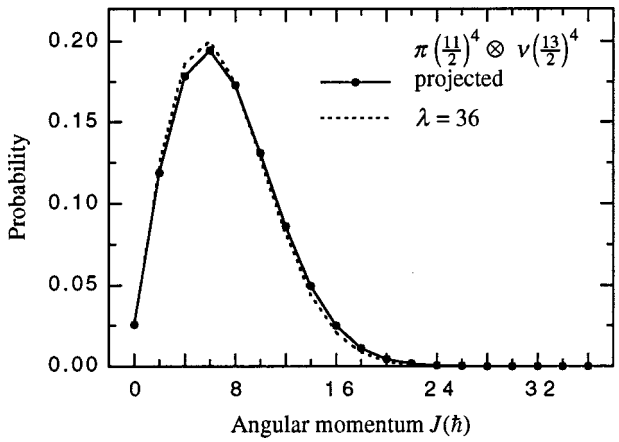

FIG. 14. Probability distribution $P_1(J)$ of angular momenta for the $\mathcal{F}_{\pi\nu}[\pi(\frac{11}{2})^4\otimes\nu(\frac{13}{2})^4]$ $\mathcal{IS}$ compared to the corresponding distribution for the SU(3) $\mathcal{F}_K[\lambda_{\rm eq}=36,0]$ $\mathcal{IS}$. See related discussion in Sec. VI A.

where $e_{\pi(\nu)}$ are the effective charges for protons(neutrons). We want to evaluate the reduced matrix elements

$$(J_f\|Q_e\|J_i)=e_\pi(J_f\|Q_\pi\|J_i)+e_\nu(J_f\|Q_\nu\|J_i) \tag{114}$$

of Q_e between the projected states $|J\rangle$ of Eq. (109). Using this equation and Eq. (1A-72a) of Ref. [20], we obtain

$$(J_f\|Q_\pi\|J_i)=\sqrt{(2J_f+1)(2J_i+1)}$$
$$\times\sum_{J'_\pi}\sum_{J_{\nu'}}\sum_{J_\pi}\sum_{J_\nu}A[J_f:J'_\pi,J'_\nu]A[J_i:J_\pi,J_\nu]$$
$$\times\left[(-1)^{J'_\pi+J'_\nu+J_i+2}\begin{Bmatrix}J_\pi & J_\nu & J_i\\ J_f & 2 & J'_\pi\end{Bmatrix}\right.$$
$$\left.\times(J'_\pi\|Q_\pi\|J_\pi)\,\delta_{J'_\nu J_\nu}\right] \tag{115}$$

and

$$(J_f\|Q_\nu\|J_i)=\sqrt{(2J_f+1)(2J_i+1)}$$
$$\times\sum_{J'_\pi}\sum_{J'_\nu}\sum_{J_\pi}\sum_{J_\nu}A[J_f:J'_\pi,J'_\nu]A[J_i:J_\pi,J_\nu]$$
$$\times\left[(-1)^{J_\pi+J_\nu+J_f+2}\begin{Bmatrix}J_\pi & J_\nu & J_i\\ 2 & J_f & J'_\nu\end{Bmatrix}\right.$$
$$\left.\times(J'_\nu\|Q_\nu\|J_\nu)\,\delta_{J'_\pi J_\pi}\right]. \tag{116}$$

For the system under consideration, $(J'_\pi\|Q_\pi\|J_\pi)$ and $(J'_\nu\|Q_\nu\|J_\pi)$ are just the reduced matrix elements $[(\frac{11}{2},4);J'\|Q\|(\frac{11}{2},4);J]$ and $[(\frac{13}{2},4);J'\|Q\|(\frac{13}{2},4);J]$, respectively, given in Table XIII. We use these values to calculate the matrix elements $(J_f\|Q_\pi\|J_i)$ and $(J_f\|Q_\nu\|J_i)$.

The $B(E2{:}J\to J-2)$ values with effective charges $e_\pi=e_\nu=1e$ are plotted in Fig. 15(a) for $J=0$ to $J=J_{\max}=J_{\pi\ \max}+J_{\nu\ \max}=36$. The values obtained with the effective charges $e_\pi=1.5e, e_\nu=0.5e$ were quite similar and are not shown.

We recall that the $B(E2{:}J\to J-2)$ values for the projected $\pi(\frac{11}{2})^4$ and $\nu(\frac{13}{2})^4$ states show two maxima [see Fig. 8(b)]. They are smoothed out for the coupled $\pi(\frac{11}{2})^4\otimes\nu(\frac{13}{2})^4$ system, as shown in Fig. 15(a). The equivalent SU(3) representation $[\lambda_{\rm eq},0]$ for this system (see Table III) is given by $\lambda_{\rm eq}=\lambda_{\pi\ \rm eq}+\lambda_{\nu\ \rm eq}=16+20=36$. The $B(E2{:}\mathrm{SU3}[\lambda_{\rm eq},0];J\to J-2)$ values normalized to the $B[E2{:}\mathrm{proj}(\frac{11}{2},4)\otimes(\frac{13}{2},4);2\to0]$ value are also shown in Fig. 15(a). The trend of the SU(3) $[\lambda_{\rm eq}=36,0]$ values is significantly less collective than that for the projected states. The SU(3) representation $[\lambda_{B(E2)},0]$ for which the $B(E2{:}\mathrm{SU3}[\lambda_{B(E2)},0];J\to J-2)$ trend best agrees with the $B(E2{:}\mathrm{proj};J\to J-2)$ trend is found to have $\lambda_{B(E2)}=54$, which is appreciably larger than $\lambda_{\rm eq}=36$.

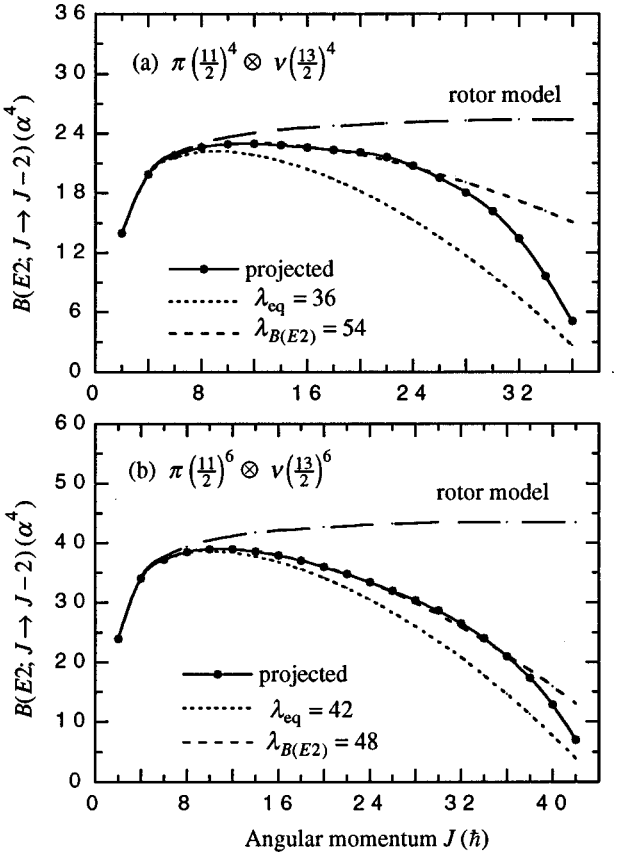

FIG. 15. $B(E2{:}J\to J-2)$ values for the yrast band projected from the coupled $\pi\nu$ intrinsic states (see Sec. VI B). The SU(3) and rotor $B(E2{:}J\to J-2)$ values are normalized to the $B(E2{:}\mathrm{proj};2\to0)$ values.

A reason for this large value of $\lambda_{B(E2)}$ may be the pronounced second hump in the $B(E2{:}\mathrm{proj};J\to J-2)$ vs J trend for the j_a^4 configurations [see Fig. 8(b)]. This feature tends to increase the $B(E2{:}\mathrm{proj};J\to J-2)$ values for the coupled $\pi\nu$ system at higher values of J and makes the $B(E2)$ vs J trend decrease more slowly. Hence the $\lambda_{B(E2)}$ value for which the $B(E2{:}\mathrm{SU3};J\to J-2)$ trend agrees with the $B(E2{:}\mathrm{proj};J\to J-2)$ trend for the $\pi\nu$ system is larger than the $\lambda_{\rm eq}$ value. To verify this conjecture we carried out a calculation of the $B(E2{:}\mathrm{proj};J\to J-2)$ values for the yrast band projected from the $\mathcal{IS}$

$$\mathcal{F}_{\pi\nu\ a}(N_{\pi a}=6,N_{\nu a}=6)=\mathcal{F}_{\pi a}\left(\frac{11}{2},6\right)\otimes\mathcal{F}_{\nu a}\left(\frac{13}{2},6\right). \tag{117}$$

As can be seen in Fig. 8(c), the projected $B(E2)$ trends for the $(\frac{11}{2})^6$ and $(\frac{13}{2})^6$ bands do not have the pronounced second maxima noted for the $(\frac{11}{2})^4$ and $(\frac{13}{2})^4$ bands. In addition, as shown in Figs. 9(a) and 9(b), these projected trends for the $(\frac{11}{2})^6$ and $(\frac{13}{2})^6$ bands are in good agreement with the SU3 trends with $\lambda_{\pi\ B(E2)}=20$ and $\lambda_{\nu\ B(E2)}=28$, respectively. On the basis of these observations, one expects that the projected $B(E2)$ trend for the coupled $\pi(\frac{11}{2})^6\otimes\nu(\frac{13}{2})^6$ band might

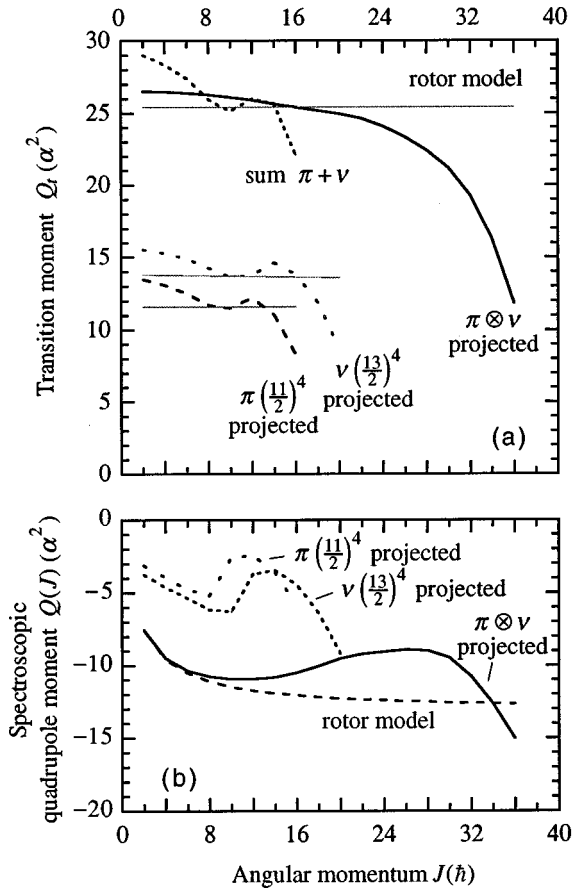

FIG. 16. (a) Transition moments $Q_t(J)$ and (b) spectroscopic quadrupole moments $Q(J)$ for the yrast band projected from the $\mathcal{F}_{\pi\nu}[\pi(\frac{11}{2})^4\otimes\nu(\frac{13}{2}4]$ $\mathcal{IS}$. See related discussion in Sec. VI B.

resemble the SU3 $B(E2)$ trend with $\lambda_{\pi\nu\ B(E2)}=48$. This is indeed the case, as is shown in Fig. 15(b). Also shown in Fig. 15(b) is the SU3 $B(E2)$ trend corresponding to the equivalent $\lambda_{\pi\nu\ \mathrm{eq}}=\lambda_{\pi\ \mathrm{eq}}+\lambda_{\nu\ \mathrm{eq}}=42$ (see Table III). For the coupled system, the equivalent SU(3) trend is significantly less collective than the projected trend.

The transition moments $Q_t(J)$ deduced from the $B(E2{:}J-2\rightarrow J)$ values for the projected $\pi\nu$ band are compared with the rotor-model values in Fig. 16(a). The $Q_t(J)$ values for the rotor model are constant and was set equal to the total intrinsic quadrupole moment: $Q_0(\pi\nu\mathrm{rot})=Q_0[\pi,(\frac{11}{2})^4]+Q_0[\nu,(\frac{13}{2})^4]=25.49\alpha^2$ (see Table V). The trend of the projected Q_t values is close to the rotor-model trend for the states up to $J=24$. A smooth but rapid decrease in the projected Q_t values relative to the rotor values occurs for states with $J>24$. For comparison, we also show in Fig. 16(a) the $Q_{t\pi}$ and $Q_{t\nu}$ values as a function of J_π and J_ν. The bumps in these Q_t values have been smoothed out in the $Q_t(J)$ values for the coupled $\pi\nu$ yrast band.

The spectroscopic quadrupole moments $Q(J)$ of the states J of the projected $\pi\nu$ band are compared with the rotor-band values in Fig. 16(b). The latter values are normalized to the projected $Q(J=2)$ value. The trend of the projected $Q(J)$ values differs significantly from the rotor-model trend beyond $J=8$. The results of this section show that for the coupled $\pi\nu$ system, both the distribution of angular momenta and the $B(E2{:}J\rightarrow J-2)$ vs J trends show approximate SU3-like ''additive'' property, namely, $\lambda_{\pi\nu}=\lambda_\pi+\lambda_\nu$.

VII. CONTRIBUTIONS OF NUCLEONS IN THE NORMAL- AND ABNORMAL-PARITY STATES TO THE YRAST BAND

In this section, we use the properties of the projected states $|(j_a,N_{\alpha a});J_{\alpha a}K_{\alpha a}\rangle$ ($\alpha=\pi$ or ν) of a nucleons discussed in the previous sections together with the properties of the states $|(j_n,N_{\alpha n});J_{\alpha n}K_{\alpha n}\rangle$ of n nucleons projected from their $\mathcal{IS}$'s to estimate the relative contributions of the a and n nucleons to (i) the total angular momentum J of the yrast band of a deformed nucleus and (ii) the $B(E2{:}J\rightarrow J-2)$ value for an yrast-band transition.

In a simple description of an axially symmetrically deformed nucleus within the configuration space of a single major shell, the Nilsson $\mathcal{IS}$ of the nucleus consists of $N_{\pi n}$ valence protons and $N_{\nu n}$ valence neutrons in the n states and $N_{\pi a}$ valence protons and $N_{\nu a}$ valence neutrons in the a states. The total numbers of valence particles in the n and a states are $N_n=N_{\pi n}+N_{\nu n}$ and $N_a=N_{\pi a}+N_{\nu a}$. The total Nilsson $\mathcal{IS}$ is a product of the Nilsson states of the n and a nucleons.

For deformed nuclei, we have listed in Table VIII of Ref. [3] the partition of the N valence nucleons in a major shell into $N_{\pi n}$, $N_{\nu n}$, $N_{\pi a}$, and $N_{\nu a}$. In a portion of this table, which is reproduced herein in Table XX, we have listed the effective pseudo-SU(3) representations $[\tilde{\lambda}^n_{\mathrm{eff}},0]$ appropriate for the different number of nucleons occupying the n orbitals. The distribution of angular momenta $|J_n\rangle$ contained in the representation $[\tilde{\lambda}^n_{\mathrm{eff}},0]$ can be determined using Eq. (3).

The Nilsson $\mathcal{IS}$ of a particles is specified in each major shell by the number N_a listed in Table XX. These $\mathcal{IS}$'s are exactly the $\mathcal{IS}$'s $\mathcal{F}_K(j_a,N_a)$ described in Sec. II B. In Table XX, we have also listed the average SU(3) representations $[\lambda_{a\ \mathrm{ave}},0]$ (taken from Table III) for which the distributions of angular momenta are close to those for the $\mathcal{IS}$'s $\mathcal{F}_k(j_a,N_a)$.

In Ref. [4], we showed that the distribution of angular momenta in the coupled proton-neutron $\mathcal{IS}$ $\mathcal{F}_{\pi\nu}=\mathcal{F}(j_{\pi a},N_{\pi a})\mathcal{F}(j_{\nu a},N_{\nu a})$ (of ^{238}U or ^{168}Er) is almost identical to that in the SU(3) $\mathcal{IS}$ with $[\lambda_{\pi\nu a}=\lambda_{\pi a}+\lambda_{\nu a},0]$. Such a result is even more valid for the coupled $\pi\nu$ $\mathcal{IS}$'s of n nucleons for which the pseudo-SU(3) symmetry exists. In the following section we use the information contained in Table XX to calculate the contribution of n and a nucleons to the total angular momentum J of the yrast band of a deformed nucleus.

A. Contribution of *a* nucleons to the angular momentum of an yrast state

The total Nilsson $\mathcal{IS}$ of an even-even nucleus with N valence nucleons can be written as

$$\mathcal{F}_K(N)=\mathcal{F}_{K_n}(N_n)\mathcal{F}_{K_a}(N_a), \tag{118}$$

with $K_n=K_a=0$ and $K=K_n+K_a=0$. The states $\mathcal{F}(N_n)$ and $\mathcal{F}(N_a)$ can be expanded as $\mathcal{F}(N_n)=\Sigma_{J_n}C_{J_n}|J_n\rangle$ and $\mathcal{F}(N_a)=\Sigma_{J_a}C_{J_a}|J_a\rangle$. The total $\mathcal{IS}$ $\mathcal{F}_K$ can be expanded as

$$\mathcal{F}_K(N)=\sum_J \sum_{J_n} \sum_{J_a} C_{J_n}C_{J_a}(J_nJ_a00|J0)|[J_n\otimes J_a]J\rangle. \tag{119}$$

The yrast state $|J\rangle$ of the nucleus is the state with this J projected from $\mathcal{F}_K(N)$ and can be expressed as

$$|J\rangle=N_J\sum_{J_n} \sum_{J_a} C_{J_n}C_{J_a}(J_nJ_a00|J0)|[J_n\otimes J_a]J\rangle \tag{120a}$$

$$=\sum_{J_n} \sum_{J_a} A(J;J_n,J_a)[J_n\otimes J_a]J\rangle, \tag{120b}$$

where the normalization coefficient N_J is given by

$$N_J=\left[\sum_{J_n} \sum_{J_a} |C_{J_n}C_{J_a}(J_nJ_a00|J0)|^2\right]^{-1/2} \tag{121}$$

and

$$A(J;J_n,J_a)=N_JC_{J_n}C_{J_a}(J_nJ_a00|J0). \tag{122}$$

The probability $P(J;J_nJ_a)$ that the yrast state $|J\rangle$ contains angular momenta J_n and J_a is given by $|A(J;J_nJ_a)|^2$. The probabilities $P(J;J_n)$ and $P(J;J_a)$ that the n or a nucleons contribute angular momentum J_n or J_a to the yrast state $|J\rangle$ are given by

$$P(J;J_n)=\sum_{J_a} |A(J;J_n,J_a)|^2, \tag{123a}$$

$$P(J;J_a)=\sum_{J_n} |A(J;J_n,J_a)|^2. \tag{123b}$$

To illustrate the usefulness of Table XX, we ask the question: What is the probability that the angular momentum of the $J=4$ yrast state of $^{156}_{64}Gd_{92}$ is contributed entirely by the n or a nucleons? To answer this question, we note that $^{156}_{64}Gd_{92}$ has $N_\pi=14$ valence protons in the 50–82 shell with $N_{\pi n}=8$ protons in the n states and $N_{\pi a}=6$ protons in the $1h_{11/2}$ a state. The pseudo-SU(3) representation of the eight n protons is $[\widetilde{\lambda_{\pi n}}=10,\widetilde{\mu_{\pi n}}=4]$ and, hence, its effective SU(3) representation for the $K_{\pi n}=0$ band is $[\lambda_{\pi n\ \mathrm{eff}},0]=[14,0]$, which is listed in Table XX. The average SU(3) representation for the six a protons in the $h_{11/2}$ state is $[\lambda_{\pi a\ \mathrm{ave}},0]=[14,0]$ from Table III. For the $N_\nu=10$ valence neutrons in the 82–126 shell, $N_{\nu n}=6$, and $N_{\nu a}=4$. The pseudo-SU(3) representation of 6 neutrons in this n shell is [18,0]; consequently, its effective SU(3) representation is also $[\lambda_{\nu n\ \mathrm{eff}},0]=[18,0]$. The average SU(3) representation of the four a neutrons in the $i_{13/2}$ state is $[\lambda_{\nu a\ \mathrm{ave}},0]=[22,0]$. Thus the total effective representations $[\lambda_n,0]$ and $[\lambda_a,0]$ are given by $\lambda_n=\lambda_{\pi n\ \mathrm{eff}}+\lambda_{\nu n\ \mathrm{eff}}$ and $\lambda_a=\lambda_{\pi a\ \mathrm{ave}}+\lambda_{\nu a\ \mathrm{ave}}$. These representations are $[\lambda_n,0]=[32,0]$ and $[\lambda_a,0]=[36,0]$. The distributions of the total angular momenta J in the Nilsson $\mathcal{IS}$ of ^{156}Gd will be very similar to the distribution of angular momenta in the SU(3) representation $[\lambda,0]=[\lambda_n+\lambda_a,0]=[68,0]$. The yrast state $|J\rangle$ of ^{156}Gd can be expressed in terms of the coupled states $|[J_n\otimes J_a]J\rangle$ of its n and a nucleons as [see Eq. (120b)]

$$|J,\mathrm{yrast}\rangle=N_J\sum_{J_n} \sum_{J_a} C_{J_n}[32,0]C_{J_a}[36,0](J_nJ_a00|J0)| \times[J_n\otimes J_a]J\rangle. \tag{124}$$

The expansion coefficients $C_{J_n}[32,0]$ are obtained for different J_n values from Eq. (3) using $\lambda=\lambda_n=32$. Similarly, the coefficients $C_{J_a}[36,0]$ are calculated for different J_a values using $\lambda=\lambda_a=36$. Equations (121)–(124) can be used, for example, to compare the probabilities that $n(a)$ nucleons contribute angular momentum $J_{n(a)}=4$ to the yrast state $|J=4\rangle$ of ^{156}Gd. If $J_n=4$ in the yrast state $|J=4\rangle$, the a nucleons can have angular momenta $J_a=0$, 2, 4, 6, and 8. Similarly, if $J_a=4$, the allowed angular momenta for the n nucleons are also $J_n=0$, 2, 4, 6, and 8 in the $|J=4\rangle$ state. Using Eqs. (121)–(124), we obtain $P_n(J_n=4,J=4)=0.273$ and $P_a(J_a=4,J=x)=0.269$. Both n and a nucleons contribute almost equally to the low-lying yrast states.

We can pose a more detailed question such as, ''What is the average angular momentum contributed by the four $i_{13/2}$ neutrons to the yrast state $|J\rangle$ of ^{156}Gd with $J=14$?'' To answer this question, we express the yrast state as

$$|J\rangle=N_J\sum_{J_s} \sum_{J_{\nu a}} C_{J_s}[\lambda-\lambda_{\nu a},0]C_{J_{\nu a}}[\lambda_{\nu a},0]|[J_f\otimes J_{\nu a}]J\rangle, \tag{125}$$

where J_s is the angular momentum of the spectator nucleons s, which are the nucleons other than the neutrons in the $i_{13/2}$ orbit. The effective SU(3) representation of the spectators is given by $\lambda_s=\lambda-\lambda_{\nu a}=68-22=46$. The probability for the a neutrons to have an angular momentum $J_{\nu a}$ in the yrast state $|J\rangle$ is given by [see Eq. (123)]

$$P(J;J_{\nu a})=\sum_{J_s} |A(J;J_s,J_{\nu a}|^2, \tag{126}$$

where

$$A(J;J_s,J_{\nu a})=N_JC_{J_s}[46,0]C_{J_{\nu a}}[22,0](J_sJ_{\nu a}00|J0). \tag{127}$$

The average value $\overline{J_{\nu a}(J)}$ of the angular momentum contributed by the a neutrons to the yrast state $|J\rangle$ is defined by

$$\overline{J_{\nu a}(J)} = [\langle J^2_{\nu a}\rangle_J]^{1/2} \tag{128a}$$

$$= \left[\sum_{J_{\nu a}} P(J;J_{\nu a}) J_{\nu a}(J_{\nu a}+1)\right]^{1/2}. \tag{128b}$$

The value of $\overline{J_{\nu a}(J)}$ in the $|J=14\rangle$ yrast state of ^{156}Gd given by Eq. (128) is $\overline{J_{\nu a}}(J=14)=7.2$. Similarly the six *a* protons in the $i_{13/2}$ orbit contribute an average angular momentum $\overline{J_{\pi a}}(J=14)=5.6$ to the yrast state with $J=14$. As far as the *n* nucleons are concerned, we find $\overline{J_{\pi n}}(J=14)=5.6$ for the six *n* protons and $\overline{J_{\nu n}}(J=14)=6.4$ for the six *n* neutrons. Thus each group of nucleons contributes approximately an equal amount of angular momentum (on an average) to the $J=14$ yrast state with the contribution of the neutrons in the 82–126 shell being 20% larger than that of protons in the 50–82 shell.

Table XX can be used similarly to determine, to a good approximation, the relative contribution of the *n* and *a* nucleons to the angular momentum of an yrast state of any deformed nucleus projected from its Nilsson $\mathcal{IS}$ within a major shell. The SU(3)-like structure of the distributions of angular momenta in the $\mathcal{IS}$ allows one to calculate, with relative ease, the separate contributions of the protons and neutrons in *a* or *n* states to the total angular momentum of an yrast state.

B. Contribution of *a* nucleons to a $B(E2:J\rightarrow J-2)$ value

We next determine the relative contribution of *a* and *n* nucleons to a $B(E2,J\rightarrow J-2)$ value for an $E2$ transition between the states $|J_i\rangle$ and $|J_f\rangle$ projected from the Nilsson $\mathcal{IS}$ of a nucleus. The $B(E2,J_i\rightarrow J_f)$ value is given by

$$B(E2,J_i\rightarrow J_f)=\frac{5}{16\pi}\frac{(J_f\|Q_e\|J_i)^2}{2J_i+1}, \tag{129}$$

which differs from Eq. (63) in the fact that the operator Q_e above is the electric quadrupole operator, whereas in Eq. (63) we considered only the mass quadrupole operator. The operator Q_e can be written as

$$Q_e = e_{\pi a}Q_{\pi a}+e_{\nu a}Q_{\nu a}+e_{\pi n}Q_{\pi n}+e_{\nu n}Q_{\nu n}. \tag{130}$$

Here, $Q_{\alpha n(a)}$ (with $\alpha=\pi$ or ν) are the mass quadrupole operators for the $n(a)$ nucleons and $e_{\alpha n(a)}$ their effective charges. Because the *n* nucleons in deformed nuclei are known to possess pseudo-SU(3) symmetry to a good approximation, it is convenient to express the quadrupole operators $Q_{\pi n}$ and $Q_{\nu n}$ in terms of the pseudo operators $\widetilde{Q_{\pi n}}$ and $\widetilde{Q_{\nu n}}$ with $Q_{\alpha n}=1.2\widetilde{Q_{\alpha n}}$ [28]. We rewrite Eq. (130) as

$$Q_e = e_{\pi a}Q_{\pi a}+e_{\nu a}Q_{\nu a}+e_{\pi n}1.2\widetilde{Q_{\pi n}}+e_{\nu n}1.2\widetilde{Q_{\nu n}}. \tag{131}$$

The reduced matrix element is written as

$$(J_f\|Q_e\|J_i)=e_{\pi a}(J_f\|Q_{\pi a}\|J_i)+e_{\nu a}(J_f\|Q_{\nu a}\|J_i) + 1.2e_{\pi n}(J_f\|\widetilde{Q_{\pi n}}\|J_i)+1.2e_{\nu n}(J_f\|\widetilde{Q_{\nu n}}\|J_i). \tag{132}$$

The contribution of just the protons in the *a* state is contained in $(J_f\|Q_{\pi a}\|J_i)$. Similar expressions give the contributions of other groups of nucleons to the total reduced matrix element.

1. Effective charges

Calculation of the reduced electric quadrupole matrix elements requires values for the effective charges $e_{\pi n}$, $e_{\nu n}$, $e_{\pi a}$, and $e_{\nu a}$, all of which may be considered to be free parameters. As a result of a previous study [3] of the $B(E2:0^+_1\rightarrow 2^+_1)$ systematics throughout the periodic table within the framework of the single-shell asymptotic Nilsson model, we recommended that the charges $e_\pi=[1+(Z/A)]e$ and $e_\nu=2.1(Z/A)e$ be used. We follow this recommendation and take $e_{\pi n}=e_{\pi a}=[1+(Z/A)]e$ and $e_{\nu n}=e_{\nu a}=2.1(Z/A)e$.

2. Evaluation of the reduced matrix elements

We now discuss how the four terms contained in Eq. (132) are calculated. Consider first the evaluation of the matrix element $(J_f\|Q_{\pi a}\|J_i)$. We begin by expressing the projected yrast state $|J\rangle$ of the nucleus in terms of the angular momenta $J_{\pi a}$ of the *a* protons and J_s of spectator nucleons. We write

$$|J\rangle=\sum_{J_s}\sum_{J_{\pi a}} A[J:J_{\pi a}J_s]|[J_{\pi a}\otimes J_s]J\rangle, \tag{133}$$

where

$$A[J:J_{\pi a},J_s]=N_J C_{J_{\pi a}}(j_{\pi a},N_{\pi a})C_{J_s}[\lambda_s=\lambda-\lambda_{\pi a},0] \times(J_{\pi a}J_s 0\,0|J\,0) \tag{134}$$

and

$$N_J=\left[\sum_{J_{\pi a}}\sum_{J_s}|C_{J_{\pi a}}(j_{\pi a},N_{\pi a})C_{J_s}[\lambda_s=\lambda-\lambda_{\pi a},0] \times(J_{\pi a}J_s 00|J0)|^2\right]^{-1/2}. \tag{135}$$

The $|C_{J_{\pi a}}(j_{\pi a},N_{\pi a})|^2$ values are listed in Table II, and the $|C_{J_s}[\lambda_s,0]|^2$ values can be calculated using Eq. (3). Using Eq. (133), the desired reduced matrix element can be expressed as

$$(J_f\|Q_{\pi a}\|J_i)=\sum_{J'_{\pi a}}\sum_{J'_s}\sum_{J_{\pi a}}\sum_{J_s} A[J_f,J'_{\pi a}J'_s]A[J_i,J_{\pi a}J_s] \times\langle[J'_{\pi a}\otimes J'_s]J_f\|Q_{\pi a}\|[J_{\pi a}\otimes J_s]J_i\rangle. \tag{136}$$

The reduced matrix element on the right-hand side of the Eq. (136) is given by

$$\langle [J'_{\pi a}\otimes J'_s]J_f\|Q_{\pi a}\|[J_{\pi a}\otimes J_s]J_i\rangle = [(2J_f+1)(2J_i+1)]^{1/2}\delta_{J'_sJ_s} \times\left[(-)^{J'_{\pi a}+J'_s+J_i+2}\begin{Bmatrix} J_{\pi a} & J_s & J_i \\ J_f & 2 & J'_{\pi a}\end{Bmatrix} \times\langle J'_{\pi a}\|Q_{\pi a}\|J_{\pi a}\rangle\right]. \quad (137)$$

The reduced matrix elements $\langle J'_{\pi a}\|Q_{\pi a}\|J_{\pi a}\rangle$ are tabulated in Table XIII. All other quantities in Eqs. (136) and (137) are known; hence, one can calculate the matrix element $(J_f\|Q_{\pi a}\|J_i)$ and, therefore, the contribution of *a* protons to the total reduced $E2$ matrix element $(J_f\|Q_e\|J_i)$. The reduced matrix elements involving neutrons in the *a* state can be obtained in a similar manner.

Just as for the *a* nucleons, the matrix elements $(J_f\|\widetilde{Q_{\alpha n}}\|J_i)$ for the *n* nucleons can be expressed in terms of $(J'_{\alpha n}\|\widetilde{Q_{\alpha n}}\|J_{\alpha n})$. Because of pseudo-SU(3) symmetry, the latter matrix elements can be approximated by the matrix elements between the states $|[\widetilde{\lambda_{\alpha n},\mu_{\alpha n}}]K=0,J_{\alpha n}\rangle$ belonging to the $K=0$ band of the pseudo-SU(3) representation $[\widetilde{\lambda_{\alpha n},\mu_{\alpha n}}]$ appropriate for the given number of valence *n* nucleons. Hence, we may use

$$(J'_{\alpha n}\|\widetilde{Q_{\alpha n}}\|J_{\alpha n}) \approx([\widetilde{\lambda_{\alpha n},\tilde{\mu}_{\alpha n}}]K=0,J'_{\alpha n}\|\widetilde{Q_{\alpha n}}\|[\widetilde{\lambda_{\alpha n},\mu_{\alpha n}}]K=0,J_{\alpha n}). \quad (138)$$

If an SU(3) representation $[\lambda,\mu]$ has $\lambda\gg\mu$, one expects that

$$([\lambda,\mu]K=0,J'\|Q\|[\lambda,\mu]K=0,J) \approx([\lambda_{\rm eff}=\lambda+\mu,0]J'\|Q\|[\lambda_{\rm eff}=\lambda+\mu,0]J). \quad (139)$$

We have explicitly verified that this approximation holds for the $[\lambda,2]$ representation. In view of this result, we write

$$(J'_{\alpha n}\|\widetilde{Q_{\alpha n}}\|J_{\alpha n}) \approx([\widetilde{\lambda^{\rm eff}_{\alpha n}},0]K=0,J'_{\alpha n}\|\widetilde{Q_{\alpha n}}\|([\widetilde{\lambda^{\rm eff}_{\alpha n}},0]K=0,J_{\alpha n}). \quad (140)$$

The values of $\widetilde{\lambda^{\rm eff}_{\alpha n}}=\widetilde{\lambda_{\alpha n}}+\widetilde{\mu_{\alpha n}}$ are listed in Table XX. For a representation $[\lambda,0]$, the values of the matrix elements $([\lambda,0]K=0,J'\|Q\|[\lambda,0]K=0,J)$ are given by Eq. (70). We use the same expression to calculate $(J'_{\alpha n}\|\widetilde{Q_{\alpha n}}\|J_{\alpha n})$ with $\widetilde{\lambda^{\rm eff}_{\alpha n}}$ in the place of λ.

C. $Q_t(J)$ values for $^{160}_{70}$Yb$_{90}$, $^{162}_{70}$Yb$_{92}$, $^{164}_{70}$Yb$_{94}$, and $^{166}_{70}$Yb$_{96}$

We use the results obtained in Sec. VII B to calculate the contributions of protons and neutrons in both *n* and *a* states to the $B(E2:J\to J-2)$ values for transitions within the yrast bands of the Yb isotopes (with $A=160$–166) projected from their Nilsson $\mathcal{IS}$'s. For some of these nuclei, the $B(E2)$ values or equivalently the transition moments $Q_t(J)$ have been measured up to $J\sim 36$. We carry out the calculations in the configuration space in which the valence protons and neutrons are confined to the 50–82 and 82–126 major shells, respectively.

Consider the nucleus $^{160}_{70}$Yb$_{90}$ with $N_\pi=20$ valence protons and $N_\nu=8$ valence neutrons. From Table XX, we obtain $N_{\pi n}=12$, $N_{\pi a}=8$, $N_{\nu n}=6$, and $N_{\nu a}=2$ in the Nilsson $\mathcal{IS}$. Note that $j_{\pi a}=0h_{11/2}$ and $j_{\nu a}=0i_{13/2}$. The ranges of angular momenta contained in this $\mathcal{IS}$ are $J_{\pi n}=0,2,4,\ldots,12$, $J_{\pi a}=0,2,4,\ldots,16$, $J_{\nu n}=0,2,4,\ldots,18$, and $J_{\nu a}=0,2,4,\ldots,12$. The yrast band of ^{160}Yb projected from this $\mathcal{IS}$ contains even angular momenta up to $J_{\max}=58$. Thus the equivalent total SU(3) representation for the Nilsson $\mathcal{IS}$ of ^{160}Yb is [58,0]. If we assume that the *a* nucleons are coupled to a $\nu=0$ state, the yrast band will terminate at a smaller $J_{\max}=J_{n\ \max}=J_{\pi n\ \max}+J_{\nu n\ \max}=12+18=30$, and the equivalent SU(3) representation for the yrast band will be [30,0].

When the *a* protons are contributing to the matrix element, the *a* neutrons and all the *n* nucleons are spectators. Their effective λ_s value is $\lambda_s=\lambda-\lambda_{\pi a}$. Using $\lambda=58$ and $\lambda_{\pi a}=\lambda_{\pi a\ \rm eq}=16$ (see the $\lambda_{\rm eq}$ value in Table IV for eight protons in the $0h_{11/2}$ orbit), we get $\lambda_s=42$. With this information, the reduced matrix elements $(J_f\|Q_{\pi a}\|J_i)$ can be calculated for ^{160}Yb using Eqs. (136) and (137). The remaining reduced matrix elements $(J_f\|Q_{\nu a}\|J_i)$, $(J_f\|Q_{\pi n}\|J_i)$, and $(J_f\|Q_{\nu n}\|J_i)$ can be similarly calculated by identifying in each case the group of spectator nucleons. For example, in the calculation of $(J_f\|Q_{\nu a}\|J_i)$, the protons in the *a* states and both protons and neutrons in the *n* states are spectator nucleons. The spectator λ_s value is, therefore, $\lambda_s=\lambda_s-\lambda_{\nu a}=58-12=46$.

For the ground-state yrast band in ^{160}Yb, the calculated values for each of the four terms contained in Eq. (132) are listed in Table XXI. We note that the contribution of each group of nucleons to the reduced matrix element is approximately proportional to the intrinsic quadrupole moment of the group. For example,

$$\frac{(J_f\|\widetilde{Q_{\pi n}}\|J_i)}{(J_f\|\widetilde{Q_{\pi a}}\|J_i)}\approx\frac{Q_0(N_{\pi n})}{Q_0(N_{\pi a})}\approx\frac{2\times 12}{14.55}\approx 1.65, \quad (141)$$

which is quite reasonable for nucleons sharing the same mean field.

In ^{160}Yb, when the *a* nucleons are not forced to couple to a $\nu=0$ state, both *a* and *n* nucleons contribute to the reduced matrix elements over the entire projected band up to $J=58$, with the dominant contribution coming from the *n* nucleons. When the *a* nucleons are forced to couple to a $\nu=0$ state, not only are the contributions from the *a* nucleons zero throughout but also those from the *n* nucleons end abruptly at $J=30$.

We calculated the reduced electric quadrupole matrix elements $(J_f||Q_e||J_i)$ using the matrix elements $(J_f||Q_{\alpha\beta}||J_i)$ and the standard effective charges discussed in Sec. VII B 1. The transition moment is given by

TABLE XXI. Individual components (in units of α^2) of the total reduced matrix element of the electric quadrupole operator [see Eq. (134) with J_f replaced by J and J_i by $J-2$]. The listed values are for the yrast band in ^{160}Yb which extends up to $J=58$. The effective charges used in Eq. (134) to calculate the $Q_t(J)$ values (in units of e b) are $e_{\pi n}=e_{\pi a}=1.44e$ and $e_{\nu n}=e_{\nu a}=0.92e$.

J	$(J_f \|\|Q_{\pi a}\|\| J_i)$	$(J_f \|\|Q_{\nu a}\|\| J_i)$	$(J_f \|\|\widetilde{Q_{\pi n}}\|\| J_i)$	$(J_f \|\|\widetilde{Q_{\nu n}}\|\| J_i)$	$Q_t(J)$
2	14.961	7.548	24.613	36.919	6.119
4	23.970	12.145	39.413	59.119	6.113
6	30.188	15.400	49.585	74.377	6.102
8	35.242	18.127	57.798	86.698	6.085
10	39.580	20.525	64.786	97.179	6.061
12	43.407	22.647	70.876	106.315	6.030
14	46.834	24.492	76.247	114.371	5.991
16	49.928	26.033	81.005	121.507	5.943
18	52.732	27.237	85.217	127.825	5.886
20	55.275	28.086	88.927	133.390	5.819
22	57.574	28.578	92.162	138.242	5.742
24	59.641	28.731	94.938	142.407	5.655
26	61.481	28.581	97.263	145.895	5.559
28	63.095	28.173	99.139	148.708	5.453
30	64.479	27.551	100.558	150.838	5.337
32	65.625	26.761	101.511	152.267	5.211
34	66.520	25.837	101.980	152.970	5.075

$$Q_t(J)=\frac{1}{(J200|J-2\,0)}\frac{(J-2||Q_e||J)}{\sqrt{2J+1}}, \qquad (142)$$

The $Q_t(J)$ values for ^{160}Yb calculated using Eq. (142) are listed in Table XXI. We have carried out similar calculations of the $Q_t(J)$ values for the yrast bands in $^{162}_{70}\mathrm{Yb}_{92}$, $^{164}_{70}\mathrm{Yb}_{94}$, and $^{166}_{70}\mathrm{Yb}_{96}$ also. The results are summarized in Fig. 17. The calculated values are shown as full curves and are then normalized (see the dashed curves) to the most accurately determined $Q_t(J)$ value for each isotope, which is $Q_t(J=2)$. The normalization factor is 0.86 for ^{160}Yb. These factors are much closer to unity for the other three Yb isotopes. The calculated $Q_t(J)$ trends do not resemble the available experimental data [38–40] closely for ^{160}Yb and ^{162}Yb, but they do so for ^{164}Yb and ^{166}Yb. The pseudo-SU(3) model values, obtained by assuming that $v_{\pi a}=v_{\nu a}=0$, are also shown in Fig. 17. As a function of J, they decrease much faster than the projected values.

The $Q_t(J)$ trend calculated for the projected band can also be described equally well [see the solid and dashed lines in Fig. 18(a)] by the trend obtained for the band belonging to the SU(3) representation $[\lambda=J_{\max},0]$. For ^{160}Yb, $J_{\max}=58$. That is one of the surprising results to emerge from this work.

The $Q_t(J)$ trend for ^{160}Yb, calculated [40] using the cranked Hartree-Fock-Bogoliubov (HFB) model, is shown in Fig. 18(b). There is a significant drop at $J=22$, whereas the data seem to suggest an increase at this J value. Both the projected and cranked HFB trends are smooth. On the other hand, the trend predicted [41] by the fermion dynamic symmetry model (with suitable extensions) has some structure, as shown in Fig. 18(b). A question for the experimentalists is whether the overall trend of the $Q_t(J)$ values is relatively smooth as it is in the ^{164}Yb case or jagged as it is in the ^{160}Yb case [see Figs. 17(c) and 17(a)]. If the trend is indeed jagged, it would pose a serious problem to existing theories.

The $Q_t(J)$ values calculated for the yrast band projected from a single $\mathcal{I}S$ show a slowly decreasing trend with J. How would this trend be interpreted in the cranking model in which there is a different $\mathcal{I}S$ for each J? In that model, the $Q_t(J)$ values are given by

$$Q_t(\mathrm{crank},J)=\frac{6}{\sqrt{15\pi}}Zer_0^2A^{2/3}\beta_2(1+0.36\beta_2)\cos(30^\circ+\gamma), \qquad (143)$$

where β_2 and γ are parameters of deformation. Consider ^{160}Yb in which the measurements extend up to $J=34$. The calculated projected $Q_t(J)$ values (see Table XXI) of $Q_t(J=2)=5.2e$ b and $Q_t(J=34)=4.4e$ b would then correspond to $\gamma(J=2)=3^\circ$ and $\gamma(J=34)=16^\circ$ if we take $\beta_2=0.222$ and use Eq. (143). The γ value at the $J=58$ termination point would be 44.6°. In other words, for a fixed value of β_2, the cranking model would interpret the decrease of $0.8e$ b in the $Q_t(J)$ value as a consequence of an increase in γ by 29°. In our projection calculation, the intrinsic state does not undergo such a change of shape.

D. $Q_t(J)$ values for $^{156}_{66}\mathrm{Dy}_{90}$ and $^{158}_{66}\mathrm{Dy}_{92}$

The $Q_t(J)$ values calculated for the yrast states up to $J=40$ projected from the single-shell asymptotic Nilsson $\mathcal{I}S$'s

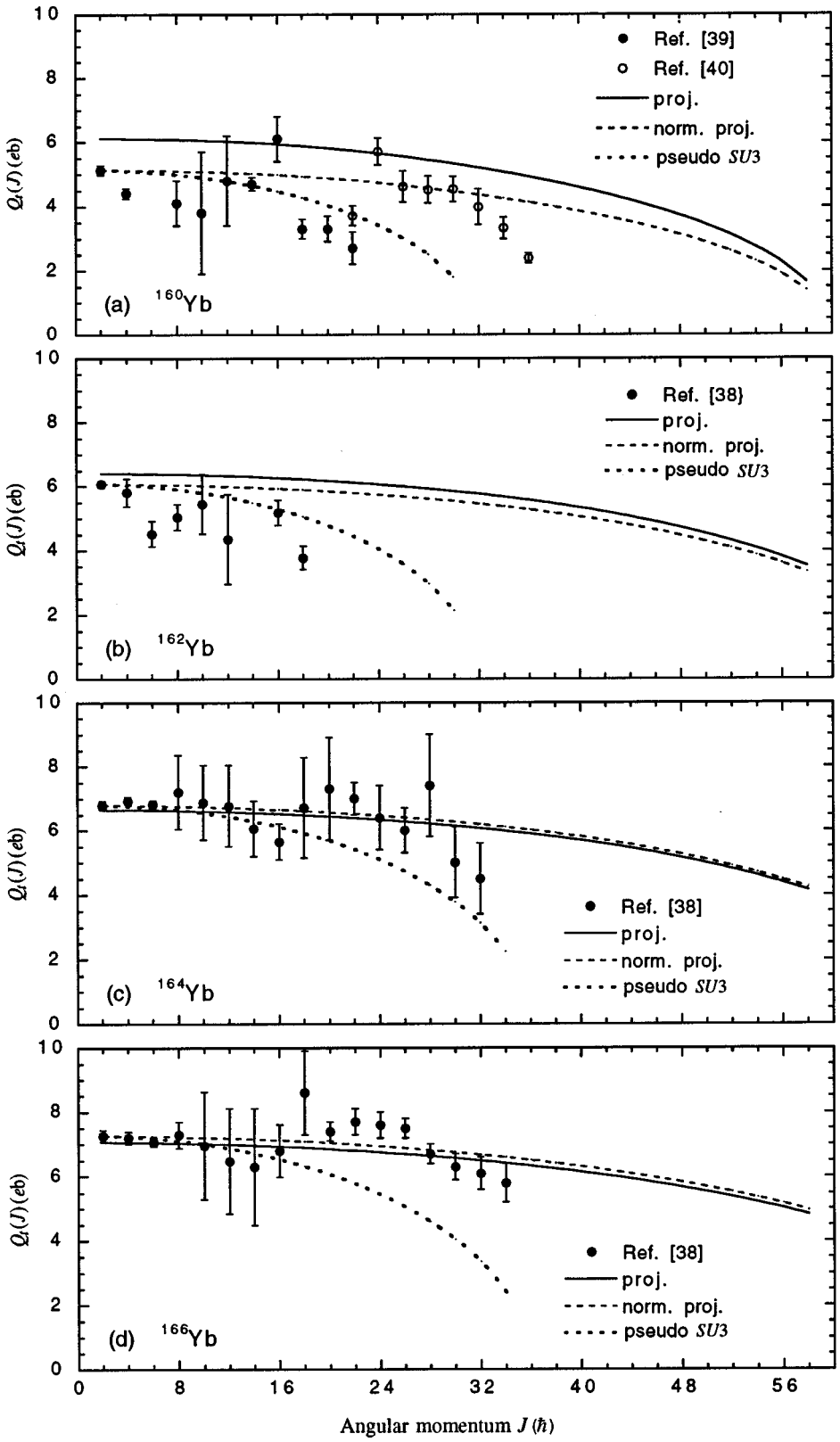

FIG. 17. Measured transition moments $Q_t(J)$ for the yrast bands in four ytterbium isotopes compared with calculated values using the effective charges given in Sec. VII B 1. The projected values (solid lines) are normalized to the measured $Q_t(J=2)$ in each case and redrawn as dashed lines. The pseudo-SU(3) model values are normalized in a similar way. See related discussion in Sec. VII C.

of ^{156}Dy and ^{158}Dy are shown in Fig. 19. The projected values are normalized to the measured $Q_t(J=2)$ values. The normalization factors are 0.937 and 0.986, respectively, for ^{156}Dy and ^{158}Dy. For these isotopes, if the *a* nucleons are assumed to be inert as a result of pairing, the $Q_t(J)$ values for the yrast bands are given by the pseudo-SU(3) representations $[\lambda_{\text{eff}},0]=[32,0]$ and $[38,0]$, respectively. The $Q_t(J)$ trends for these representations, also normalized to the measured $Q_t(J=2)$ values, are shown in Fig. 19 by the dotted lines. The existing data [42] for states with spins up to *J*

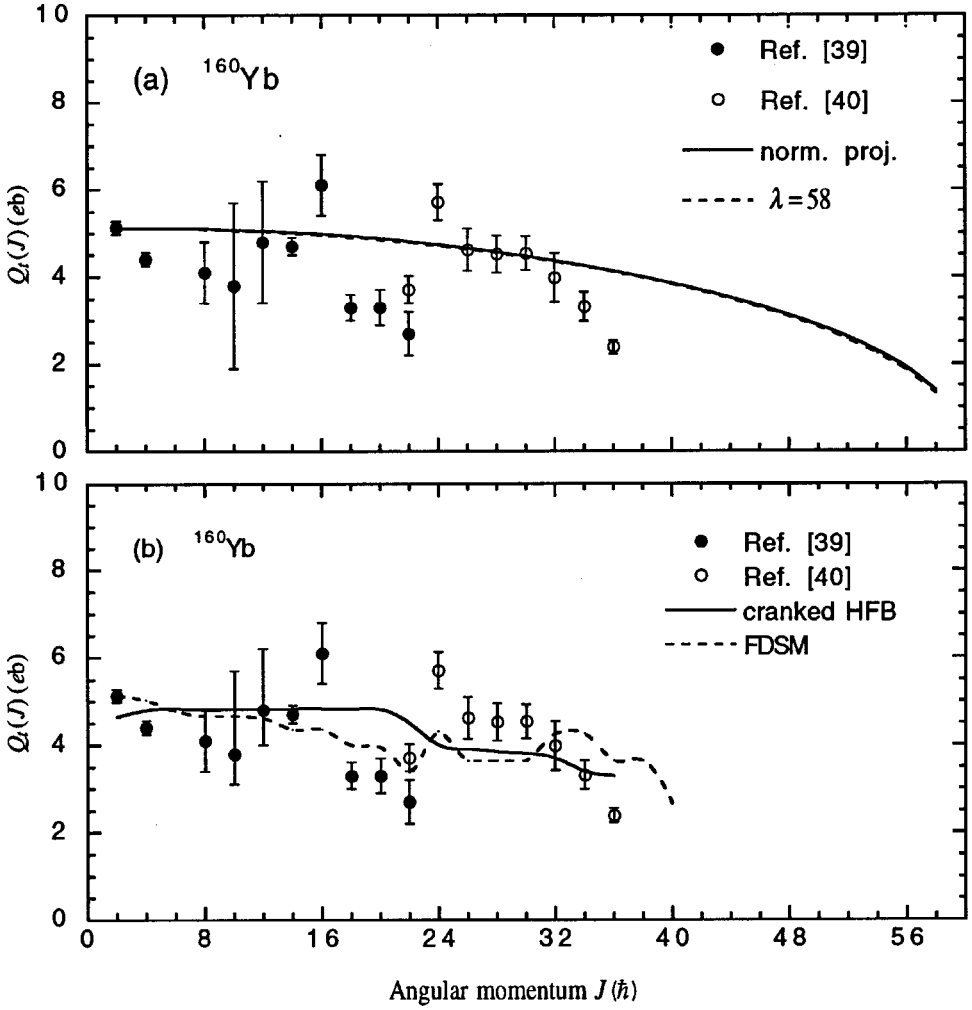

FIG. 18. (a) Normalized transition moments $Q_t(J)$ for the projected yrast bands in ^{160}Yb compared with the corresponding values for the equivalent SU(3) $[\lambda_{eq}=58,0]$ band. (b) Predictions of the cranked HFB and fermion dynamic symmetry models. The latter values are normalized to the measured $Q_t(J=2)$. See related discussion in Sec. VII C.

$=24$ in ^{156}Dy and up to $J=26$ in ^{158}Dy favor the pseudo-SU(3) descriptions.

E. Transition matrix elements in $^{232}_{90}Th_{142}$, $^{234}_{90}U_{144}$, and $^{236}_{90}U_{146}$

Ower *et al.* [43] have deduced the $E2$ transition matrix elements for the yrast band up to $J=28$ in ^{232}Th. For this nucleus, the number of valance nucleons and their distribution in the n and a states are $[N_\pi=8,\ N_{\pi n}=4$, and $N_{\pi a}=4$ (in the $0i_{13/2}$ state)] and $[N_\nu=16,\ N_{\nu n}=16$, and $N_{\nu a}=4$ (in the $0j_{15/2}$ state)]. The appropriate SU(3) $[\lambda,0]$ values for these particle numbers are $\lambda_{\pi n}=14$, $\lambda_{\nu n}=24$, $\lambda_{\pi a}=20$, and $\lambda_{\nu a}=30$. The yrast band projected from the Nilsson intrinsic state extends up to $J_{max}=88$. We use the formulation given in Sec. VII to calculate the total reduced matrix element given by Eq. (132) for each combination of J_f and J_i. These calculated values are related to the matrix elements $(J+2||E2||J)$ deduced by Ower *et al.* [43] from their experiment via

$$(J+2||Q_e||J)=\sqrt{\frac{16\pi}{5}}(J+2||E2||J). \qquad (144)$$

The measured and calculated values, the latter normalized to the $(2||Q_e||0)$ value, are shown in Fig. 20(a). Also shown in this figure are the rotor model and the pseudo-SU(3) model values. Experimental data for the $J>24$ states are needed to distinguish between different model predictions.

Ower *et al.* [43] also give the reduced $E2$ matrix elements for ^{234}U and ^{236}U from their measurements. The comparison between theory and experiment for these two cases is shown in Fig. 20(b) and Fig. 20(c), respectively. In ^{236}U, the experimental values are larger than both the rotor model and projected model values for $J>18$. Thus the behavior of ^{236}U is apparently different from the behaviors of ^{232}Th and ^{234}U.

VIII. SUMMARY AND CONCLUSIONS

We have examined, for the first time, in a systematic way, the quadrupole collectivity of nucleons in the abnormal-parity single-particle states $j_a=\frac{9}{2}$, $\frac{11}{2}$, $\frac{13}{2}$, and $\frac{15}{2}$ in the Nilsson intrinsic states of deformed nuclei. We have used some well-known criteria to describe the collectivity of a nucleons. This property is not amenable to analytical study by group theory.

We have calculated the collective properties of the intrinsic states of these abnormal-parity nucleons and of the states with angular momenta J projected from each of these intrinsic states. The properties studied include (i) the distribution

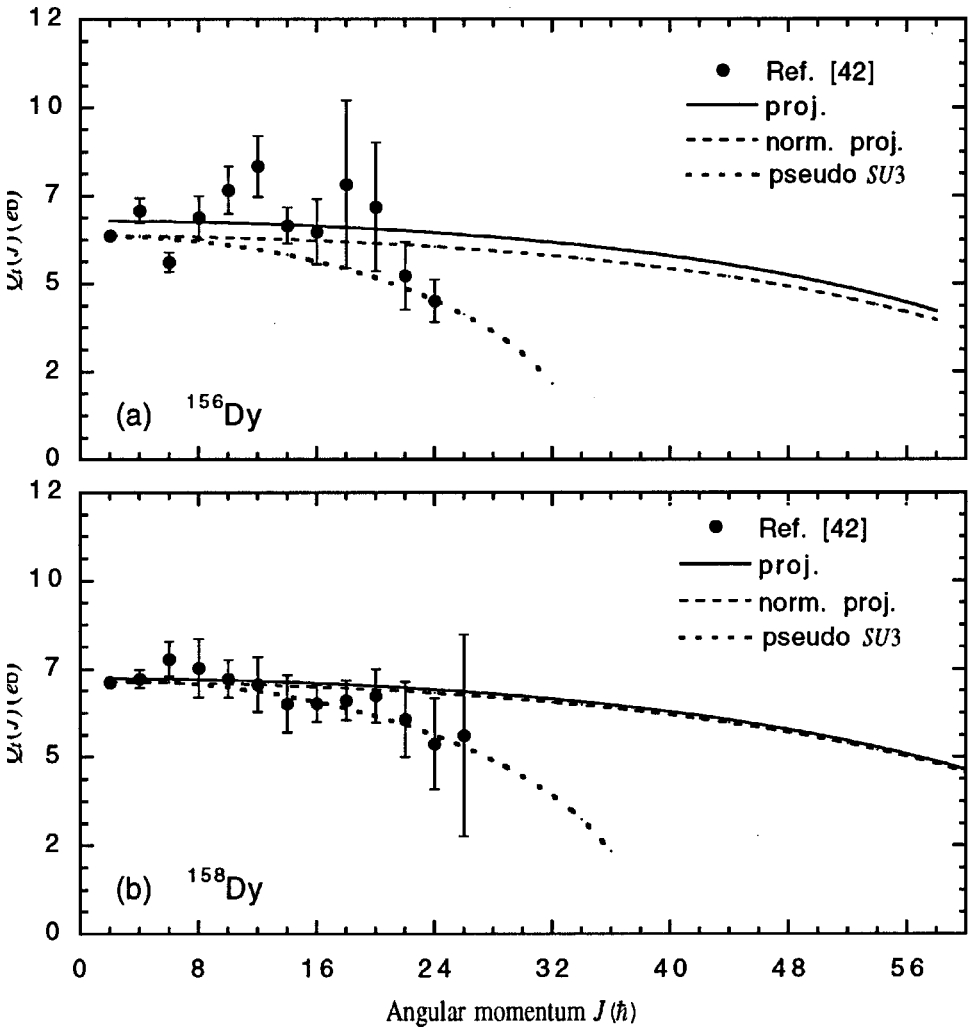

FIG. 19. Measured transition moments $Q_t(J)$ for the yrast bands in two dysprosium isotopes compared with calculated values using the effective charges given in Sec. VII B 1. The projected values (solid lines) are normalized to the measured $Q_t(J=2)$ in each case and redrawn as dashed lines. The pseudo-SU(3) model values are normalized in a similar way. See related discussion in Sec. VII D.

of angular momenta contained in the prolate Nilsson intrinsic state of different number of *a* particles and (ii) the relationship between the quadrupole moment of the intrinsic state and the maximum angular momentum contained in it. This numerical description of the collectivity of the intrinsic states of *a* nucleons is put in some perspective by comparing it with the standard quadrupole collectivity of the intrinsic states of nucleons having SU(3) symmetry. This comparison is instructive because the $j_a^{N_a}$ configuration space available to the *a* nucleons cannot support any SU(3) symmetry at the microscopic level and yet the distribution of angular momenta in the intrinsic states of *a* nucleons was found to be very similar to the distribution of angular momenta in an intrinsic state with SU(3) symmetry.

An interesting feature of the quadrupole collectivity of the intrinsic states of *a* nucleons brought out by analogy with that of an SU(3) intrinsic state is the linear relation between the particle-hole averaged quadrupole moment $\langle Q_{\rm ph}\rangle_{\rm ave}$ and the maximum angular momentum $J_{\rm max}$ contained in an axially symmetric j^N intrinsic state. The result, $\langle Q_{\rm ph}\rangle \approx 0.8 J_{\rm max}$, appears to be a new relation not available in the literature. The relationship between the quadrupole moment Q_0 of an axially symmetric SU(3) intrinsic state and the $J_{\rm max}$ contained in it is $Q_0 = 2J_{\rm max}$. (Both $\langle Q_{\rm ph}\rangle$ and Q_0 are in units of the size parameter α^2 of the harmonic oscillator wave functions used in their calculation.) An inference from the above results is that the $j_a^{N_a}$ intrinsic state is less collective than an SU(3) intrinsic state with the same $J_{\rm max}$ by a factor of about 2.5.

In the next stage, we considered the quadrupole collectivity of the states of definite *J* projected from the prolate j_a^N Nilsson intrinsic state. This collectivity is characterized quatitatively by the complete set of the matrix elements $(J_f||Q||J_i)$ between all the projected states. The calculation of these matrix elements with high accuracy involved a major computational effort. We have listed all these matrix elements for the states projected from the various j_a^N intrinsic states. Although the matrix elements $(J_f||Q||J_i)$ contain all the information about collectivity, a more familiar display of this collectivity is also presented in the form of (i) the trend of the $B(E2, J \rightarrow J-2)$ vs *J* values for transitions within the projected band and (ii) the variation of the transition moments $Q_t(J)$ and the spectroscopic quadrupole moments $Q(J)$ of the projected states. Once again the variations of these quantities for the projected *a* states are compared with the variations of the same quantities for the states with SU(3) and SO(6) symmetry. This comparison leads to a surprising

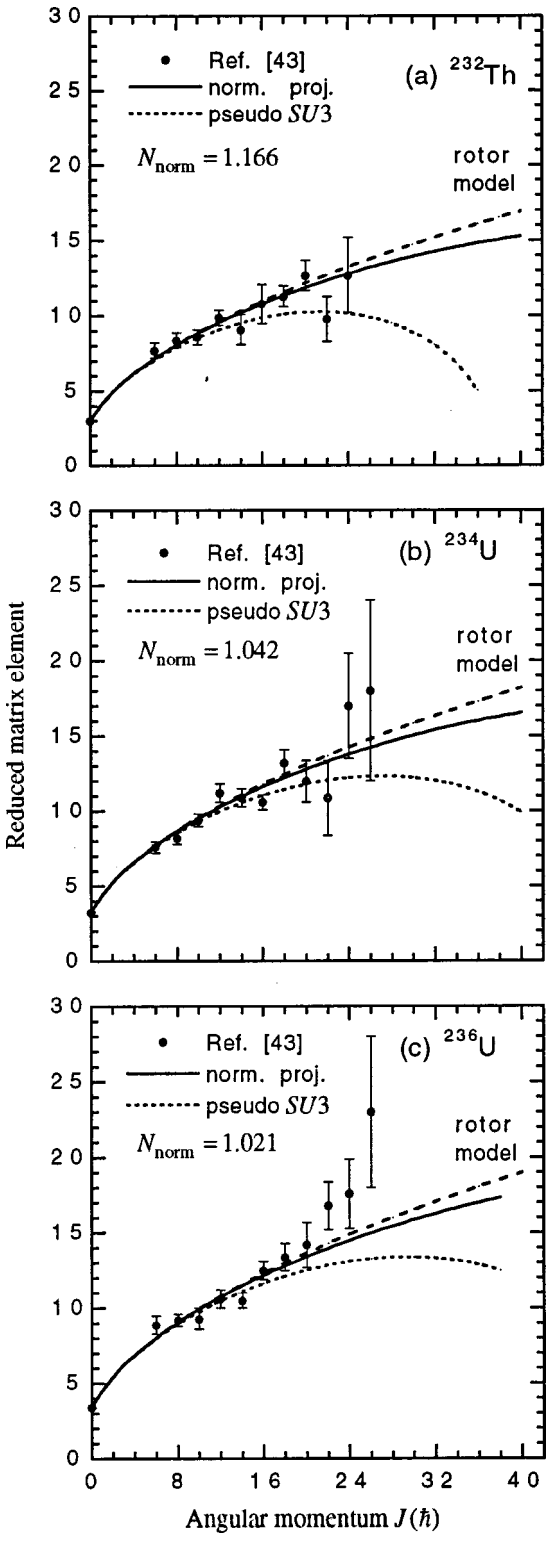

FIG. 20. Measured reduced matrix elements $(J+2||Q_e||J)$ for ^{232}Th, ^{234}U, and ^{236}U compared with calculated values using the effective charges given in Sec. VII B 1. In each case, the projected, rotor, and pseudo-SU(3) model values are normalized to the measured $(2||Q_e||0)$ value for that particular isotope. The normalization factors $N_{\rm norm}$ for the projected matrix elements are listed in (a), (b), and (c). See related discussion in Sec. VII E.

result that the trend of the $B(E2,J\rightarrow J-2)$ vs J values for the projected states is *more* collective than that of the equivalent SU(3) or SO(6) representations. In addition, we find the projected trend over about $\frac{3}{4}$ of the band can be well described by the trend obtained for a single SU(3) band of representation $[\lambda_{BE2},0]$.

Up to this point we described the collectivity of different numbers of particles occupying only the abnormal-parity orbits in the Nilsson intrinsic states. In the next step, we determined the specific coupling between the collective projected proton and neutron states induced by the mean field to produce the yrast band of the proton-neutron system of a nucleons, projected from their combined (product) intrinsic states. The $B(E2,J\rightarrow J-2)$ trend for the $\pi\nu$ coupled band of a nucleons is more SU(3)-like than the trends for the individual groups of a protons or a neutrons.

We finally considered the a nucleons sharing the mean field with other valence nucleons in the n single-particle states. We obtained the wave functions of the yrast states of even-even deformed nuclei in terms of the quadrupole collective states of the n and a nucleons. The transition moments Q_t for the members of the yrast band, calculated with these projected wave functions, are in good agreement with the measured values. The cranking model achieves similar results without using wave functions for the specific yrast states of the nucleus.

In a previous work [4], we showed that the distribution of the *total* angular momentum in the asymptotic single-shell Nilsson $\mathcal{IS}$ of ^{238}U is remarkably close, over 27 orders of magnitude, to the corresponding one obtained for the SU(3) representation $[\lambda=J_{\rm max},0]$, where $J_{\rm max}$ is the maximum angular momentum contained in the intrinsic state. In this work, we showed that the $B(E2,J\rightarrow J-2)$ trend for the projected yrast band of ^{160}Yb is also surprisingly SU(3)-like. Thus, although the SU(3) symmetry is absent at the microscopic level, SU(3)-like features keep cropping up at the macroscopic level. We can think of two reasons: (i) The prolate intrinsic states of a nucleons considered here and the corresponding SU(3) intrinsic states both have the maximum quadrupole moment within their respective configuration spaces and (ii) the same projection procedure is used to obtain the states of definite angular momenta from both of these intrinsic states.

ACKNOWLEDGMENTS

The authors are especially grateful to Igal Talmi for deriving Eq. (97). We also acknowledge the help of J.D. Garrett, N.R. Johnson, and P. Tikkanen. The current work was sponsored by the U.S. Department of Energy, under Contract No. DE-AC05-96OR22464 with Lockheed Martin Energy Research Corporation. Two of the authors (S.K and K.H.B) were supported in part by the Joint Institute of Heavy-Ion Research. This institute is supported by the U.S. Department of Energy, under Contract No. DE-FG05-87ER40361 with The University of Tennessee, and is operated jointly by The University of Tennessee, Vanderbilt University, and Oak Ridge National Laboratory.

[1] S. Raman, C. W. Nestor, Jr., and K. H. Bhatt, Phys. Rev. C **37**, 805 (1988).
[2] S. Raman, C. W. Nestor, Jr., S. Kahane, and K. H. Bhatt, Phys. Rev. C **43**, 556 (1991).
[3] K. H. Bhatt, C. W. Nestor, Jr., and S. Raman, Phys. Rev. C **46**, 164 (1992).
[4] S. Kahane, S. Raman, and K. H. Bhatt, Phys. Rev. C **55**, 2885 (1997).
[5] J. P. Elliott, Proc. R. Soc. London **A245**, 128 (1958).
[6] J. P. Elliott, Proc. R. Soc. London **A245**, 562 (1958).
[7] R. D. Ratna Raju, J. P. Draayer, and K. T. Hecht, Nucl. Phys. **A202**, 422 (1973).
[8] A. de-Shalit and I. Talmi, *Nuclear Shell Theory* (Academic, New York, 1963).
[9] I. Talmi, *Simple Models of Complex Nuclei* (Harwood Academic, Chur, Switzerland, 1993).
[10] A. K. Dhar, D. R. Kulkarni, and K. H. Bhatt, Phys. Lett. **47B**, 133 (1973).
[11] K. H. Bhatt, J. C. Parikh, and J. B. McGrory, Nucl. Phys. **A224**, 301 (1974).
[12] J. P. Draayer and K. J. Weeks, Ann. Phys. (N.Y.) **156**, 41 (1984).
[13] S. Raman, C. W. Nestor, Jr., S. Kahane, and K. H. Bhatt, At. Data Nucl. Data Tables **42**, 1 (1989).
[14] P. Ring and P. Schuck, *The Nuclear Many Body Problem* (Springer, New York, 1980).
[15] F. Iachello and A. Arima, *The Interacting Boson Model* (Cambridge University Press, Cambridge, England, 1987).
[16] F. Iachello and P. Van Isacker, *The Interacting Boson-Fermion Model* (Cambridge University Press, Cambridge, England, 1991).
[17] C. -L. Wu, D. H. Feng, and M. Guidry, in *Advances in Nuclear Physics*, edited by J. W. Negele and E. Vogt (Plenum, New York, 1994), Vol. 21, p. 227.
[18] S. Raman, S. Kahane, and K. H. Bhatt, J. Phys. G **25**, 905 (1999).
[19] C. S. Warke and M. R. Gunye, Phys. Rev. **155**, 1084 (1967).
[20] A. Bohr and B. R. Mottelson, *Nuclear Structure* (Benjamin, New York, 1969), Vols. 1 and II.
[21] J. D. Vergados, Nucl. Phys. **A111**, 687 (1968).
[22] G. F. Bertsch, *The Practitioner's Shell Model* (Elsevier, New York, 1972), p. 28.
[23] J. P. Elliott, The University of Rochester Report No. NYO-2271, 1958 (unpublished), p. 50.
[24] D. M. Brink and G. R. Satchler, *Angular Momentum* (Clarendon, Oxford, England, 1967), p. 36.
[25] T. Otsuka, A. Arima, and F. Iachello, Nucl. Phys. **A309**, 1 (1978).
[26] A. Bohr and B. R. Mottelson, Phys. Scr. **22**, 468 (1980).
[27] B. E. Chi, Nucl. Phys. **83**, 97 (1966).
[28] O. Castaños, J. P. Draayer, and Y. Leschber, Ann. Phys. (N.Y.) **180**, 290 (1987).
[29] J. P. Draayer, in *International Workshop on Nuclear Structure Models*, edited by R. Bengtsson, J. Draayer, and W. Nazarewicz (World Scientific, Singapore, 1992), p. 61.
[30] D. P. Ahalpara, A. Abzouzi, and K. H. Bhatt, in *Progress in Particle and Nuclear Physics*, edited by A. Faessler (Pergamon, Oxford, 1985), Vol. 15, p. 135.
[31] K. L. G. Heyde, *The Nuclear Shell Model* (Springer-Verlag, Berlin, 1990), p. 320.
[32] V. K. B. Kota and Y. D. Devi, *Nuclear Shell Model and the Interacting Boson Model: Lecture Notes for Practitioners* (Inter University Consortium for D.A.E. Facilities, Calcutta, 1998), p. 183.
[33] M. R. Gunye and C. S. Warke, Phys. Rev. **159**, 885 (1967).
[34] K. Hara and Y. Sun, Int. J. Mod. Phys. E **4**, 637 (1995).
[35] F. Villars, in *Many-Body Description of Nuclear Structure and Reactions*, edited by C. Bloch (Academic, New York, 1966), p. 14.
[36] K. Hara, A. Hayashi, and P. Ring, Nucl. Phys. **A385**, 14 (1982).
[37] I. Talmi (private communication).
[38] H. Xie, Ph. D thesis, The University of Tennessee, 1990.
[39] H. Xie, F. K. McGowan, C. Baktash, J. D. Garrett, J. H. Hamilton, N. R. Johnson, I. Y. Lee, J. C. Wells, R. Wyss, and C.-H. Yu, Nucl. Phys. **A599**, 560 (1996).
[40] N. R. Johnson, F. K. McGowan, D. F. Winchell, C. Baktash, J. D. Garrett, I. Y. Lee, J. C. Wells, L. Chaturdevi, W. B. Gao, W. C. Ma, S. Pilotte, and C.-H. Yu, Phys. Rev. C **53**, 671 (1996).
[41] C.-L. Wu (private communication).
[42] H. Emling, E. Grosse, R. Kulessa, D. Schwalm, and H. J. Wollersheim, Nucl. Phys. **A419**, 187 (1984).
[43] H. Ower, Th. W. Elze, J. Idzko, K. Stelzer, E. Grosse, H. Emling, P. Fuchs, D. Schwalm, H. J. Wollersheim, N. Kaffrell, and N. Trautmann, Nucl. Phys. **A388**, 421 (1982).